STOCHASTIC STRUCTURAL CONTROL OF BRIDGES SUBJECT TO WIND-INDUCED VIBRATIONS USING SEPARATED SURFACES

By

Diego Andrés Alvarez Marín

diegoandresalvarez@gmx.net

Supervisor:

Jorge Eduardo Hurtado Gómez

SUBMITTED IN PARTIAL FULFILLMENT OF THE
REQUIREMENTS FOR THE DEGREE OF
MASTER ON INDUSTRIAL AUTOMATION
AT THE
UNIVERSIDAD NACIONAL DE COLOMBIA
MANIZALES, COLOMBIA
NOVEMBER 2003

UNIVERSIDAD NACIONAL DE COLOMBIA
FACULTY OF
ELECTRIC AND ELECTRONIC ENGINEERING

The undersigned hereby certify that they have read and recommend to the Faculty of Faculty of Engineering for acceptance a thesis entitled "**Stochastic Structural Control of Bridges Subject to Wind-Induced Vibrations Using Separated Surfaces**" by **Diego Andrés Alvarez Marín** in partial fulfillment of the requirements for the degree of **Master on Industrial Automation**.

Dated: November 2003

Supervisor:

Jorge Eduardo Hurtado Gómez

Readers:

First Reader

Second Reader

UNIVERSIDAD NACIONAL DE COLOMBIA

Date: **November 2003**

Author: **Diego Andrés Alvarez Marín**

Title: **Stochastic Structural Control of Bridges Subject to Wind-Induced Vibrations Using Separated Surfaces**

Faculty: **Electric and Electronic Engineering**

Degree: **M.Sc.** Convocation: **November** Year: **2003**

To all those who hold me in their hearts

Contents

List of Tables

List of Figures

Abstract

This thesis studies the use of separated control surfaces attached beneath the deck of a long-span bridge as an effective method for controlling wind induced vibrations, namely, buffeting and fluttering, making stress on the influence of the former. In this work, a state space formulation of the controlled bridge was developed. This formulation was analyzed varying the different parameters involved in the structural control. As it was seen that the state space formulation was dependent on the mean wind speed a variable gain approach was employed, showing an efficient performance of the control algorithm on the wind design range; however in turbulent winds the performance of the control system may not be as good as expected, in as much as the buffeting forces have a great influence on the heaving vibration mode. Since the wind fluctuations are a stochastic process a parametric analysis of the system was carried out, showing also that the use of control surfaces is not a very effective system for controlling the turbulent component of the wind.

Resumen

Esta tesis estudia el control activo de puentes de gran luz utilizando superficies de control fijadas debajo del tablero, como un método efectivo para controlar las vibraciones inducidas por el viento, en particular, buffeting y fluttering, haciendo especialmente énfasis en la primera. En este trabajo, se desarrolló una formulación en espacio de estados la cual fue analizada variando los diferentes parámetros involucrados en el control activo del puente. Se observó que esta formulación es dependiente de la velocidad media del viento, por lo tanto se utilizó en enfoque de control estocástico con que utiliza ganancias variables, el cual demostró un eficiente desempeño en el para el rango de velocidades de viento deseadas; sin embargo, el funcionamiento del sistema de control no es tan bueno como se podría esperar cuando se tienen vientos altamente turbulentos, en razón a que las fuerzas de buffeting tienen una gran influencia en el modo de vibración vertical. Como las fluctuaciones del viento son un proceso estocástico, se realizó un análisis paramétrico del sistema, demostrando que el uso de superficies de control no son tan eficientes como se desearía para la mitigación de las vibraciones inducidas por la turbulencia del viento.

Acknowledgements

I would like to thank Prof. Jorge E. Hurtado, my tutor and supervisor, for his many suggestions and constant support during this work, and the most important, for being my mentor during these five years. I am also thankful to Prof. Germán Castellanos, for instilling in me the research spirit.

Of course, I am grateful to my parents for their patience and love.

Also, I would like to say thanks to Prof. Nicholas Jones, Dr. Xinzhong Chen and Prof. Krzysztof Wilde for his help through the internet.

Finally, I wish to thank the following: Carolina, for teach me what courage is; Diego Alejandro Patiño for his useful comments concerning the control system of the bridge, the guys of the Control and Digital Signal Processing Group, for their useful discussions about machine learning, girls, control, computers, music, signal processing and life; Naile, for helping me with the typesetting of some equations; and all others, you know who you are!

This research was financially supported by the agreement 069 of 2002 between the Universidad Nacional de Colombia Sede Manizales - DIMA and Colciencias, program "Jóvenes Investigadores."

Manizales, Colombia — Diego Andrés Alvarez

September 26, 2003

Chapter 1

Introduction

> *"... the Tacoma Narrows bridge failure has given us invaluable information ... It has shown [that] every new structure which projects into new fields of magnitude involves new problems for the solution of which neither theory nor practical experience furnish an adequate guide. It is then that we must rely largely on judgment and if, as a result, errors or failures occur, we must accept them as a price for human progress."*
>
> *Othmar Ammann,*
> *leading bridge designer and member of the Federal Works Agency Commission*
> *investigating the collapse of the Tacoma Narrows Bridge*

Bridges are structures subjected to traffic-, seismic- and wind-induced forces. Wind forces impel on the structure vibrations which could make collapse it: that was the case of the Brighton Chain suspended-bridge in 1836, of a bridge over the Ohio river in West Virginia in 1854 and the well-known case of the Tacoma Narrows Bridge (Figure 1.1) in November 7, 1940 (Billah and Scanlan (1991)). Thenceforth, wind effects on structures have become a new topic of research, becoming of primal importance the study of aerodynamic and aeroelastic stability of structures. Thus, engineers, nowadays, face the problem of making each time longer bridges, which at the same time promotes the study of wind effects on those structures.

On the other side, a recent field of concern in structural engineering is the mitigation of vibrations

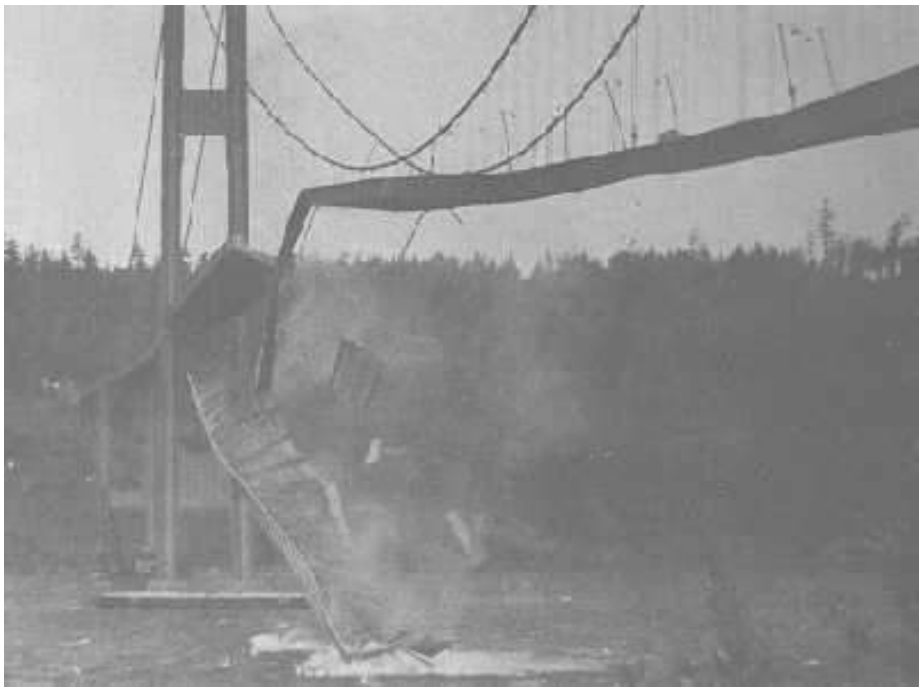

Figure 1.1: Collapse of the Tacoma Narrows Bridge (source Billah and Scanlan (1991))

induced by environmental loads as those caused by earthquakes and wind as a method to reduce structural damage inasmuch as they represent a threat to human lives and the infrastructure. Recently, active control of structures has been regarded as an effective method of hazard reduction which has becoming increasingly popular (Yao (1972); Housner et al. (1997)). Its main idea is that through the application of actuators and sensors the structural forces and vibrations can be kept between serviceability and safety bounds, such that desirable performance criteria are achieved. However, the main strides made in last years have aimed the development of structural control for seismic protection, leaving its application to bridges subjected to wind-induced loading in a second place (Housner et al. (1997)). Notwithstanding, some developments have been carried out, as will be briefly discussed in the following.

1.1 Previous work

After the Tacoma Narrows Bridge collapse[1], structural engineering community realized the fact that wind stability is one of the design government criteria in long-span bridges. Ever since,

[1]The Tacoma Narrows had a main span of 854 m

several strategies have been used to increase the flutter and torsional divergence velocity in bridges. In the first suspension bridges erected after the disaster, torsional stiffening of the truss girder was a very common strategy employed to reach aerodynamic/aeroelastic stability; however these torsional rigid girders have large structural dead loads and also are prone to higher wind loading than box girders (particularly drag forces), in addition to difficult and expensive manufacturing, erecting and maintenance processes. The construction in 1966 of the Severn Bridge (United Kingdom), showed that bridge stability could be achieved by the use of a flat-box-aerodynamic shaped girder. Nevertheless box girder decks are not useful anymore beyond certain span lengths. For example, the 1991-m-span-length Akashi Kaykio Bridge, built in Japan, the up-to-date longest suspension bridge in the world, was constructed using again a torsional rigid truss girder.

In recent years, several alternatives have been proposed to increase the wind stability of long-span bridges: the use of tuned mass dampers (TMD) (Nobuto et al. (1988)), the use of a twin-deck system (Richardson (1981)), the movement of the center of gravity of the deck by means of tanks filled with water, as was implemented in the Humber Bridge in the United Kingdom (Branceleoni (1992)), the use of active tendons (Ackkire and Preumont (1996); Bossens and Preumont (2001)), the change of shape in the cable configuration (Astiz (1998)), the use of aerodynamic appendages (Cobo del Arco and Aparicio (1998)) and the use of actively controlled winglets as a modification of the latter (Raggett (1987); Wilde and Fujino (1998), Huynh and Thoft-Christensen (2001)).

Nobuto et al. (1988) studied the use of TMDs on a sectional model of a bridge deck. They placed two TMDs on the leading and trailing edges of the girder and their frequencies were tuned to the resulting flutter frequency, increasing in this way the flutter velocity on 14% approximately; however the performance of the system resulted very sensible to the tuning of the TMDs.

Ackkire and Preumont (1996) and Bossens and Preumont (2001) have studied the use of active tendons in cable-stayed brides. This method places strategically along the deck several actuators which control the deformation of different cables, such that the actuators hinder the girder vibration. This method is only useful for cable-stayed bridges and has the advantage that it also is useful for controlling vibrations induced by earthquakes and traffic.

The aerodynamic appendages strategy was proposed in Raggett (1987) and Ostenfeld and Larsen (1992). They described along general lines two methods which could serve as means of active

control of bridges: the use of wings separated of the deck, and the use of ailerons next to the bridge girder. Ostenfeld and Larsen (1992, 1997) also proposed the active control of these control surfaces as a way to generate forces; the rotation of the surfaces produces the aeroelastic forces that are used to stabilize the structure, cancelling or reducing the vibrations induced by wind loading on the bridge. In other words, the idea proposes to attach by means of aerodynamically shaped pylons one or two control surfaces above or below the bridge deck running parallel to the girder and far enough from the deck that it lies in the undisturbed flow field, so that the control surfaces modify the flow around the deck, increasing in this way the flutter speed. Cobo del Arco and Aparicio (1998) suggested the use of winglets as aerodynamic appendages attached to the deck, fixed or actively controlled; they located the wings in different configurations and concluded that the use of winglets can increase the flutter speed of the bridge, however the use of symmetrically placed wings can increase the flutter speed, but not the torsional divergence speed, so there is a maximum length in bridges using wings as an active control method.

Kobayashi and Nagaoka (1992) reported the first experimental research of the active aerodynamic flutter suppression on a wind tunnel test bridge model deck section with winglets positioned above the girder, obtaining an increase of 100% on the flutter speed, based on an algorithm proposed in Ostenfeld and Larsen (1992). They varied the angle of rotation of the wings in time as a predetermined function of the angle of rotation of the girder, so that if the bridge is rotating in a sinusoidal motion at a frequency ω, the flap is rotating at the same frequency but out of phase, that is, the deck rotation is modelled as $\alpha_d(t) = \alpha_0 \sin(\omega t)$ and the winglet rotation as $\alpha_w(t) = a\alpha_0 \sin(\omega t + \phi)$, where a controls the amplitude of the winglet and ϕ is the out-of-phase angle between the movement of the flap and the movement of the girder; those parameters must be carefully set by the designer.

On the other hand, Wilde and Fujino (1998) directly addressed the control of winglets to control flutter in bridge decks using active control theory, under the assumption that there is no flow interaction within the control surfaces and the deck, deriving a state space formula describing the motion of a sectional model of a wind-bridge-control surfaces (BWCS) system. Since the developed equation of motion was dependent on average wind velocity, they proposed a variable-gain output feedback control law, defined over the possible wind velocity range in which the bridge would be exposed to. The main assumption of Wilde and Fujino (1998), which deserves further experimental study, is that neither the flow around the control surfaces is not disturbed

by the presence of the deck nor by the wake of the leading flap. It is further supposed that the flow around the deck is not disturbed by the presence of the wings, so that the total load on the cross section can be obtained by the superposition of the load acting on the deck and the load acting on the winglets.

Huynh and Thoft-Christensen (2001) also studied the use of control surfaces attached below the deck. They did not address the active control of such wings, however they analyzed the flap configuration and the flap rotation angles as parameters for analyzing the flutter velocity, concluding that the best position of the control surfaces is one where the leading control surface is twisted in an angle opposed in sign to the one of the deck and the trailing flap, an angle with the same sign as the deck.

The use of ailerons next to the bridge deck, studied independently by Hansen and Thoft-Christensen (1998) and Wilde et al. (2001), actively changes the geometry, and therefore the aerodynamic parameters of the bridge girder, modifying the flow pattern around the girder to lessen the wind-impelled excitation. These authors showed also that this method is an efficient one for controlling wind-induced excitations.

1.2 Main objectives of the thesis

The publications reported to date on the use control surfaces as a method of controlling wind induced vibrations have especially focused the control of the fluttering phenomenon using deterministic approaches. Nevertheless, up to the author's knowledge no research addressed explicitly the interaction between self-excited and buffeting vibrations nor considered the vibrations of the controlled bridge as parametric. For this reason, the following are the objectives of the present work:

- Propose a linear structural stochastic control for controlling self excited and buffeting-induced vibrations using the current approaches as a starting point.
- Analyze the stability of the uncontrolled and controlled bridge using stochastic differential equations which model the parametric vibration of the bridge caused by the wind excitation.

Finally, it must be said, that the present study will focus exclusively on the approach of the separated control surfaces located beneath the bridge deck using a two degree of freedom structural model (pitching and heaving modes).

1.3 Structure of the document

With the aim of making this document as self-contained as possible, it is included a chapter on wind effects on bridges, a chapter on synthetic wind fields simulation, and one explaining the simulation of the different aerodynamic and aeroelastic parameters of a wing; also the novel state space approach developed by Boonyapinyo et al. (1999) and Chen et al. (2000) is explained in chapter 5; the development of the state space equations which represent the dynamics of the BWCS system is addressed in chapter 6; next, the proposed stochastic control and the parametric stochastic stability of the winged bridge is developed in chapters 7 and 8 respectively. The document ends with a summary of the main results found in the research and offers suggestions for future work.

Chapter 2

Wind effects on bridges

Bridge design must ensure that the aerodynamic[1] and aeroelastic[2] effects of wind will not be present under normal serviceability conditions and that the bridge will not vibrate excessively under gusty winds. In this way, its design must take in care several types of vibrations, among those we have: vortex shedding induced vibrations, torsional divergence, flutter, buffeting and galloping. In the following, a brief description of the wind-induced vibrations will be developed after Simiu and Scanlan (1996), Morguental (2000) and Jurado and Hernández (2000).

2.1 Vortex shedding induced vibrations

A bluff body inside a flow produces a wake behind it; the flow within the wake is turbulent, but in certain intervals of the Reynolds number[3] (between 250 and 2×10^5) it can be observed that the body causes a vortex trail, moving downstream, that is shed from the flow. This vortex trail, known as *von Karman vortex street* (see Figure 2.1), has a periodic behaviour in time and space which induces on the structure an oscillating force actuating perpendicularly to the flow. The

[1] *Aerodynamic effects* are those induced in a structure by the wind considering its geometry before deformation.

[2] *Aeroelastic effects* are those impelled in a structure by the wind taking seriously into account the movement and deformation of the structure.

[3] The *Reynolds number* expresses a relationship between the inertial forces and the viscous forces present in a flow. It is given by $Re = Ul\rho/\mu$ where U is the flow speed, l expresses a characteristic length, ρ is the flow density and μ its dynamic viscosity. When this number is small, it is said that the flow is *laminar* or *steady*; on the other hand, when the Re is high (greater than 10^5 approximately), the flow is said to be *turbulent*.

periodic frequency of this vortex trail is largely dependent on the body geometry, the speed of the flow and the density and viscosity of the fluid. This trail of vortices induces on the structure

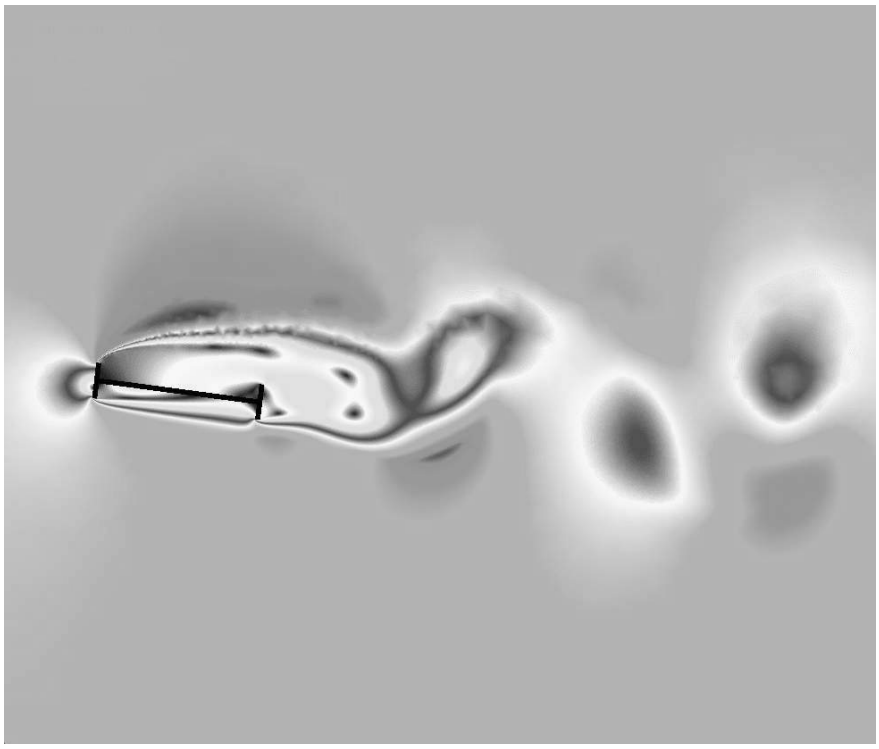

Figure 2.1: Von Karman vortex street (source Frandsen (2002))

a vertical (lift) force $L(t)$, expressed by,

$$L(t) = \frac{1}{2}\rho U^2 D C_L \sin(2\pi N_s t) \tag{2.1}$$

where ρ is the air density, C_L is the lift coefficient and N_s is the vortex shedding frequency.

If the body has a degree of freedom associated with a certain stiffness in the direction of the periodic force, it will exercise an oscillation due to its inertia and the forcing action. In this way, when the vortex shedding frequency is near the natural frequency of oscillation of the body, a phenomenon known as *resonance* is produced, which has a bounded maximum amplitude. This vortex-induced vibrations can also be experienced by bridges which in this case becomes a serviceability problem, however it generally may be overcome by either increasing the damping or stiffening the structure to shift the natural frequency away; this maybe done by the application of tuned mass dampers and changing the arrangement of additional cables.

2.2 Divergence

It is an instability phenomenon usually present on structures subjected to high wind speeds, like airplane airfoils. It is characterized by a sudden torsional movement of the structure; in this way it can be associated to the buckling phenomenon present in columns.

2.3 Fluttering

There are various kinds of fluttering, however, here is merely discussed the one related to bridges. The classical fluttering is an aeroelastic phenomenon in which several degrees of freedom of a structure becomes coupled in an unstable oscillation driven by the wind (see Figure 2.2). This movement inserts energy to the bridge during each cycle so that it neutralizes the natural damping of the structure, thus the new system (bridge-fluid) behaves like if had an effective negative damping, leading to a exponentially growing response, and finally driving the bridge toward failure due to excessive deflection and stresses. It can be concluded that flutter is a stability problem as opposed to vortex induced vibrations being a response problem. The wind speed which causes the beginning of the fluttering phenomenon (when the effective damping becomes zero) is known as the *flutter velocity*. Flutter analysis is usually based on a linear and elastic behaviour of the compound system fluid-structure. This is justified because the bridge oscillations are usually small. Fluttering occurs even in steady flow, so that it is recognized as a self-exciting phenomenon. Hence, bridge design must ensure that flutter velocity will be higher that the maximum mean wind speed present at the site. This is worth to mention that, usually

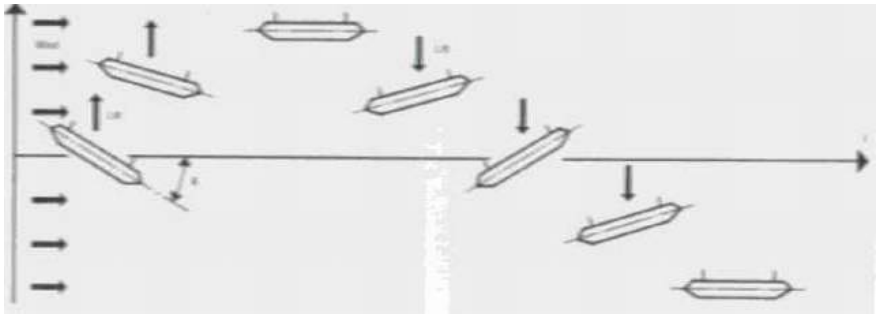

Figure 2.2: Fluttering (source Walther et al. (1988))

in physics courses it is taught that the Tacoma Narrows Bridge collapsed because of vortex

shedding-induced resonance (it was the initial hypothesis of von Karman). However Billah and Scanlan (1991) clearly states that it collapsed due to fluttering.

2.4 Buffeting

When the vibrations on a structure are caused by the variations on wind speed and direction (turbulence), it is said that the structure vibrates due to *buffeting*. This vibrations can occur for example when the body is inside the wake left by another body upstream. Buffeting response does not generally lead to catastrophic failures, however, it may cause fatigue damage of the structure and may affect the safety of passing vehicles because of excessive vibrations, hence, it is a serviceability problem.

2.5 Galloping

Galloping is a instability usually present on slender structures such cables with an ice coating fixed to it. This instability is characterized by an along wind oscillation of the structure with amplitudes large many times the characteristic dimension of the structure. It is an important issue in the design of cable-stayed bridges, and power transmission lines.

Chapter 3

Simulation of wind velocity fluctuation fields

Wind as a natural phenomenon random in nature can be modelled as a stochastic process. As the analysis of the structural response to wind-induced load can be carried out by means of a Monte Carlo simulation, it is mandatory to accurately describe the random properties of wind velocity. Wind velocity is a non-stationary process, composed of a fluctuating part $u(t)$ and a imposed steady part $\bar{U}$ which represents the mean; the fluctuations about $\bar{U}$ can be modelled as a Gaussian ergodic stationary non-homogeneous three dimensional and multivariate (since it varies along the span of the bridge) stochastic process. However, the simulation can be further simplified modelling the wind velocity fluctuation field as three one-dimensional multivariate process, with the coherence between different dimensions ignored inasmuch as the error in this way included is frequently small.

There are several approaches for simulating sample functions from a stochastic process, among them we have, (a) the spectral representation method, (b) the auto-regressive modelling method, (c) the turning band method, (d) the noise shower method, (e) the scale refinement methods and (f) the covariance decomposition method.

3.1 The spectral representation method

The spectral representation method is widely used today. Its origin dates back to Rice (1954) who setup the foundation of the method, however, were Shinozuka (1972) and Shinozuka and Jan (1972) who first applied it to simulate multidimensional, multivariate, non-stationary and non-Gaussian stochastic processes. Yang (1972, 1973) and Shinozuka (1974) made use of the FFT technique to drastically speed up the computational efficiency of the method, applying it also to multidimensional cases. Yamazaki and Shinozuka (1988) extended the application of the method to the simulation of non-Gaussian stochastic fields by means of an iterative procedure, whereas, Deodatis and Shinozuka (1989) built a method to simulate stochastic waves. Shinozuka et al. (1989) developed a method to generate ergodic multivariate stochastic processes using the idea of double-indexing the frequencies, but this algorithm simulated sample functions which were not ergodic. Later Deodatis (1996) further developed the spectral representation method and used it to successfully simulate ergodic multivariate stochastic processes. Cao et al. (2000) improved Deodatis (1996) method making it computationally more efficient in the particular case of homogeneous processes when the cross spectral density matrix is real and used it to simulate one-dimensional wind velocity fields on long-span bridges.

In the following lines the method is briefly summarized after Deodatis (1996) and Cao et al. (2000). Let us consider a one dimensional n-variate (1-D,n-V) stochastic processes vector $\{f_j(t)\}$ with components $f_j(t)$, $j = 1, \ldots, n$, zero mean

$$E\left[f_j(t)\right] = 0 \quad j = 1, \ldots, n \tag{3.1}$$

and cross-spectral density matrix given by

$$\mathbf{S}(\omega) = \begin{bmatrix} S_{11}(\omega) & S_{12}(\omega) & \cdots & S_{1n}(\omega) \\ S_{21}(\omega) & S_{22}(\omega) & \cdots & S_{2n}(\omega) \\ \vdots & \vdots & \ddots & \vdots \\ S_{n1}(\omega) & S_{n2}(\omega) & \cdots & S_{nn}(\omega) \end{bmatrix} \tag{3.2}$$

where $S_{jj}(\omega)$, $j = 1, \ldots, n$ are the power spectral density functions of the n components of the process and $S_{jk}(\omega)$, $j, k = 1, \ldots, n$, $j \neq k$ are the corresponding cross-spectral density functions. It can be demonstrated that $\mathbf{S}(\omega)$ is a Hermitian and usually complex non-negative definite matrix. Shinozuka (1972) stated that the stochastic process $f_j(t)$, $j = 1, \ldots, n$ can be simulated

by

$$f_j(t) = \sqrt{2\Delta\omega} \sum_{m=1}^{j} \sum_{l=1}^{N} |H_{jm}(\omega_{ml})| \cos(\omega_{ml} t - \theta_{jm}(\omega_{ml}) + \Phi_{ml}) \quad j = 1, \ldots, n \tag{3.3}$$

as $N \to \infty$, where H_{jm} is a component of a lower-triangular matrix $\mathbf{H}(\omega)$, which can be obtained by means of a Cholesky decomposition of the cross-spectral density matrix $\mathbf{S}(\omega)$, that is,

$$\mathbf{S}(\omega) = \mathbf{H}(\omega)\mathbf{H}^{T*}(\omega) \tag{3.4}$$

The elements of $\mathbf{H}(\omega)$ can be expressed in polar form as

$$H_{jm}(\omega_m) = |H_{jm}(\omega)| \exp(i\theta_{jm}(\omega)) \qquad j = 1, \ldots, n \quad m = 1, \ldots, n \quad j \geq m \tag{3.5}$$

where $i^2 = -1$ and

$$\theta_{jm}(\omega) = \tan^{-1}\left(\frac{\mathrm{Im}[H_{jm}(\omega)]}{\mathrm{Re}[H_{jm}(\omega)]}\right) \tag{3.6}$$

The double-indexing of the frequency originally proposed by Shinozuka et al. (1989) is given by

$$\omega_{ml} = \left(l + \frac{m}{n} - 1\right)\Delta\omega \quad l = 1, \ldots, N \tag{3.7}$$

where the frequency increment $\Delta\omega$ stands for

$$\Delta\omega = \frac{\omega_u}{N} \tag{3.8}$$

In the last equation, ω_u is a fixed upper cutoff frequency (a constant) beyond which the elements of the cross-spectral density matrix, S_{jk} are assumed to be zero, that is, $|\omega| = 0$ for $\omega \geq \omega_u$. As ω_u is a fixed value and $\Delta\omega N = \omega_u$, then $N \to \infty$ as $\Delta\omega \to 0$

In equation (3.3) $\{\Phi_{ml}\}$ is a sequence of random variables uniformly distributed over the interval $[0, 2\pi)$ which can be understood as random phase angles.

The stochastic process $f_j(t)$ simulated by equation (3.3) is periodic with period given by

$$T = n\frac{2\pi}{\Delta\omega} \tag{3.9}$$

which indicates that the smaller $\Delta\omega$, the longer the period T of the stochastic process.

A sample function $\{f_j^0(t)\}$ of the stochastic process $\{f_j(t)\}$, $j = 1, \ldots, N$ is obtained after sampling values $\{\phi_{ml}\}$ from the random variables $\{\Phi_{ml}\}$ and taking in care that they must obey the Nyquist's sampling theorem condition,

$$\Delta t \leq \frac{2\pi}{2\omega_u} \tag{3.10}$$

in order to avoid aliasing (Mitra (1998)).

The simulation method expressed in equation (3.3) has the following properties (the reader is referred to Deodatis (1996) for detailed proofs):

1. The ensemble expected value of the simulated stochastic process $E[f_j(t)]$ and their targets $E[f_j^0(t)]$ are identical and equal to zero, i.e.,

$$E[f_j(t)] = E[f_j^0(t)] = 0 \quad j = 1, \ldots, n \tag{3.11}$$

2. The ensemble auto/cross correlation function $R_{jk}(\tau)$ of the generated stochastic process and their targets $R_{jk}^0(\tau)$ are identical,

$$R_{jk}(\tau) = R_{jk}^0(\tau) \quad j, k = 1, \ldots, n \tag{3.12}$$

where $\mathbf{R}(\tau)$ and $\mathbf{S}(\omega)$ are related by the *Wiener-Khintchine formulas*, that is,

$$\mathbf{S}(\omega) = \frac{1}{2\pi} \int_{-\infty}^{\infty} \mathbf{R}(\tau) \exp(-i\omega\tau) \mathrm{d}\tau \tag{3.13}$$

$$\mathbf{R}(\tau) = \int_{-\infty}^{\infty} \mathbf{S}(\omega) \exp(i\omega\tau) \mathrm{d}\omega \tag{3.14}$$

3. The sample function of the generated stochastic process are bounded as follows

$$f_j^0(t) \leq \sqrt{2\Delta\omega} \sum_{m=1}^{j} \sum_{l=1}^{N} |H_{jm}(\omega_{ml})| \quad j = 1, \ldots, n \tag{3.15}$$

4. Each and every sample function given by (3.3) is ergodic in the mean

$$\left\langle f_j^0(t) \right\rangle_{T_0} = E\left[f_j^0(t)\right] = 0 \quad j = 1, \ldots, n \quad \text{when } T = T_0 \tag{3.16}$$

and in correlation

$$\left\langle f_j^0(t) f_k^0(t+\tau) \right\rangle_{T_0} = R_{jk}^0(\tau) \quad j, k = 1, \ldots, n \quad \text{when } T = T_0 \tag{3.17}$$

where the operator $\langle \cdot \rangle$ stands for

$$\langle g(t) \rangle_T \equiv \frac{1}{T} \int_0^T g(t) \mathrm{d}t \tag{3.18}$$

as $\Delta\omega \to 0$ and $N \to \infty$ in (3.3) while keeping in mind that $\omega_u = N\Delta\omega$ and $S_{jk}(\omega) = 0$ for $|\omega| \geq \omega_u$ and $j, k = 1, \ldots, n$.

5. The simulated stochastic process is Gaussian as $N \to \infty$ in (3.3) because of the central limit theorem.

3.1.1 Generation of the one-dimensional multivariate stochastic process using the FFT technique

By using the FFT technique, we can increase the computational efficiency of the algorithm. We can recast (3.3) in the following form,

$$f_j^0\left(p\Delta t\right) = \sum_{m=1}^{j} \mathrm{Re}\left\{ g_{jm}\left(q\Delta t\right) \exp\left(i\left(\frac{m\Delta\omega}{n}\right)\left(p\Delta t\right)\right)\right\} \quad p = 0,\ldots,nM-1 \quad j = 1,\ldots,n \tag{3.19}$$

where $q \equiv \mathrm{mod}(p, M)$ is the remainder of the division of p and M and

$$g_{jm}\left(q\Delta t\right) = \sum_{l=0}^{M-1} B_{jm}(l\Delta\omega) \exp\left(i\left(l\Delta\omega\right)\left(q\Delta t\right)\right) \quad q = 0,\ldots,M-1 \tag{3.20}$$

with

$$B_{jm}(l\Delta\omega) = \begin{cases} \sqrt{2\Delta\omega}\left|H_{jm}\left(\omega_{lmn}\right)\right| \exp\left(-i\theta_{jm}\left(\omega_{lmn}\right) + i\phi_{ml}\right) & \text{when } 0 \le l \le N-1 \\ 0 & \text{when } N \le l \le M-1 \end{cases} \tag{3.21}$$

for $j, m = 1,\ldots,n$, $j \ge m$ and $l = 0,\ldots,M-1$, where $\omega_{lmn} = l\Delta\omega + \frac{m\Delta\omega}{n}$. The second case in (3.21), that is, when $N \le l \le M-1$ accounts for the assumption that $S(\omega) = 0$ for $|\omega| \ge \omega_u$.

The sample function $f_j^0(p\Delta t)$, $j = 1,\ldots,n$ stated in (3.19) is periodic with period $T = 2\pi n/\Delta\omega$, therefore $nM\Delta t = 2\pi n/\Delta\omega$ which can be written as $\Delta t\Delta\omega = 2\pi/M$ or

$$\Delta t = \frac{2\pi}{\Delta\omega M} \tag{3.22}$$

Replacing the above equation in (3.20) we have

$$g_{jm}\left(q\Delta t\right) = \sum_{l=0}^{M-1} B_{jm}(l\Delta\omega) \exp\left(i\frac{2\pi}{M}lq\right) \quad j,m = 1,\ldots,n \quad j \ge m \quad q = 0,\ldots,M-1 \tag{3.23}$$

Using (3.8), (3.10) and (3.22) the following condition is established

$$M \ge 2N \tag{3.24}$$

The sample function is therefore calculated using (3.19), after applying the FFT technique to (3.23) as $g_{jm}\left(q\Delta t\right)$ is M times the inverse discrete Fourier transform of $B_{jm}(l\Delta\omega)$, resulting in a drastically increase of the computational efficiency.

3.1.2 Particularization of the method for generating a wind velocity field

The method outlined above can be particularized to the case in which the random field is homogeneous, that is, $S_{11}(\omega) = S_{22}(\omega) = \cdots = S_{nn}(\omega) = S(\omega)$. On the other hand, as the orthogonal spectrum of wind velocity fluctuations in the atmosphere is usually neglected because it is very small, then $S_{jk}(\omega)$ can usually be treated as real, and therefore $\mathbf{S}(\omega)$ can be treated as a real matrix. The elements of $\mathbf{S}(\omega)$ can be expressed as

$$\begin{aligned} &S_{jj}(\omega) = S_j(\omega) \quad j = 1, \ldots, n \\ &S_{jk}(\omega) = \sqrt{S_j(\omega) S_k(\omega)} \mathrm{Coh}\left(\Delta_{jk}, \omega\right) \quad j, k = 1, \ldots, n, j \neq k \end{aligned} \tag{3.25}$$

where $S_j(\omega)$ is the power spectral density function of the process and $\mathrm{Coh}\left(\Delta_{jk}, \omega\right)$ is known as the coherence function between the stochastic processes $f_j^0(t)$ and $f_k^0(t)$.

Kaimal and et. al. (1972) stated a power spectral density function which relates the longitudinal wind velocity fluctuations at different heights,

$$S_{uu}\left(z, \omega\right) = \frac{200 z u_*^2}{U(z)\left(1 + 50 \frac{\omega z}{2\pi U(z)}\right)^{5/3}} \tag{3.26}$$

likewise, Simiu and Scanlan (1996) proposed a spectrum of vertical wind velocity fluctuations,

$$S_{vv}\left(z, \omega\right) = \frac{3.36 z u_*^2}{U(z)\left(1 + 10\left(\frac{\omega z}{2\pi U(z)}\right)^{5/3}\right)} \tag{3.27}$$

where,

$$u_* = \frac{0.4 U(z)}{\ln\left(\frac{z}{z_0}\right)} \tag{3.28}$$

and z is the height in meters, ω is the frequency in rad/s, u_* is the friction velocity as a function of the surface roughness in m/s, $U(z)$ is the mean wind speed at height z in m/s and z_0 is the surface roughness.

On the other hand, Davenport (1968) suggested a model of the coherence function between the velocity fluctuations at two different heights z_j and z_m (however in this case $z_j = z_m = z$),

$$\mathrm{Coh}\left(\Delta_{jm}, \omega\right) = \exp\left(-\frac{\omega}{2\pi} \frac{C_z \Delta_{jm}}{\frac{1}{2}\left(U(z_j) + U(z_m)\right)}\right) \tag{3.29}$$

where Δ_{jm} is the distance between points j and m and C_z is a constant which can be fixed to 10 for structural design purposes.

Considering the case of n uniformly distributed points along the bridge span, with a distance interval Δ between adjacent points, then $\Delta_{jm} = |j-m|\,\Delta$, therefore, (3.29) can be rewritten as,

$$\mathrm{Coh}\,(\Delta_{jm},\omega) = \exp\left(-\frac{\omega}{2\pi}\frac{C_z\Delta}{U(z)}\right)^{|j-m|} = C(\omega)^{|j-m|} \tag{3.30}$$

where,

$$C \equiv C(\omega) = \exp\left(-\frac{\omega}{2\pi}\frac{C_z\Delta}{U(z)}\right) \tag{3.31}$$

Taking in mind (3.25) and (3.29), $\mathbf{S}(\omega)$ can be recast as follows

$$\mathbf{S}\,(\omega) = S(\omega)\begin{bmatrix} 1 & C & C^2 & \cdots & C^{n-1} \\ C & 1 & C & \cdots & C^{n-2} \\ C^2 & C & 1 & \cdots & C^{n-3} \\ \vdots & \vdots & \vdots & \ddots & \vdots \\ C^{n-1} & C^{n-2} & C^{n-3} & \cdots & 1 \end{bmatrix} \tag{3.32}$$

It is possible to show that $\mathbf{S}(\omega)$ in the above equation has a corresponding $\mathbf{H}(\omega)$ matrix, obtained by means of Cholesky's decomposition, as indicated by (3.4) and given by

$$\mathbf{H}(\omega) = \sqrt{S(\omega)}\mathbf{G}(\omega) \tag{3.33}$$

where,

$$\mathbf{G}\,(\omega) = \begin{bmatrix} 1 & & & & & 0 \\ C & \sqrt{1-C^2} & & & & \\ C^2 & C\sqrt{1-C^2} & \sqrt{1-C^2} & & & \\ C^3 & C^2\sqrt{1-C^2} & C\sqrt{1-C^2} & \sqrt{1-C^2} & & \\ \vdots & \vdots & \vdots & \vdots & \ddots & \\ C^{n-1} & C^{n-2}\sqrt{1-C^2} & C^{n-3}\sqrt{1-C^2} & C^{n-4}\sqrt{1-C^2} & \cdots & \sqrt{1-C^2} \end{bmatrix} \tag{3.34}$$

that, is

$$G_{_{jm}}(\omega) = \begin{cases} 0 & \text{when } 1 \le j \le m \le n \\ C^{|j-m|} & \text{when } m = 1, m \le j \le n \\ C^{|j-m|}\sqrt{1-C^2} & \text{when } 2 \le m \le j \le n \end{cases} \tag{3.35}$$

inasmuch as $0 < C < 1$ then $\sqrt{1-C^2} > 0$ and therefore $H(\omega)$ is a real matrix. In this case, it can be proved that $\theta_{jk}(\omega) = 0$, $j, m = 1, \ldots, n$, $j \geq k$. Finally, replacing (3.33) into (3.3) we have,

$$f_j(t) = \sqrt{2\Delta\omega} \sum_{m=1}^{j} \sum_{l=1}^{N} \sqrt{S_{jm}(\omega_{ml})} G_{jm}(\omega_{ml}) \cos(\omega_{ml} t + \Phi_{ml}) \quad j = 1, \ldots, n \tag{3.36}$$

as $N \to \infty$, therefore, (3.21) changes to,

$$B_{jm}(l\Delta\omega) = \begin{cases} \sqrt{2\Delta\omega S\left(l\Delta\omega + \frac{m\Delta\omega}{n}\right)} G_{jm}\left(l\Delta\omega + \frac{m\Delta\omega}{n}\right) \exp(i\phi_{ml}) & \text{when } 0 \leq l \leq N-1 \\ 0 & \text{when } N \leq l \leq M-1 \end{cases} \tag{3.37}$$

for $j, m = 1, \ldots, n$, $j \geq m$ and $l = 0, \ldots, M-1$.

3.2 The auto-regressive modelling method

Papoulis (1991) and Chen and Kareem (2001) describe this method. It models the multi-correlated wind fluctuations as the output of a filtered vector Gaussian white noise $\mathbf{w}(t)$. The filter in this case is a linear system described by an auto-regressive (AR) model and the input has zero mean and identity covariance matrix. The AR model is expressed as

$$\mathbf{f}(t) = \sum_{k=1}^{p} \mathbf{P}_k \mathbf{f}(t - k\Delta t) + \mathbf{L}\mathbf{w}(t) \tag{3.38}$$

where p is the order of the AR model, Δt is the sampling interval and $\mathbf{P}_k$ for $k = 1, \ldots, p$ are the coefficient matrices of the *Yule-Walker equations*:

$$\mathbf{R}(j\Delta t) = \sum_{k=1}^{p} \mathbf{R}((j-k)\Delta t)\mathbf{P}_k^{\mathrm{T}}, \quad \text{for } j = 1, \ldots, p \tag{3.39}$$

In the last equation, $\mathbf{R}(j\Delta t), \quad j = 1, \ldots, p$ stands for the correlation matrix of the wind fluctuation vector $\mathbf{f}(t)$. As was seen above, they can be obtained from the cross-spectral density matrix $\mathbf{S}(\omega)$ using the Wiener-Khintchine formula (3.14). Also, matrix $\mathbf{L}$ in (3.38) can be obtained from the Cholesky decomposition,

$$\mathbf{L}^{\mathrm{T}}\mathbf{L} = \mathbf{R}(0) - \sum_{k=1}^{p} \mathbf{P}_k \mathbf{R}(k\Delta t) \tag{3.40}$$

The RHS of the last equation can be understood as the cross power spectral density of the white noise input (Papoulis (1991)). The AR model can be written in terms of the controllable canonical discrete state-space format:

$$\mathbf{x}_w(t) = \mathbf{A}_{dw}\mathbf{x}_w(t-\Delta t) + \mathbf{B}_{dw}\mathbf{w}(t) \tag{3.41}$$

$$\mathbf{f}(t) = \mathbf{C}_{dw}\mathbf{x}_w(t) + \mathbf{D}_{dw}\mathbf{w}(t) \tag{3.42}$$

where

$$\mathbf{x}_w(t) = \begin{bmatrix} \mathbf{x}_{w1}(t) \\ \mathbf{x}_{w2}(t) \\ \vdots \\ \mathbf{x}_{wn}(t) \end{bmatrix}; \quad \mathbf{A}_{dw} = \begin{bmatrix} \mathbf{0} & \mathbf{I} & \mathbf{0} & \cdots & \mathbf{0} \\ \mathbf{0} & \mathbf{0} & \mathbf{I} & \cdots & \mathbf{0} \\ \vdots & \vdots & \vdots & \ddots & \vdots \\ \mathbf{0} & \mathbf{0} & \mathbf{0} & \cdots & \mathbf{I} \\ \mathbf{P}_p & \mathbf{P}_{p-1} & \mathbf{P}_{p-2} & \dots & \mathbf{P}_1 \end{bmatrix}; \quad \mathbf{B}_{dw} = \begin{bmatrix} \mathbf{0} \\ \mathbf{0} \\ \vdots \\ \mathbf{I} \end{bmatrix}; \tag{3.43}$$

$$\mathbf{C}_{dw} = \begin{bmatrix} \mathbf{P}_p\mathbf{L} & \mathbf{P}_{p-1}\mathbf{L} & \cdots & \mathbf{P}_1\mathbf{L} \end{bmatrix}; \quad \mathbf{D}_{dw} = \mathbf{L} \tag{3.44}$$

Using the relationships,

$$\mathbf{A}_{dw} = \exp(\mathbf{A}_w\Delta t); \quad \mathbf{B}_{dw} = (\exp(\mathbf{A}_w\Delta t) - I)\mathbf{A}_w^{-1}\mathbf{B}_w; \quad \mathbf{C}_{dw} = \mathbf{C}_w; \quad \mathbf{D}_{dw} = \mathbf{D}_w \tag{3.45}$$

the equivalent continuous state space representation can be obtained,

$$\dot{\mathbf{x}}_w(t) = \mathbf{A}_w\mathbf{x}_w(t) + \mathbf{B}_w\mathbf{w}(t) \tag{3.46}$$

$$\mathbf{f}(t) = \mathbf{C}_w\mathbf{x}_w(t) + \mathbf{D}_w\mathbf{w}(t) \tag{3.47}$$

3.3 Generation of the wind velocity fluctuation field

An artificial wind velocity fluctuation field was simulated using the spectral representation method. The multivariate wind field was made of 18 waves, setting the distance between consecutive points as 250m. For computational reasons the parabolic camber of the deck was neglected in the simulation, inasmuch as the assumption of a non-homogeneous multivariate process makes the algorithm simulation, using Cao et al. (2000) approach, 148 times faster as the one by Deodatis (1996); this is explained by the fact that wind fluctuation power spectral density is dependent on

the height of the points. The algorithm was run on a 650 MHz-Pentium III processor with 256 MB of RAM, using MATLAB v6.0 and it took approximately 32 minutes to make the simulation.

The simulation conditions of the algorithm were as follows:

- Number of simulated points: $n = 18$.
- Distance between simulated points: $\Delta = 250$ m.
- Sampling frequency: $\frac{1}{\Delta t} = 4$ Hz.
- Upper cutoff frequency: $\omega_u = 4\pi$ rad/s.
- Number of divisions in frequency: $N = 1024$.

Kaimal's spectrum was selected as the target power spectral density. Davenport formula was selected as the coherence function between simulated points; in this way, those formulas require the parameters detailed below:

- Height above the ground: $z = 84$ m.
- Ground surface roughness length: $z_0 = 0.03$ m.
- Davenport's formula constant $C_z = 10$.

The wind speed was set to 40 m/s. In this way, the period of the simulated multivariate stochastic process was $T = 9216$ seconds. Figure 3.1 shows the first 200 seconds of the generated field for points 1, 2 and 18 in order to distinguish the similitudes and differences among the three realizations, while Figure 3.2 shows the auto-cross correlation functions of the realizations at different points of the simulated multivariate stochastic process. As can be seen realizations 1 and 2 have a strong correlation between them since they are near to each other, while on the contrary realizations 1 and 18 have a weaker correlation since they are far apart. If the simulated points were closer among them (say $\Delta = 30$ m) one could see in Figure 3.1 that nearer realizations would have a similar shape and low frequency behaviour, however here it is not the case because there is a strong loss of coherence for $\Delta = 250$ m, in view of the fact that the coherence decays exponentially with distance, as is stated by equation (3.29).

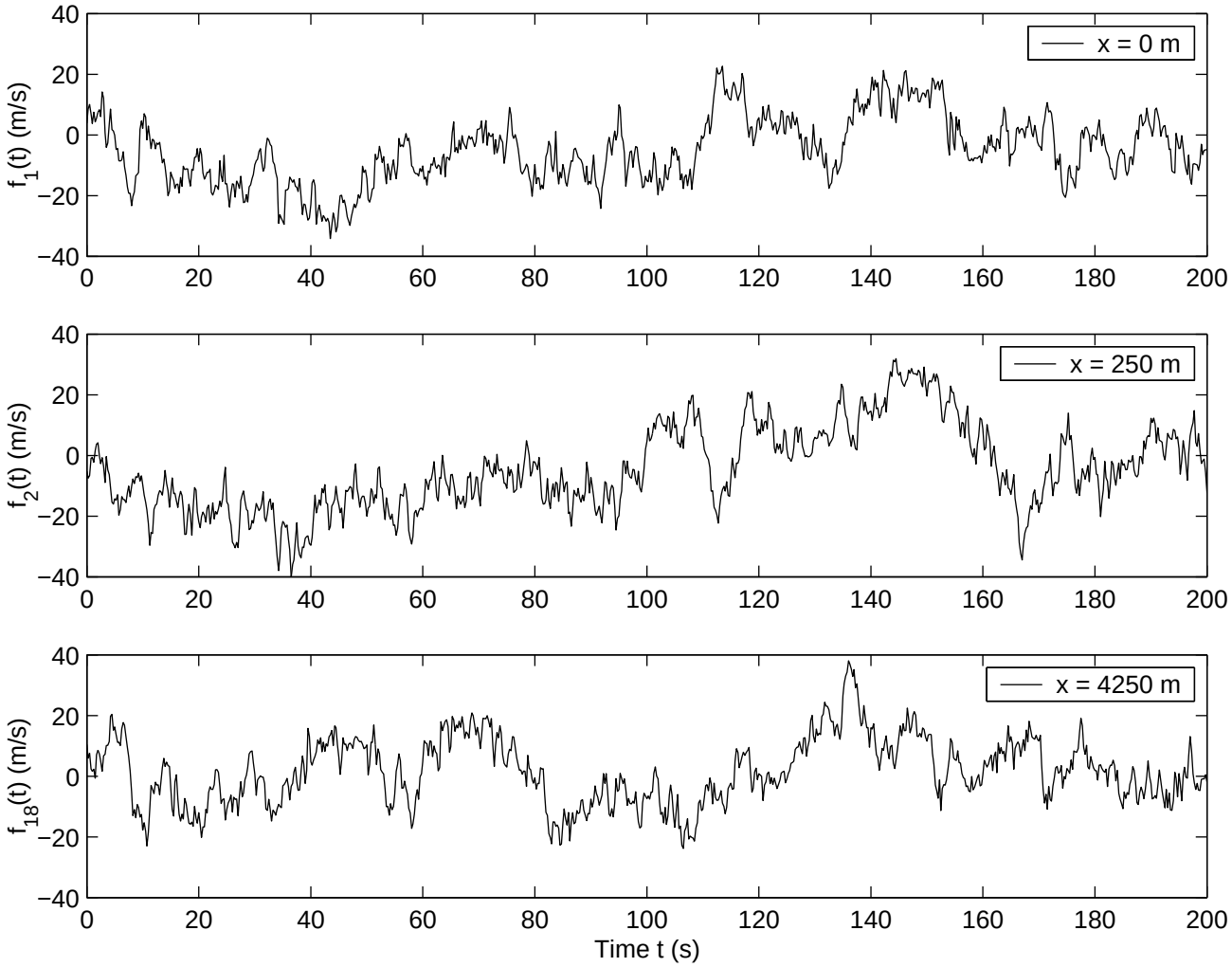

Figure 3.1: Simulation of horizontal wind velocity fluctuations at points 1, 2 and 18, for a mean wind velocity of 40 m/s.

Finally, Figure 3.3 shows the power spectral density check of the simulated wind velocity horizontal fluctuations field. The spectrum check was made using the Yule-Walker AR method. As can be observed, some deviations can be seen between the simulated spectra and the target at low frequencies. However, this error is negligible.

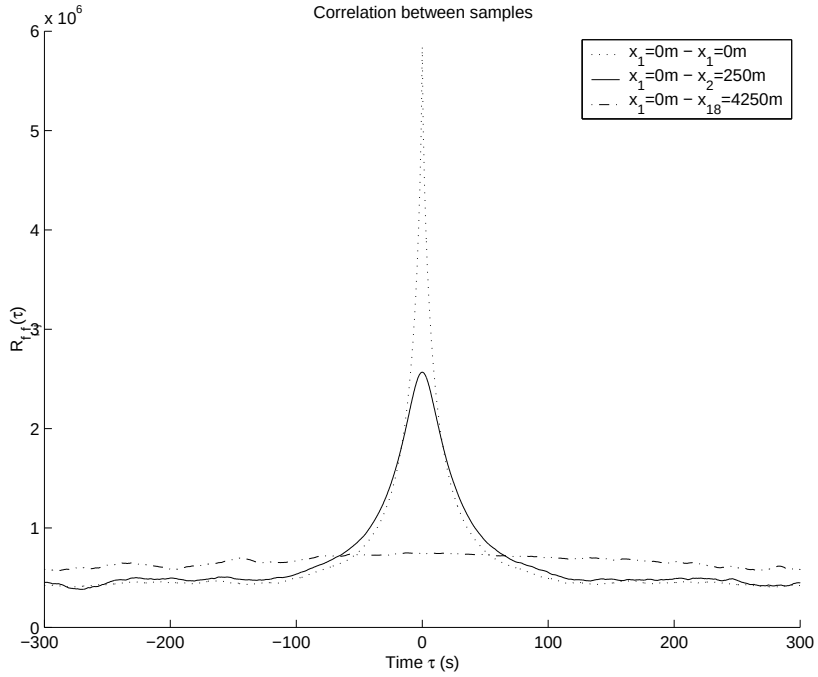

Figure 3.2: Auto and cross correlation functions of the simulated horizontal wind velocity fluctuations at points 1, 2 and 18, for an average wind speed of 40 m/s

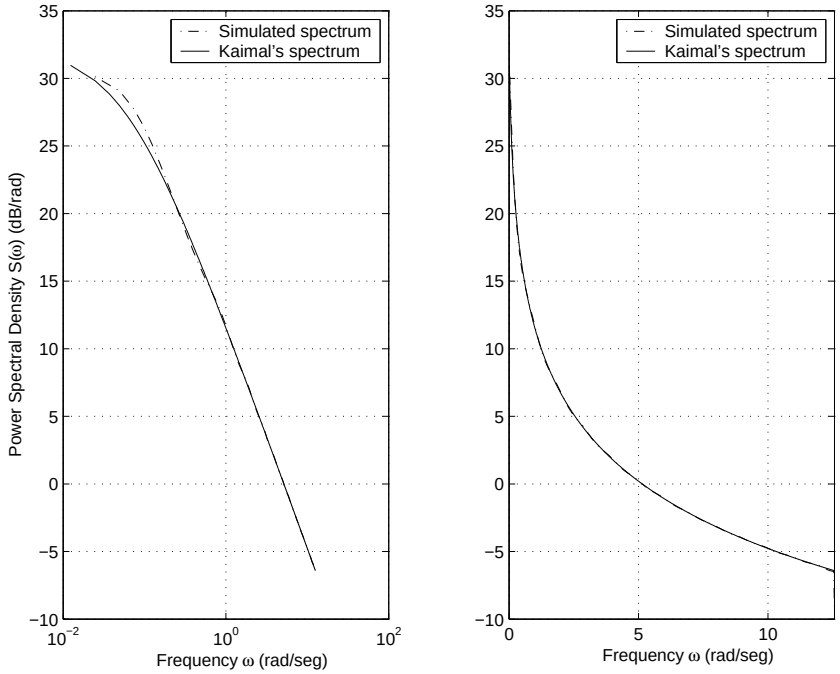

Figure 3.3: Power spectral density check of the simulated wind velocity horizontal fluctuations field, for an average wind speed of 40 m/s

Chapter 4

Aerodynamic and aeroelastic parameters of bridge decks and airfoils

Since the infamous collapse of the Tacoma Narrows Bridge, wind engineers have made great efforts to understand aeroelastic and aerodynamic analysis associated with long span bridges. Many of their developments were rooted on classical analysis of aircraft airfoils. However, this is only an approximation, because airfoils are designed to be aerodynamically efficient, inasmuch as the flow about them is usually undisturbed; this is not the case of bridge-deck-bluff bodies. Therefore, it is mandatory to accurately adjust airfoil theory to compensate for the differences between the behaviour of an airfoil and a bridge deck section.

As will be seen in the following, the equations of bridge aeroelastic and aerodynamic analysis have several coefficients which must be determined. In this chapter the analytic determination of this coefficients is addressed.

Theodorsen's theory

Theodorsen developed in his seminal paper of 1935 (Theodorsen (1935)) a theory used extensively in aircraft design, which is useful for estimating the aeroelastic forces acting on a flat plate of width $B = 2b$ moving in a fluid at velocity U (see Figure 4.1). Using potential flow theory,

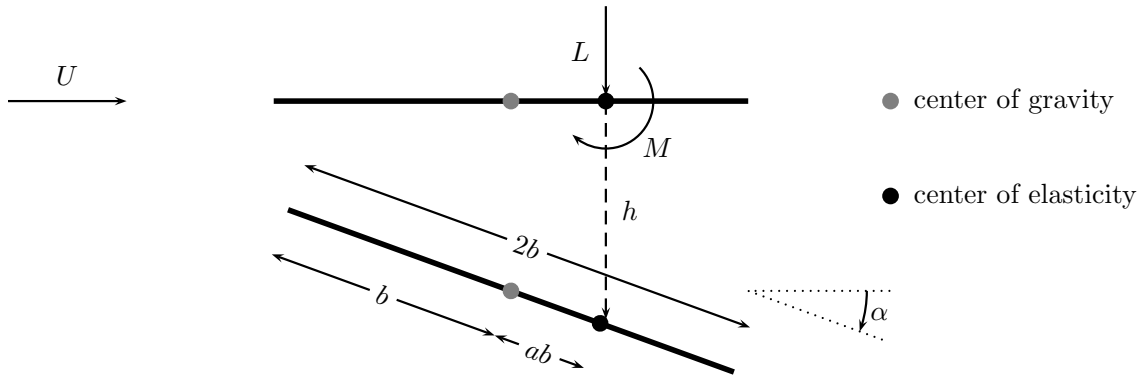

Figure 4.1: Scheme of Theodorsen's flat plate

Theodorsen stated that the aeroelastic (self-excited) forces, lift $L_{se}(t)$ and moment $M_{se}(t)$ acting over the flat plated per unit length can expressed by (Jurado and Hernández (2000)),

$$\begin{aligned} L_{se}(t) &= -\frac{1}{2}\rho U^2 B\left\{2\pi F\frac{\dot{h}(t)}{U}+\frac{\pi}{2}\left[1+\frac{4G}{K}+2\left(\frac{1}{2}-a\right)F\right]\frac{B}{U}\dot{\alpha}(t)+\right. \\ &\left.\pi\left[2F-\left(\frac{1}{2}-a\right)GF+\frac{K^2 a}{4}\right]\alpha(t)-\frac{\pi}{2}K^2\left[1+\frac{4G}{K}\right]\frac{h(t)}{B}\right\} \qquad (4.1) \\ M_{se}(t) &= \frac{1}{2}\rho U^2 B^2\left\{\pi F\left(\frac{1}{2}+a\right)\frac{\dot{h}(t)}{U}-\frac{\pi}{2}\left[\frac{1}{2}\left(\frac{1}{2}+a\right)-\left(\frac{1}{2}+a\right)\frac{2G}{K}+F\left(a^2-\frac{1}{4}\right)\right]\frac{B}{U}\dot{\alpha}(t)\right. \\ &+\frac{\pi}{2}\left[\frac{K^2}{4}\left(a^2+\frac{1}{8}\right)+2F\left(\frac{1}{2}+a\right)+GK\left(a^2-\frac{1}{4}\right)\right]\alpha(t)- \\ &\left.\frac{\pi}{2}\left[\frac{K^2 a}{2}+\left(\frac{1}{2}+a\right)2GK\right]\frac{h(t)}{B}\right\} \qquad (4.2) \end{aligned}$$

where, $K = B\omega/U$ is the *reduced frequency*, ω is the angular frequency of oscillation, a is $1/b$ times the distance which separates the mass center of inertia and the elastic center of the wing, U is the mean wind velocity of the flow, ρ is the air density ($\rho = 0.125$ Kg/m^3) and F and G are the real and imaginary terms respectively of the Theodorsen's circulation function $C(K) = F(K) + jG(K)$ (Jain et al. (1996)),

$$\begin{aligned} F &\equiv F(K) = \frac{J_1(K)\left(J_1(K)+Y_0(K)\right)+Y_1(K)\left(Y_1(K)-J_0(K)\right)}{\left(J_1(K)+Y_0(K)\right)^2+\left(Y_1(K)-Y_0(K)\right)^2} \\ G &\equiv G(K) = -\frac{Y_1(K)Y_0(K)+J_1(K)J_0(K)}{\left(J_1(K)+Y_0(K)\right)^2+\left(Y_1(K)-J_0(K)\right)^2} \qquad (4.3) \end{aligned}$$

where $J_0(K)$ and $J_1(K)$ are Bessel functions of the first kind and $Y_0(K)$ and $Y_1(K)$ are Bessel functions of the second kind. Both functions $F(K)$ and $G(K)$ and plotted in Figure 4.2.

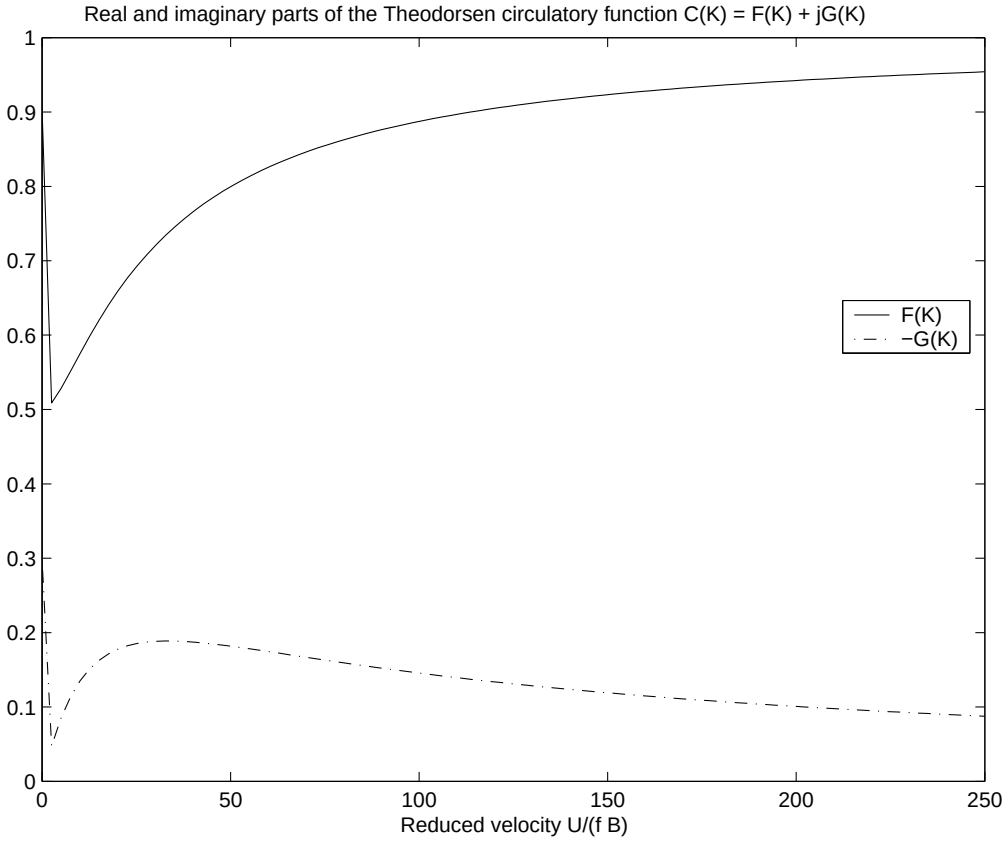

Figure 4.2: Real and Imaginary parts of the Theodorsen's circulatory function

As is currently recognized in bridge theory, identification of aeroelastic forces cannot be made using the analytical approach developed by Theodorsen, as bridge decks do not have an aerodynamic shape; instead wind tunnel test are performed to experimentally measure an appropriate description of the deck forces-movement interaction. Scanlan and Tomko (1971) developed a set of equations which define the aeroelastic forces in a similar way to that stated by equations (4.1) and (4.2),

$$L_{se}(t) = \frac{1}{2}\rho U^2 B \left(K H_1^*(K)\frac{\dot{h}(t)}{U} + K H_2^*(K)\frac{B\dot{\alpha}(t)}{U} + K^2 H_3^*(K)\alpha(t) + K^2 H_4^*(K)\frac{h(t)}{B} \right) \quad (4.4)$$

$$M_{se}(t) = \frac{1}{2}\rho U^2 B^2 \left(K A_1^*(K)\frac{\dot{h}(t)}{U} + K A_2^*(K)\frac{B\dot{\alpha}(t)}{U} + K^2 A_3^*(K)\alpha(t) + K^2 A_4^*(K)\frac{h(t)}{B} \right) \quad (4.5)$$

where the coefficients $H_i^*(K)$ and $A_i^*(K)$, $i = 1, \ldots, 4$ are functions dependent of the deck shape and of the frequency of oscillation of the deck popularly known as *flutter derivatives*, which must

be determined experimentally for a bridge deck section in a wind tunnel test by means of system identification techniques, as commented in Simiu and Scanlan (1996). The drag component (the component associated with lateral motion) is in practice usually neglected as it is not significant compared with lift or moment forces; however, when it is included (c.f. equations (5.8), (5.9) and (5.10)), the corresponding flutter derivatives can be estimated using quasi-steady theory, as follows (Chen et al. (2000)),

$$\begin{aligned}
P_1^*(K) &= -\frac{4}{K}C_D && (4.6)\\
P_2^*(K) &= -\frac{1}{K}\left(C_D' - C_L\right) && (4.7)\\
P_3^*(K) &= -\frac{4}{K^2}C_D' && (4.8)\\
P_4^*(K) &= 0 && (4.9)\\
P_5^*(K) &= \frac{2}{K}\left(C_D' - C_L\right) && (4.10)\\
P_6^*(K) &= 0 && (4.11)\\
H_5^*(K) &= \frac{4}{K}C_L && (4.12)\\
H_6^*(K) &= 0 && (4.13)\\
A_5^*(K) &= -\frac{8}{K}C_M && (4.14)\\
A_6^*(K) &= 0 && (4.15)
\end{aligned}$$

where C_L, C_D and C_M are respectively the static lift, drag and moment coefficients, and $C_D' = \frac{dC_D}{d\alpha}\Big|_{\alpha=0}$, as will be defined in Chapter 5 (c.f. page 33).

Relating equations (4.1) and (4.2) with (4.4) and (4.5) respectively, we can deduce that for a flat plate, the flutter derivatives H_i^* and A_i^*, $i = 1, \ldots, 4$ are expressed in terms of Theodorsen's circulation function as

$$\begin{aligned}
H_1^*(K) &= -\frac{2\pi}{K}F(K) && (4.16)\\
H_2^*(K) &= -\frac{\pi}{K}\left(\frac{1+F(K)}{2} + \frac{2G(K)}{K}\right) && (4.17)\\
H_3^*(K) &= -\frac{\pi}{K^2}\left(2F(K) - \frac{KG(K)}{2}\right) && (4.18)\\
H_4^*(K) &= \frac{\pi}{2}\left(1 + \frac{4G(K)}{K}\right) && (4.19)\\
A_1^*(K) &= \frac{\pi}{2K}F(K) && (4.20)
\end{aligned}$$

$$A_2^*(K) = \frac{\pi}{K}\left(\frac{F(K)-1}{8}+\frac{G(K)}{2K}\right) \tag{4.21}$$

$$A_3^*(K) = \frac{\pi}{K^2}\left(\frac{F(K)}{2}-\frac{KG(K)}{8}\right) \tag{4.22}$$

$$A_4^*(K) = -\frac{\pi}{2K}G(K) \tag{4.23}$$

assuming that $a = 0$ which is valid for most bridge deck sections because of symmetry. The corresponding airfoil flutter derivatives are plotted in Figures 4.3 and 4.4.

Finally, it must be said that Theodorsen theory is not valid for bridge deck sections because the deck shape has not an aerodynamic shape, and therefore they are not appropriate in actual design analysis, that is, only wind tunnel tests are suitable for determining an accurate bridge response (Jain et al. (1996); Jurado and Hernández (2000)).

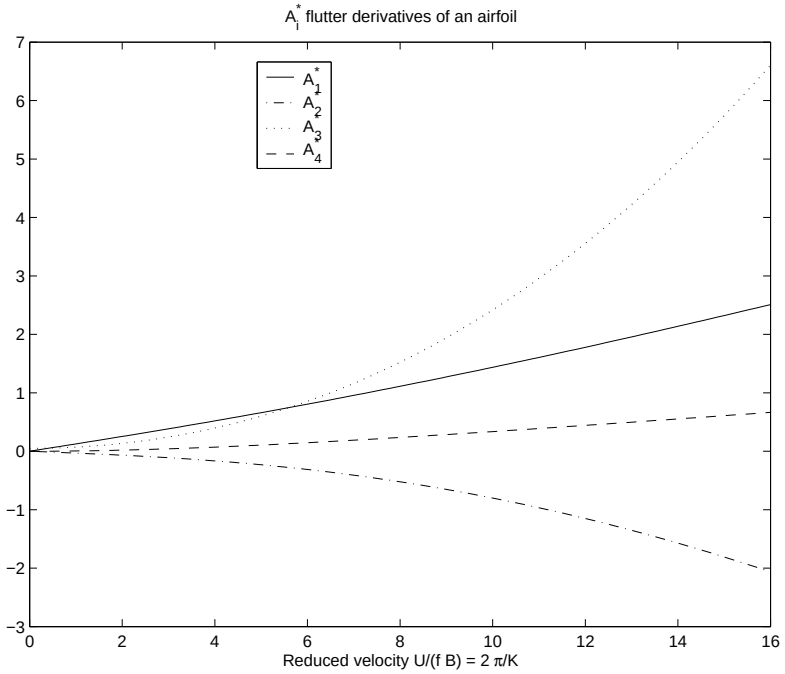

Figure 4.3: A_i^* flutter derivatives of an airfoil

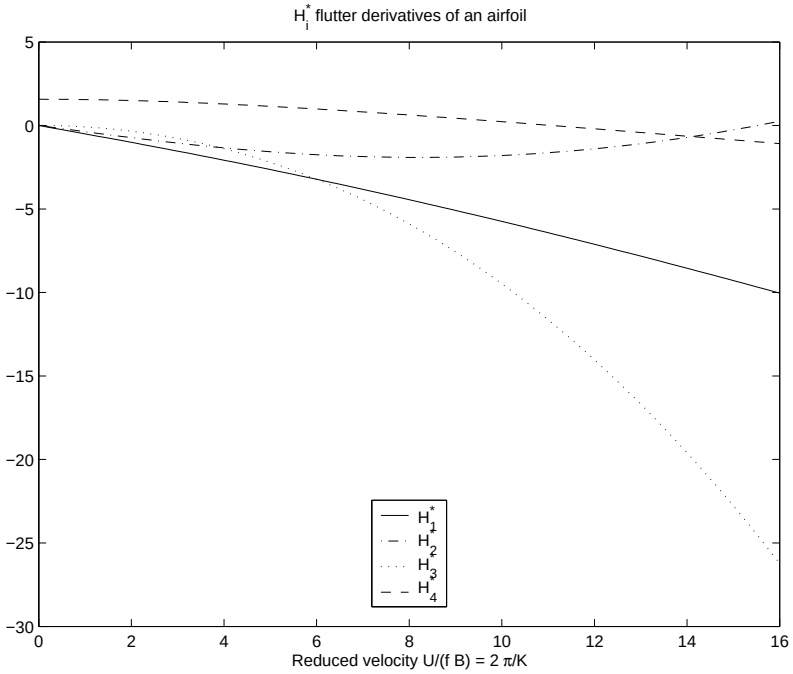

Figure 4.4: H_i^* flutter derivatives of an airfoil

Chapter 5

Self-excited response analysis

As will be seen in Chapter 8, wind turbulence may help to feed energy from the least stable vibration modes to the more stable ones, and in this way provide stabilization to the bridge. This is the main reason why coupled self-excited and buffeting response analysis is important in bridge design, as it allows the modelling of energy transfer between vibration modes. Another reason which motives the coupled response analysis is the well-known fact that low vibration frequencies of long-span bridges are crowded, and in this way, long-span bridges always vibrate in several modes at the same time.

There are many approaches to calculate the coupled self-excited and buffeting bridge response to wind forces. Jain et al. (1996) and Katsuchi et al. (1999) formulated a technique whose resulting equations of motion have frequency dependent parameters; thereby, its solution requires iterative methods for calculating the flutter speed; also the frequency dependence of their method restricts it to frequency domain solutions. Boonyapinyo et al. (1999) and Chen et al. (2000) independently proposed a state-space technique in which aerodynamic coupling among self-excited and buffeting responses of long-span bridges are considered; a state space approach like this is useful because it allows the use of tools based on the linear system theory for the analysis and control of a dynamic system. However, as the flutter derivatives are calculated only for some frequencies, approximations are necessary to define the aeroelastic mass, damping and stiffness matrices, therefore these approximations reduce the accuracy of flutter prediction, but the method is still very useful. In the following lines this method is succinctly summarized.

5.1 State-space equation of the compound bridge-wind mechanical system

A linear mechanic system (in this case a bridge) of n degrees-of-freedom can be expressed by the differential equation

$$\mathbf{m}\ddot{\mathbf{d}}(t) + \mathbf{c}\dot{\mathbf{d}}(t) + \mathbf{k}\mathbf{d}(t) = \mathbf{f}(t) \tag{5.1}$$

where $\mathbf{m}$, $\mathbf{c}$ and $\mathbf{k}$ are respectively the mass, viscous damping and stiffness matrices of the system, $\mathbf{d}(t)$ is the nodal displacement vector and $\mathbf{f}(t)$ is the external load vector.

Using a modal analysis approach, the dynamic response of the structure can be expressed in terms of natural modes of vibration $\mathbf{\Phi}(x, y, z)$ and generalized displacement coordinates $\mathbf{q}(t)$ as,

$$\mathbf{d}(x, y, z, t) \approx \sum_{i=1}^{r} \mathbf{\Phi}_i(x, y, z) q_i(t) \tag{5.2}$$

or as,

$$\mathbf{d}(x, y, z, t) \approx \mathbf{\Phi}(x, y, z)\mathbf{q}(t) \tag{5.3}$$

where r is the number of modes of vibration to take into account, $q_i(t)$ is the i-th component of $\mathbf{q}(t)$, $i = 1, \ldots, r$ and $\mathbf{\Phi} = [\mathbf{\Phi}_1, \mathbf{\Phi}_2, \ldots, \mathbf{\Phi}_r]$ is the modal shape matrix.

As the wind-induced forces per unit span acting on the bridge are defined as

$$\mathbf{f}(t) = \mathbf{f}_{se}(t) + \mathbf{f}_b(t) \tag{5.4}$$

where $\mathbf{f}_{se}(t)$ and $\mathbf{f}_b(t)$ are the self-excited (aeroelastic forces) and buffeting (aerodynamic forces) forces respectively, then the decoupled driving equation of motion of a bridge subjected to wind loads can be expressed as,

$$\mathbf{M}\ddot{\mathbf{q}}(t) + \mathbf{C}\dot{\mathbf{q}}(t) + \mathbf{K}\mathbf{q}(t) = \mathbf{Q}_{se}(t) + \mathbf{Q}_b(t) \tag{5.5}$$

or expressing it in state-space form as

$$\begin{bmatrix} \dot{\mathbf{q}}(t) \\ \ddot{\mathbf{q}}(t) \end{bmatrix} = \begin{bmatrix} \mathbf{0} & \mathbf{I} \\ -\mathbf{M}^{-1}\mathbf{K} & -\mathbf{M}^{-1}\mathbf{C} \end{bmatrix} \begin{bmatrix} \mathbf{q}(t) \\ \dot{\mathbf{q}}(t) \end{bmatrix} + \begin{bmatrix} \mathbf{0} \\ \mathbf{M}^{-1} \end{bmatrix} \mathbf{Q}_{se}(t) + \begin{bmatrix} \mathbf{0} \\ \mathbf{M}^{-1} \end{bmatrix} \mathbf{Q}_b(t) \tag{5.6}$$

where $\mathbf{M} = \mathbf{\Phi}^T\mathbf{m}\mathbf{\Phi}$, $\mathbf{C} = \mathbf{\Phi}^T\mathbf{c}\mathbf{\Phi}$, and $\mathbf{K} = \mathbf{\Phi}^T\mathbf{k}\mathbf{\Phi}$, are the mass-, damping- and stiffness-generalized matrices, each over dot means $\frac{d}{dt}$ ()), and

$$\begin{aligned} \mathbf{Q}_{se}(t) &= \mathbf{\Phi}^T\mathbf{f}_{se}(t) \\ \mathbf{Q}_b(t) &= \mathbf{\Phi}^T\mathbf{f}_b(t) \end{aligned} \tag{5.7}$$

are the generalized self-excited and buffeting forces respectively. It is a good place to remember that the essence of modal analysis is to determine the response of a n-degree-of-freedom system by approximating it into r independent single-degree-of-freedom systems, determining the response of each individual system and then combining the separate responses into the response of the original system.

The self-excited forces, lift, drag and moment, as depicted in Figure 5.1, per unit span are

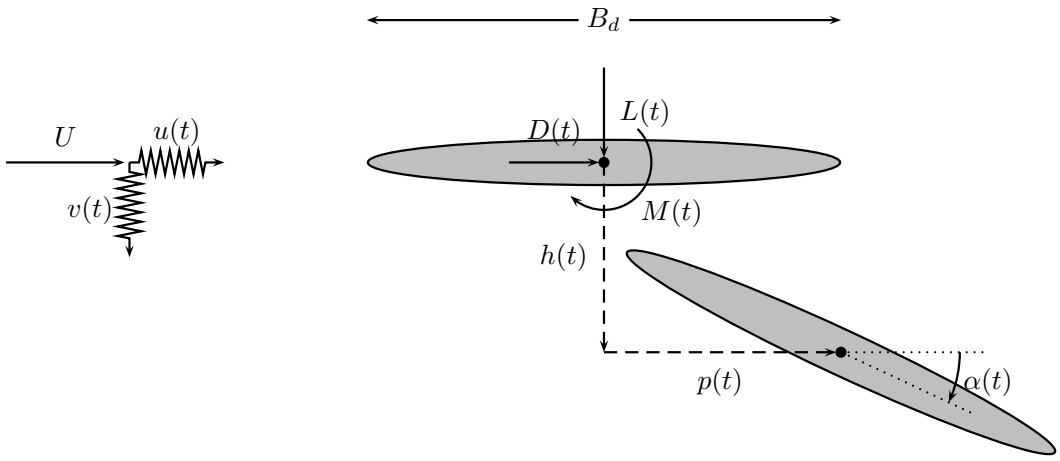

Figure 5.1: Aeroelastic forces on bridge deck section

commonly described as follows (Jain et al. (1996)):

$$\begin{aligned} L_{se}(t) &= \frac{1}{2}\rho U^2(t) B_d \left(K H_1^*(K)\frac{\dot{h}(t)}{\bar{U}} + K H_2^*(K)\frac{B_d\dot{\alpha}(t)}{\bar{U}} \right. \\ &\quad \left. + K^2 H_3^*(K)\alpha(t) + K^2 H_4^*(K)\frac{h(t)}{B_d} + K H_5^*(K)\frac{\dot{p}(t)}{\bar{U}} + K^2 H_6^*(K)\frac{p(t)}{B_d} \right) \end{aligned} \tag{5.8}$$

$$\begin{aligned} D_{se}(t) &= \frac{1}{2}\rho U^2(t) B_d \left(K P_1^*(K)\frac{\dot{p}(t)}{\bar{U}} + K P_2^*(K)\frac{B_d\dot{\alpha}(t)}{\bar{U}} \right. \\ &\quad \left. + K^2 P_3^*(K)\alpha(t) + K^2 P_4^*(K)\frac{p(t)}{B_d} + K P_5^*(K)\frac{\dot{h}(t)}{\bar{U}} + K^2 P_6^*(K)\frac{h(t)}{B_d} \right) \end{aligned} \tag{5.9}$$

$$M_{se}(t) = \frac{1}{2}\rho U^2(t) B_d^2 \left(K A_1^*(K) \frac{\dot{h}(t)}{\bar{U}} + K A_2^*(K) \frac{B_d \dot{\alpha}(t)}{\bar{U}} + K^2 A_3^*(K) \alpha(t) + K^2 A_4^*(K) \frac{h(t)}{B_d} + K A_5^*(K) \frac{\dot{p}(t)}{\bar{U}} + K^2 A_6^*(K) \frac{p(t)}{B_d} \right) \quad (5.10)$$

where ρ is the air density ($\rho = 0.125\text{kg/m}^3$), $\bar{U}$ is the average wind speed, $U(t)$ is the instantaneous wind speed, B_d is the bridge deck width, $K = \omega B_d/\bar{U}$ is the reduced frequency, ω is the circular frequency of oscillation, $p(t)$, $h(t)$ and $\alpha(t)$ are the drag, lift and torsional displacements and $H_i^*(K)$, $P_i^*(K)$ and $A_i^*(K)$, for $i = 1, \ldots, 6$ are the flutter derivatives, defined in chapter 4. Special attention must be given to the fact that expressions (5.8), (5.9) and (5.10) are supposed to be valid only for small rotations and displacements on steady flow, thus they are commonly used to define the beginning of the aeroelastic instability.

In this way the self-excited forces acting on a beam element of length $l^{(e)}$ can be expressed by

$$\mathbf{f}_{se}^{(e)}(t) = U^2(t) \mathbf{v}_d^{(e)} \left(\mathbf{a}_s^{(e)}(K) \mathbf{d}^{(e)}(t) + \frac{B_d}{\bar{U}} \mathbf{a}_d^{(e)}(K) \dot{\mathbf{d}}^{(e)}(t) \right) \quad (5.11)$$

where,

$$\mathbf{f}_{se}^{(e)}(t) = l^{(e)} \begin{bmatrix} L_{se}^{(e)}(t) \\ D_{se}^{(e)}(t) \\ M_{se}^{(e)}(t) \end{bmatrix}, \quad (5.12)$$

$$\mathbf{v}_d^{(e)} = \text{diag}\left(\frac{1}{2}\rho \begin{bmatrix} B_d & B_d & B_d^2 \end{bmatrix} \right), \quad (5.13)$$

$\mathbf{a}_s^{(e)}(K)$ is the element aerodynamic stiffness matrix,

$$\mathbf{a}_s^{(e)}(K) = l^{(e)} \mathbf{v}_d^{(e)} \begin{bmatrix} K^2 H_4^*(K) & K^2 H_6^*(K) & K^2 H_3^*(K) \\ K^2 P_6^*(K) & K^2 P_4^*(K) & K^2 P_3^*(K) \\ K^2 A_4^*(K) & K^2 A_6^*(K) & K^2 A_3^*(K) \end{bmatrix}, \quad (5.14)$$

$\mathbf{a}_d^{(e)}(K)$ is the element aerodynamic damping matrix,

$$\mathbf{a}_d^{(e)}(K) = l^{(e)} \mathbf{v}_d^{(e)} \begin{bmatrix} K H_1^*(K) & K H_5^*(K) & K H_2^*(K) \\ K P_5^*(K) & K P_1^*(K) & K P_2^*(K) \\ K A_1^*(K) & K A_5^*(K) & K A_2^*(K) \end{bmatrix} \quad (5.15)$$

$\mathbf{d}^{(e)}(t)$ is the element displacement vector,

$$\mathbf{d}^{(e)}(t) = \begin{bmatrix} h^{(e)}(t)/B_d \\ p^{(e)}(t)/B_d \\ \alpha^{(e)}(t) \end{bmatrix}, \quad (5.16)$$

and $h^{(e)}(t)$, $p^{(e)}(t)$ and $\alpha^{(e)}(t)$ are respectively the vertical, lateral and torsional displacement at the center of the deck beam element.

After assembling the contributions of all finite elements, the total self-excited forces can be expressed as

$$\mathbf{f}_{se}(t) = U^2(t)\left(\mathbf{a}_s(K)\mathbf{d}(t) + \frac{B_d}{\bar{U}}\mathbf{a}_d(K)\dot{\mathbf{d}}(t)\right) \tag{5.17}$$

and finally, replacing (5.7) and (5.3) into (5.17), we have

$$\mathbf{Q}_{se}(t) = U^2(t)\left(\mathbf{A}_s(K)\mathbf{q}(t) + \frac{B_d}{\bar{U}}\mathbf{A}_d(K)\dot{\mathbf{q}}(t)\right) \tag{5.18}$$

where $\mathbf{A}_s(K) = \mathbf{\Phi}^{\mathrm{T}}\mathbf{a}_s(K)\mathbf{\Phi}$ and $\mathbf{A}_d(K) = \mathbf{\Phi}^{\mathrm{T}}\mathbf{a}_d(K)\mathbf{\Phi}$.

On the other hand, the buffeting forces, lift, drag and moment, per unit span are given by

$$L_b(t) = \frac{1}{2}\rho\bar{U}^2 B_d\left(-2C_L\chi_{L_{bu}}(K)\frac{u(t)}{\bar{U}} + \left(C'_L + C_D\right)\chi_{L_{bw}}(K)\frac{w(t)}{\bar{U}}\right) \tag{5.19}$$

$$D_b(t) = \frac{1}{2}\rho\bar{U}^2 B_d\left(2C_D\chi_{D_{bu}}(K)\frac{u(t)}{\bar{U}} - C'_D\chi_{D_{bw}}(K)\frac{w(t)}{\bar{U}}\right) \tag{5.20}$$

$$M_b(t) = \frac{1}{2}\rho\bar{U}^2 B_d^2\left(2C_M\chi_{M_{bu}}(K)\frac{u(t)}{\bar{U}} - C'_M\chi_{M_{bw}}(K)\frac{w(t)}{\bar{U}}\right) \tag{5.21}$$

where C_L, C_D and C_M are the steady average lift, drag and moment force coefficients respectively, C'_L, C'_D and C'_M are its derivatives evaluated at $\alpha = 0$, $\chi_{L_u}(K)$, $\chi_{L_{bw}}(K)$, $\chi_{D_{bu}}(K)$ are the aerodynamic admittances and $u(t)$, $w(t)$ are the horizontal and vertical fluctuating wind speed components respectively. The *aerodynamic admittances* are frequency dependent correction terms of the quasi-steady buffeting force coefficients C_L, C_D and C_M which relate the wind speed fluctuation and the developed wind force per unit span inasmuch as these coefficients alone fail to hold when relatively quickly time-varying gust velocities are agitating the system; they typically depict a diminution with increasing frequency of the force level from that of the steady force. The aerodynamic admittances are dependent on the geometrical configuration of the deck and each of their absolute magnitude is referred as the aerodynamic admittance function. The buffeting forces are usually expressed using the quasi-steady theory setting $\chi(K) = 1$ because in this way calculations are usually conservative.

The buffeting forces acting on a deck beam element of length $l^{(e)}$ can be expressed as

$$\mathbf{f}_b^{(e)}(t) = \bar{U}^2\mathbf{v}_d^{(e)}\left(\mathbf{a}_{bu}^{(e)}\frac{u^{(e)}(t)}{\bar{U}} + \mathbf{a}_{bw}^{(e)}\frac{w^{(e)}(t)}{\bar{U}}\right) \tag{5.22}$$

where $u^{(e)}(t)$, $w^{(e)}(t)$ are the horizontal and vertical fluctuating wind speed components at the center of the deck beam element respectively, $\mathbf{f}_b^{(e)}(t)$ is the element buffeting force vector (also acting at the center of the element),

$$\mathbf{f}_b^{(e)}(t) = l^{(e)} \begin{bmatrix} L_b^{(e)}(t) \\ D_b^{(e)}(t) \\ M_b^{(e)}(t) \end{bmatrix}, \tag{5.23}$$

$$\mathbf{a}_{bu}^{(e)} = l^{(e)} \mathbf{v}_d^{(e)} \begin{bmatrix} -2C_L \chi_{L_{bu}}(K) \\ 2C_D \chi_{D_{bu}}(K) \\ 2C_M \chi_{M_{bu}}(K) \end{bmatrix} \tag{5.24}$$

and

$$\mathbf{a}_{bw}^{(e)} = l^{(e)} \mathbf{v}_d^{(e)} \begin{bmatrix} \left(C_L' + C_D\right) \chi_{L_{bu}}(K) \\ -C_D' \chi_{D_{bu}}(K) \\ -C_M' \chi_{M_{bu}}(K) \end{bmatrix} \tag{5.25}$$

After assemblage procedure of the finite element method, the total buffeting forces can be calculated by

$$\mathbf{f}_b(t) = \bar{U}^2 \left(\mathbf{a}_{bu} \frac{\mathbf{u}(t)}{\bar{U}} + \mathbf{a}_{bw} \frac{\mathbf{w}(t)}{\bar{U}} \right) \tag{5.26}$$

or as

$$\mathbf{Q}_b(t) = \bar{U}^2 \left(\mathbf{A}_{bu} \frac{\mathbf{u}(t)}{\bar{U}} + \mathbf{A}_{bw} \frac{\mathbf{w}(t)}{\bar{U}} \right) \tag{5.27}$$

where $\mathbf{A}_{bu} = \mathbf{\Phi}^{\mathrm{T}} \mathbf{a}_{bu}$, $\mathbf{A}_{bw} = \mathbf{\Phi}^{\mathrm{T}} \mathbf{a}_{bw}$.

As $\mathbf{A}_s(K)$ and $\mathbf{A}_d(K)$ are functions of the reduced frequency whilst $\mathbf{Q}_{se}(t)$ is function of time, it is better to express (5.17) as a frequency independent equation, avoiding so iterative solutions of (5.5) as those proposed in Simiu and Scanlan (1996), Jain et al. (1996) and Katsuchi et al. (1999).

Taking the Fourier transform of (5.11) we have (setting $\mathbf{f}_{se}^{(e)}(t_0) = \mathbf{0}$ and $\mathbf{d}^{(e)}(t_0) = \mathbf{0}$ at $t_0 = 0$)

$$\mathscr{F}\left\{\mathbf{f}_{se}^{(e)}(t)\right\} = U^2(t) \mathbf{v}_d^{(e)} \left(\mathbf{a}_s^{(e)} \left(\frac{\omega B_d}{\bar{U}} \right) + j \frac{\omega B_d}{\bar{U}} \mathbf{a}_d^{(e)} \left(\frac{\omega B_d}{\bar{U}} \right) \right) \mathscr{F}\left\{\mathbf{d}^{(e)}(t)\right\} \tag{5.28}$$

Since $\mathbf{f}_{se}^{(e)}(t)$ and $\mathbf{d}^{(e)}(t)$ are equal to zero for $t < 0$, the Fourier transform can be replaced by a Laplace transform making $s = j\omega, j^2 = -1$. So the above equation becomes

$$\mathscr{L}\left\{\mathbf{f}_{se}^{(e)}(t)\right\} = U^2(t) \mathbf{v}_d^{(e)} \left(\mathbf{a}_s^{(e)} \left(\frac{\omega B_d}{\bar{U}} \right) + \frac{s B_d}{\bar{U}} \mathbf{a}_d^{(e)} \left(\frac{\omega B_d}{\bar{U}} \right) \right) \mathscr{L}\left\{\mathbf{d}^{(e)}(t)\right\} \tag{5.29}$$

The matrix $\mathbf{a}_s^{(e)}\left(\frac{\omega B_d}{\bar{U}}\right)+\frac{sB_d}{\bar{U}}\mathbf{a}_d^{(e)}\left(\frac{\omega B_d}{\bar{U}}\right)$ can be either expressed in terms of *Roger's rational function approximation* (RFA) (Roger (1977)) as

$$\mathbf{a}_s^{(e)}\left(\frac{\omega B_d}{\bar{U}}\right)+\frac{sB_d}{\bar{U}}\mathbf{a}_d^{(e)}\left(\frac{\omega B_d}{\bar{U}}\right)\approx \mathbf{a}_1^{(e)}+\left(\frac{sB_d}{\bar{U}}\right)\mathbf{a}_2^{(e)}+\left(\frac{sB_d}{\bar{U}}\right)^2\mathbf{a}_3^{(e)}+\sum_{l=1}^{m}\frac{\mathbf{a}_{l+3}^{(e)}\frac{sB_d}{\bar{U}}}{\frac{sB_d}{\bar{U}}+d_l^{(e)}} \tag{5.30}$$

where $\mathbf{a}_i^{(e)}$, $i=1,\ldots,m+3$ are frequency-independent matrices, $d_l^{(e)}$, $l=1,\ldots,m$ are real positive coefficients (for the system expressed by (5.29) to be stable) and m is the order of the RFA, or the *minimum-state formula*, which was originally described by Karpel (1981) and refined by Tiffany and Adams (1988),

$$\mathbf{a}_s^{(e)}\left(\frac{\omega B_d}{\bar{U}}\right)+\frac{sB_d}{\bar{U}}\mathbf{a}_d^{(e)}\left(\frac{\omega B_d}{\bar{U}}\right)\approx \mathbf{a}_1^{(e)}+\left(\frac{sB_d}{\bar{U}}\right)\mathbf{a}_2^{(e)}+\left(\frac{sB_d}{\bar{U}}\right)^2\mathbf{a}_3^{(e)}+\mathbf{g}^{(e)}\left(\frac{sB_d}{\bar{U}}\mathbf{I}+\mathbf{R}^{(e)}\right)^{-1}\mathbf{e}^{(e)} \tag{5.31}$$

where $\mathbf{g}^{(e)}$ and $\mathbf{e}^{(e)}$ are fully populated matrices of appropriate dimensions and $\mathbf{R}^{(e)}$ is a diagonal matrix composed of m terms R_{ii} for $i=1,\ldots,m$ which must be positive to assure stability of the filter represented by (5.29).

The advantage of the minimum state method is that the number of aerodynamic states required can easily be a tenth of that required by Roger's RFA method for similar accuracy. The drawback is that its solution requires a nonlinear optimization. However, Roger's formula is more robust.

5.1.1 State-space equation using Roger's rational function approximation

Expression (5.30) can be rewritten as

$$\mathbf{a}_s^{(e)}(K)+(jK)\mathbf{a}_d^{(e)}(K)\approx \mathbf{a}_1^{(e)}+(jK)\mathbf{a}_2^{(e)}+(jK)^2\mathbf{a}_3^{(e)}+\sum_{l=1}^{m}\frac{jK\mathbf{a}_{l+3}^{(e)}}{jK+d_l^{(e)}} \tag{5.32}$$

where, $i=1,\ldots,m+3$, and

$$\mathbf{a}_s^{(e)}(K)+(jK)\mathbf{a}_d^{(e)}(K)=l^{(e)}K^2\begin{bmatrix} H_4^*(K)+jH_1^*(K) & H_6^*(K)+jH_5^*(K) & H_3^*(K)+jH_2^*(K)\\ P_6^*(K)+jP_5^*(K) & P_4^*(K)+jP_1^*(K) & P_3^*(K)+jP_2^*(K)\\ A_4^*(K)+jA_1^*(K) & A_6^*(K)+jA_5^*(K) & A_3^*(K)+jA_2^*(K)\end{bmatrix} \tag{5.33}$$

This approximation can be carried by means of optimization techniques in a least square sense, that is, making a regression of experimental data points we can find $\mathbf{a}_i^{(e)}, i=1,\ldots,m+3$.

Boonyapinyo et al. (1999) suggested to take m varying from 1 to 3, depending on the number of terms needed to adequately adjust the flutter derivatives.

Replacing (5.30) into (5.29) and taking inverse Laplace transform on both sides of (5.29) one obtains,

$$\mathbf{f}_{se}^{(e)}(t) = U^2(t)\mathbf{v}_d^{(e)}\left(\mathbf{a}_1^{(e)}\mathbf{d}^{(e)}(t) + \left(\frac{B_d}{\bar{U}}\right)\mathbf{a}_2^{(e)}\dot{\mathbf{d}}^{(e)}(t) + \left(\frac{B_d}{\bar{U}}\right)^2\mathbf{a}_3^{(e)}\ddot{\mathbf{d}}^{(e)}(t) + \sum_{l=1}^{m}\mathbf{d}_{se_l}^{(e)}(t)\right) \tag{5.34}$$

where,

$$\mathbf{d}_{se_l}^{(e)}(t) = \mathscr{L}^{-1}\left\{\frac{\mathbf{a}_{l+3}^{(e)}\frac{sB_d}{\bar{U}}}{\frac{sB_d}{\bar{U}} + d_l^{(e)}}\mathscr{L}\left\{\mathbf{d}^{(e)}(t)\right\}\right\}, \quad l = 1, \ldots, m \tag{5.35}$$

Taking Laplace transforms at both sides of (5.35), it follows

$$\mathscr{L}\left\{\mathbf{d}_{se_l}^{(e)}(t)\right\} = \frac{\mathbf{a}_{l+3}^{(e)}\frac{sB_d}{\bar{U}}}{\frac{sB_d}{\bar{U}} + d_l^{(e)}}\mathscr{L}\left\{\mathbf{d}^{(e)}(t)\right\}, \quad l = 1, \ldots, m \tag{5.36}$$

so that,

$$\dot{\mathbf{d}}_{se_l}^{(e)}(t) = \mathbf{a}_{l+3}^{(e)}\dot{\mathbf{d}}^{(e)}(t) - \mathbf{d}_{se_l}^{(e)}(t)\frac{\bar{U}}{B_d}d_l^{(e)}, \quad l = 1, \ldots, m \tag{5.37}$$

After assembling, one obtains,

$$\mathbf{Q}_{se}(t) = U^2(t)\left(\mathbf{A}_1\mathbf{q}(t) + \left(\frac{B_d}{\bar{U}}\right)\mathbf{A}_2\dot{\mathbf{q}}(t) + \left(\frac{B_d}{\bar{U}}\right)^2\mathbf{A}_3\ddot{\mathbf{q}}(t) + \sum_{l=1}^{m}\mathbf{q}_{se_l}(t)\right) \tag{5.38}$$

and

$$\dot{\mathbf{q}}_{se_l}(t) = \mathbf{A}_{l+3}\dot{\mathbf{q}}(t) - \mathbf{q}_{se_l}(t)\frac{\bar{U}}{B_d}d_l, \quad l = 1, \ldots, m \tag{5.39}$$

Substituting (5.38) and (5.39) into (5.6), yields

$$\dot{\mathbf{y}}(t) = \mathbf{A}(t)\mathbf{y}(t) + \mathbf{B}(t)\mathbf{Q}_b(t) \tag{5.40}$$

where,

$$\mathbf{y}(t) = \begin{bmatrix} \mathbf{q}(t) \\ \dot{\mathbf{q}}(t) \\ \mathbf{q}_{se1}(t) \\ \vdots \\ \mathbf{q}_{sem}(t) \end{bmatrix}, \tag{5.41}$$

$$\mathbf{A}(t) = \begin{bmatrix} \mathbf{0} & \mathbf{I} & \mathbf{0} & \cdots & \mathbf{0} \\ -\bar{\mathbf{M}}^{-1}\bar{\mathbf{K}} & -\bar{\mathbf{M}}^{-1}\bar{\mathbf{C}} & U^2(t)\bar{\mathbf{M}}^{-1} & \cdots & U^2(t)\bar{\mathbf{M}}^{-1} \\ \mathbf{0} & \mathbf{A}_4 & -\frac{\bar{U}}{B_d}d_1\mathbf{I} & \cdots & \mathbf{0} \\ \vdots & \vdots & \vdots & \ddots & \vdots \\ \mathbf{0} & \mathbf{A}_{3+m} & \mathbf{0} & \cdots & -\frac{\bar{U}}{B_d}d_m\mathbf{I} \end{bmatrix}, \tag{5.42}$$

$$\mathbf{B}(t) = \begin{bmatrix} \mathbf{0} \\ \bar{\mathbf{M}}^{-1} \\ \mathbf{0} \\ \vdots \\ \mathbf{0} \end{bmatrix} \tag{5.43}$$

and

$$\bar{\mathbf{M}}(t) = \mathbf{M} - U^2(t)\frac{B_d^2}{\bar{U}^2}\mathbf{A}_3, \quad \bar{\mathbf{C}}(t) = \mathbf{C} - U^2(t)\frac{B_d}{\bar{U}}\mathbf{A}_2, \quad \bar{\mathbf{K}}(t) = \mathbf{K} - U^2(t)\mathbf{A}_1 \tag{5.44}$$

Observe that equation (5.40) combines the effect of coupled buffeting and self-excited vibrations on a single equation.

It is a good point to annotate that the added aerodynamic mass matrix $U^2(t)\frac{B_d^2}{\bar{U}^2}\mathbf{A}_3$ is usually neglected in bridge studies, however its use is very important in aircraft design (Wilde and Fujino (1998)).

5.1.2 State-space equation using Karpel's minimum-state formula for a single element

Formula (5.31) can be reexpressed as

$$\mathbf{a}_s^{(e)}(K) + (jK)\mathbf{a}_d^{(e)}(K) \approx \mathbf{a}_1^{(e)} + (jK)\mathbf{a}_2^{(e)} + (jK)^2\mathbf{a}_3^{(e)} + \mathbf{g}^{(e)}\left((jK)\mathbf{I} + \mathbf{R}^{(e)}\right)^{-1}\mathbf{e}^{(e)} \tag{5.45}$$

with $\mathbf{a}_s^{(e)}(K) + (jK)\mathbf{a}_d^{(e)}(K)$ given by (5.33).

The above approximation can carried out using a nonlinear least square fitting of the experimental data points. The approximation can be improved by increasing m until (5.45) makes an adequate fit of (5.33).

Substituting (5.31) into (5.29) and taking inverse Laplace transform on both sides of (5.29) it follows that,

$$\mathbf{f}_{se}^{(e)}(t) = U^2(t)\mathbf{v}_d^{(e)}\left(\mathbf{a}_1^{(e)}\mathbf{d}^{(e)}(t) + \left(\frac{B_d}{\bar{U}}\right)\mathbf{a}_2^{(e)}\dot{\mathbf{d}}^{(e)}(t) + \left(\frac{B_d}{\bar{U}}\right)^2\mathbf{a}_3^{(e)}\ddot{\mathbf{d}}^{(e)}(t) + \mathbf{g}^{(e)}\mathbf{x}_a^{(e)}(t)\right) \tag{5.46}$$

where $\mathbf{x}_a^{(e)}(t)$ is known as the vector of aerodynamic states of the element,

$$\mathbf{x}_a^{(e)}(t) = \mathscr{L}^{-1}\left\{\left(\frac{sB_d}{\bar{U}}\mathbf{I} + \mathbf{R}^{(e)}\right)^{-1}\mathbf{e}^{(e)}\mathscr{L}\left\{\mathbf{d}^{(e)}(t)\right\}\right\} \tag{5.47}$$

Taking Laplace transforms at both sides of (5.47), one obtains

$$\left(\frac{sB_d}{\bar{U}}\mathbf{I} + \mathbf{R}^{(e)}\right)\mathscr{L}\left\{\mathbf{x}_a^{(e)}(t)\right\} = \mathbf{e}^{(e)}\mathscr{L}\left\{\mathbf{d}^{(e)}(t)\right\} \tag{5.48}$$

in order that,

$$\dot{\mathbf{x}}_a^{(e)}(t) = \frac{\bar{U}}{B_d}\mathbf{e}^{(e)}\mathbf{d}^{(e)}(t) - \frac{\bar{U}}{B_d}\mathbf{R}^{(e)}\mathbf{x}_a^{(e)}(t) \tag{5.49}$$

Replacing (5.46) and (5.49) into (5.6), yields the state-space representation (5.40) where,

$$\mathbf{y}(t) = \begin{bmatrix} \mathbf{d}^{(e)}(t) \\ \dot{\mathbf{d}}^{(e)}(t) \\ \mathbf{x}_a^{(e)}(t) \end{bmatrix}, \tag{5.50}$$

$$\mathbf{A}(t) = \begin{bmatrix} \mathbf{0} & \mathbf{I} & \mathbf{0} \\ -\bar{\mathbf{m}}^{(e)-1}\bar{\mathbf{k}}^{(e)} & -\bar{\mathbf{m}}^{(e)-1}\bar{\mathbf{c}}^{(e)} & U^2(t)\bar{\mathbf{m}}^{(e)-1}\mathbf{v}_d^{(e)}\mathbf{g}^{(e)} \\ \frac{\bar{U}}{B_d}\mathbf{e}^{(e)} & \mathbf{0} & -\frac{\bar{U}}{B_d}\mathbf{R}^{(e)} \end{bmatrix} \tag{5.51}$$

,

$$\mathbf{B}(t) = \begin{bmatrix} \mathbf{0} \\ \bar{\mathbf{m}}^{(e)-1} \\ \mathbf{0} \end{bmatrix} \tag{5.52}$$

and

$$\bar{\mathbf{m}}^{(e)}(t) = \mathbf{m}^{(e)} - U^2(t)\frac{B_d^2}{\bar{U}^2}\mathbf{v}_d^{(e)}\mathbf{a}_3^{(e)}, \quad \bar{\mathbf{c}}^{(e)}(t) = \mathbf{c}^{(e)} - U^2(t)\frac{B_d}{\bar{U}}\mathbf{v}_d^{(e)}\mathbf{a}_2^{(e)}, \quad \bar{\mathbf{k}}^{(e)}(t) = \mathbf{k}^{(e)} - U^2(t)\mathbf{v}_d^{(e)}\mathbf{a}_1^{(e)} \tag{5.53}$$

Finally, it must be said that the number of terms used in the approximations of both, minimum-state and Roger's RFA be set and have to be chosen carefully to ensure accurate results; it is a trade off between accuracy and size of the representation. As can be seen from equations (5.42) and (5.51), the system is linear time invariant for a fixed mean wind velocity, that is for $U(t) = \bar{U}$.

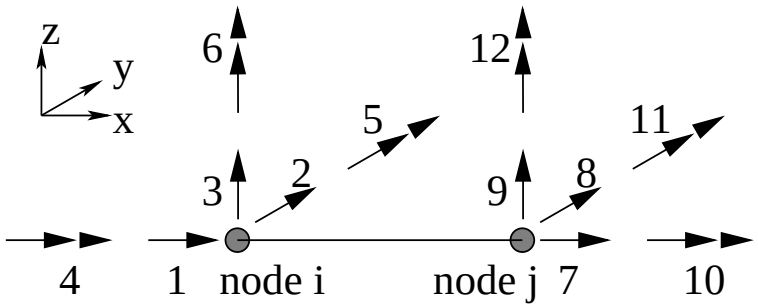

Figure 5.2: Degrees of freedom of a finite element

5.1.3 Assemblage procedure of the wind-induced forces

As a part of a finite element model, these distributed forces are converted into nodal forces by means of a lumping procedure whereby one-half of the uniform load over the element is supposed to act at each element end. Each finite element has 12 degrees of freedom, 6 at each node (3 translations and 3 rotations) as can be seen in Figure 5.2. In this way, the wind-induced force components $\mathbf{f}(t)$, drag, lift and moment, act respectively at the degrees of freedom 2, 3, 4, 8, 9 and 10.

5.2 Calculation of critical wind velocity under steady winds

Turbulent winds induce buffeting forces. Therefore, in this section, we will neglect the second term of the right hand side of equation (5.40), and will set $U(t)$ to $\bar{U}$, so we will be considering only aeroelastic forces, that is, (5.40) reduces to:

$$\dot{\mathbf{y}}(t) = \mathbf{A}\mathbf{y}(t) \tag{5.54}$$

It is well-known in linear system theory that when all of the eigenvalues $\lambda_i = \lambda_{Ri} + j\lambda_{Ii}$ of matrix $\mathbf{A}$ (called *poles*) have negative real part, the system is stable, but, when at least one of them has a real part greater or equal than zero, the system becomes unstable; in this case, the alluded stability is BIBO (Szidarovszky and Bahill (1998)). Imagine a spring-mass-damper mechanical

system subjected to a external force $f(t)$,

$$m\ddot{x}(t) + c\dot{x}(t) + kx(t) = f(t) \tag{5.55}$$

with initial conditions $\dot{x}(t_0) = 0$, and $x(t_0) = 0$ for $t_0 = 0$. The transfer function of this system is given by,

$$H(s) = \frac{1}{ms^2 + cs + k} \tag{5.56}$$

Let

$$\xi = \frac{c}{2\sqrt{km}} \tag{5.57}$$

be the viscous damping factor and let

$$\omega_n = \sqrt{\frac{k}{m}} \tag{5.58}$$

be the natural frequency of oscillation of the system, in order that the transfer function becomes,

$$H(s) = \frac{\omega_n^2}{m\left(s^2 + 2\xi\omega_n s + \omega_n^2\right)} \tag{5.59}$$

Since $k > 0$, the poles of this system are given by,

$$s_{1,2} = -\xi\omega_n \mp j\omega_n\sqrt{1 - \xi^2} \tag{5.60}$$

Relating equation (5.40) with the equation that describes the wind-bridge mechanical system, the poles of matrix $\mathbf{A}$ in (5.54) can be seen as the poles of the new mechanical system. That means that the real part of the eigenvalues of $\mathbf{A}$, λ_{Ri} can be associated to $-\xi_i\omega_{ni}$ in (5.60) because of uncoupled modes. As ω_n is always positive, if the real part of λ_{Ri} becomes greater than zero with an increasing wind speed, it means that ξ_i, the viscous damping of the wind-bridge system becomes negative. In this way, the beginning of the instability is occurs when net damping of the wind-bridge system becomes a zero, for a wind speed known as the *critical wind velocity* U_{cr}. Then, if a pair of eigenvalues of $\mathbf{A}$ becomes purely imaginary, the bridge will fail in an exponentially-increasing oscillation movement, the aforementioned *flutter*. As the viscous damping at the flutter velocity is zero, the flutter frequency can be easily found from the imaginary part of the eigenvalue (making $\xi = 0$ in equation (5.60)). In contrast, if the imaginary part of one eigenvalue becomes zero, the bridge becomes unstable, failing with a non-oscillating diverging movement. In this case, the bridge is said to fail by *divergence* (Bucher and Lin (1988)).

5.3 Application of the method in a two-degree-of-freedom deck section model

To illustrate the application of the method a two-degree-of-freedom bridge section was chosen with vertical and torsional degrees of freedom considered here as an example. The working model corresponds to a 1:150 scaled version of one the preliminary models of the Akashi-Kaikyo Bridge (Fujino et al. (1992)). Figure 5.3 shows one of those proposed models. The bridge parameters are summarized in Table 5.1, and the flutter derivatives are assumed to be modelled by Theodorsen's theory.

Figure 5.3: Model of the Akashi-Kaikyo suspension bridge (source Simiu and Scanlan (1996))

Table 5.1: Structural and geometric parameters of the working model (per unit length)

Parameter	**Value**
Deck width (B_d)	0.292 m
Frequency of heaving mode (ω_h)	7.879 rad/s
Frequency of pitching mode (ω_α)	25.057 rad/s
Damping of heaving mode (ξ_h)	0.111 %
Damping of pitching mode (ξ_α)	0.095 %
Mass of heaving mode (m_h)	0.191 Kg
Mass moment of inertia of pitching mode (I_α)	1.935×10^{-03} Kg m^2

For the aforementioned bridge, the equation of motion in frequency domain is given by,

$$\left(s^2\begin{bmatrix} mB_d & 0 \\ 0 & I_\alpha \end{bmatrix} + s\begin{bmatrix} c_hB_d & 0 \\ 0 & c_\alpha \end{bmatrix} + \begin{bmatrix} k_hB_d & 0 \\ 0 & k_\alpha \end{bmatrix}\right)\mathscr{L}\left\{\begin{bmatrix} h(t)/B_d \\ \alpha(t) \end{bmatrix}\right\} = \mathscr{L}\left\{\mathbf{f}_{se}(t)\right\} \quad (5.61)$$

where m is the deck mass per unit length, I_α is the mass moment of inertia, c_h, c_α, k_h, k_α symbolizes the damping and stiffness coefficients of the vertical and torsional degrees of freedom respectively, $\mathbf{f}_{se}(t)$ is the vector of self-excited forces, expressed by,

$$\mathscr{L}\left\{\mathbf{f}_{se}(t)\right\} = U^2(t)\mathbf{V}_d\mathbf{Q}_d\mathscr{L}\left\{\begin{bmatrix} h(t)/B_d \\ \alpha(t) \end{bmatrix}\right\} \quad (5.62)$$

where,

$$\mathbf{V}_d = \begin{bmatrix} -\frac{1}{2}\rho B_d & 0 \\ 0 & \frac{1}{2}\rho B_d^2 \end{bmatrix} \quad (5.63)$$

and

$$\mathbf{Q}_d \equiv \mathbf{Q}_d(K) = \begin{bmatrix} K^2\left(H_4^*(K) + jH_1^*(K)\right) & K^2\left(H_3^*(K) + jH_2^*(K)\right) \\ K^2\left(A_4^*(K) + jA_1^*(K)\right) & K^2\left(A_3^*(K) + jA_2^*(K)\right) \end{bmatrix} \quad (5.64)$$

As the flutter derivatives were calculated using Theodorsen's theory, the above equation was expanded in Karpel's minimum state representation as

$$\hat{\mathbf{Q}}_d(K) = \mathbf{a}_1 + (jK)\mathbf{a}_2 + \mathbf{g}\left((jK)\mathbf{I} + \mathbf{R}\right)^{-1}\mathbf{e} \quad (5.65)$$

Calculation of matrices $\mathbf{a}_1$, $\mathbf{a}_2$, $\mathbf{g}$, $\mathbf{R}$ and $\mathbf{e}$ was as will be explained below. Matrices $\mathbf{Q}_d(K)$, $K \in \mathcal{K}$, for $\mathcal{K} = \{0.1 : 0.01 : 0.2,\ 0.3 : 0.1 : 1.0,\ 5.0\}$ were calculated; as can be seen $\mathcal{K}$ covers the range in which fits were required. Then, beginning from initial random matrices $\mathbf{a}_{10}$, $\mathbf{a}_{20}$, $\mathbf{g}_0$, $\mathbf{R}_0$ and $\mathbf{e}_0$, a nonlinear regression was made, to fit (5.65) to (5.64) in the set $\mathcal{K}$ solving the following optimization problem:

$$\begin{aligned} &\min_{\mathbf{a}_1,\mathbf{a}_2,\mathbf{g},\mathbf{R},\mathbf{e}} \sum_{K\in\mathcal{K}} \left\|\mathbf{Q}_d(K) - \left(\mathbf{a}_1 + (jK)\mathbf{a}_2 + \mathbf{g}\left((jK)\mathbf{I} + \mathbf{R}\right)^{-1}\mathbf{e}\right)\right\|^2 \\ &\text{subject to } \inf\mathcal{K} \le R_{ii} \le \sup\mathcal{K}, \text{ for } i = 1, \ldots, m \end{aligned} \quad (5.66)$$

where, the operator $\|\cdot\|$ stands for $\|\mathbf{A}\| = \sum_{i=1}^{p}\sum_{j=1}^{q}|a_{ij}|, \mathbf{A} \in \mathcal{R}^{p\times q}$

Approximations using 1, 2, 3, 5 and 10 lag terms were calculated. It was noted that using only a lag term, the fit was not good at some points, while it was seen that using two lag terms the approximation error was only slightly inferior that employing a higher degree in the rational

function approximation, that is, using 3, 5 and 10 terms; hence two lag terms in this example were employed. Also, the regression was made with an additional matrix $\mathbf{a}_3$; it was observed that it has an insignificant effect on the improvement of the rational function approximation in low frequencies, inasmuch as the term $(jK)^2$ in (5.45) becomes negligible for a small K, which is the general case in bridge analysis.

Figures 5.4 and 5.5 show the flutter derivatives approximation made by equation (5.65); aeroelastic data for the set $\mathcal{K}$ were denoted by the different symbols ($\times$, $+$, $\circ$, $*$), while the approximation using two lag terms was symbolized by a solid line. As can be seen, Karpel's minimum state representation fits very well the data set generated from Theodorsen's theory. The following matrices were obtained:

$$\begin{gathered}\mathbf{a}_1 = \begin{bmatrix} 1.3040330 & 3.5334140 \\ 0.3354198 & 0.8738144 \end{bmatrix}; \mathbf{a}_2 = \begin{bmatrix} 3.3842200 & 2.3575520 \\ 0.7988867 & -0.1875175 \end{bmatrix}; \\ \mathbf{g} = \begin{bmatrix} 3.4690530 & 3.2669750 \\ 0.8526074 & 0.8640608 \end{bmatrix}; \mathbf{R} = \begin{bmatrix} 0.1911883 & 0 \\ 0 & 0.7477236 \end{bmatrix}; \\ \mathbf{e} = \begin{bmatrix} -0.01446793 & 0.07817446 \\ -0.23044170 & 0.25954960 \end{bmatrix}\end{gathered} \tag{5.67}$$

The *deterministic* stability of the model was checked by means of a complex eigenvalue analysis. Figure A.1 shows how the position of the poles of the system (5.61), the damping and the oscillation frequency of the different modes of vibration of the bridge change with an increasing mean wind speed. It can be seen that the system is stable in the mean wind velocity interval $\bar{U} = [0, 10.4)\,\mathrm{m/s}$, becoming marginally stable at the critical velocity, $\bar{U}_{cr} = 10.4\mathrm{m/s}$, which corresponds to the flutter onset, as the pitching mode damping becomes negative. From this point, for a increasing wind speed, there exists at least one eigenvalue with positive real part, meaning that the system is unstable. Figure 7.5 shows the fluttering phenomenon in the analyzed bridge, for a wind speed of 12 m/s. On the other hand, it can be noted that the heaving and pitching frequencies tend to keep constant for low mean wind speeds, and for high wind speeds they tend to gather, nevertheless, these frequencies maintain separate until failure.

It is also interesting to note that with an increasing deck width, the critical speed decreases for a given section, as can be seen from Figure 5.6. This figure was calculated using the same parameters of the deck section specified above but girder width, which varies. However, it must

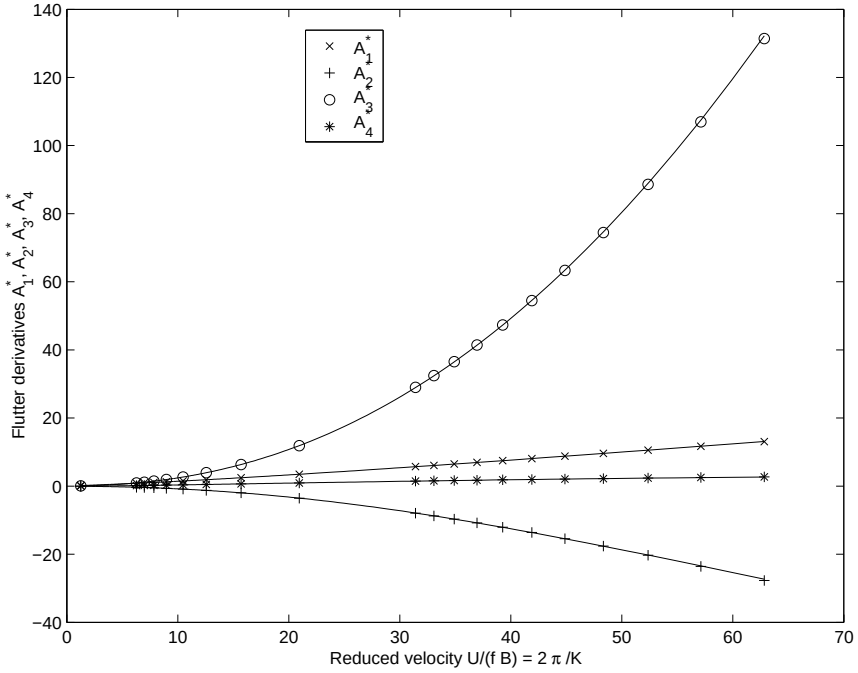

Figure 5.4: Approximation of the flutter derivatives A_i^* made by Karpel's minimum state formula

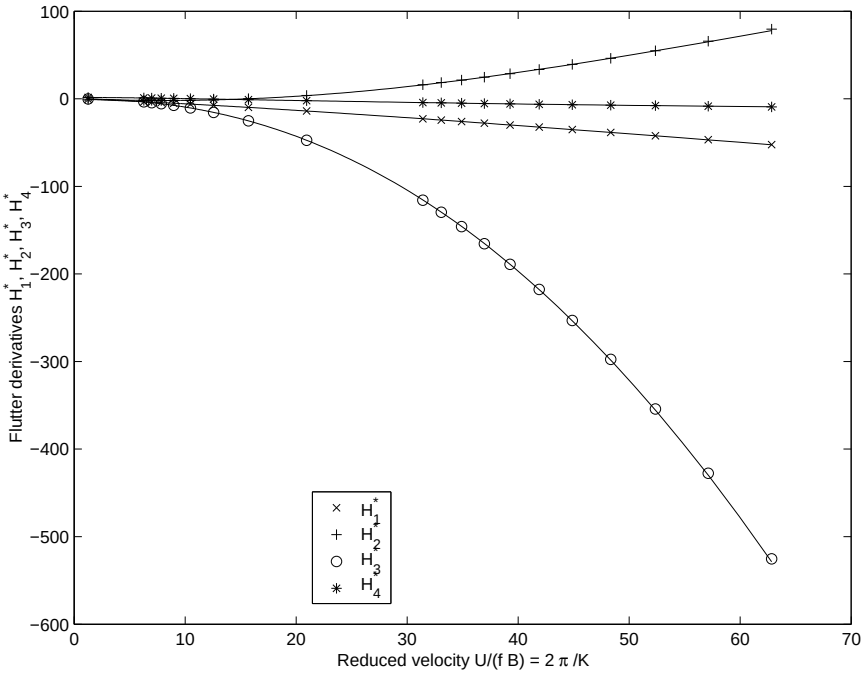

Figure 5.5: Approximation of the flutter derivatives H_i^* made by Karpel's minimum state formula

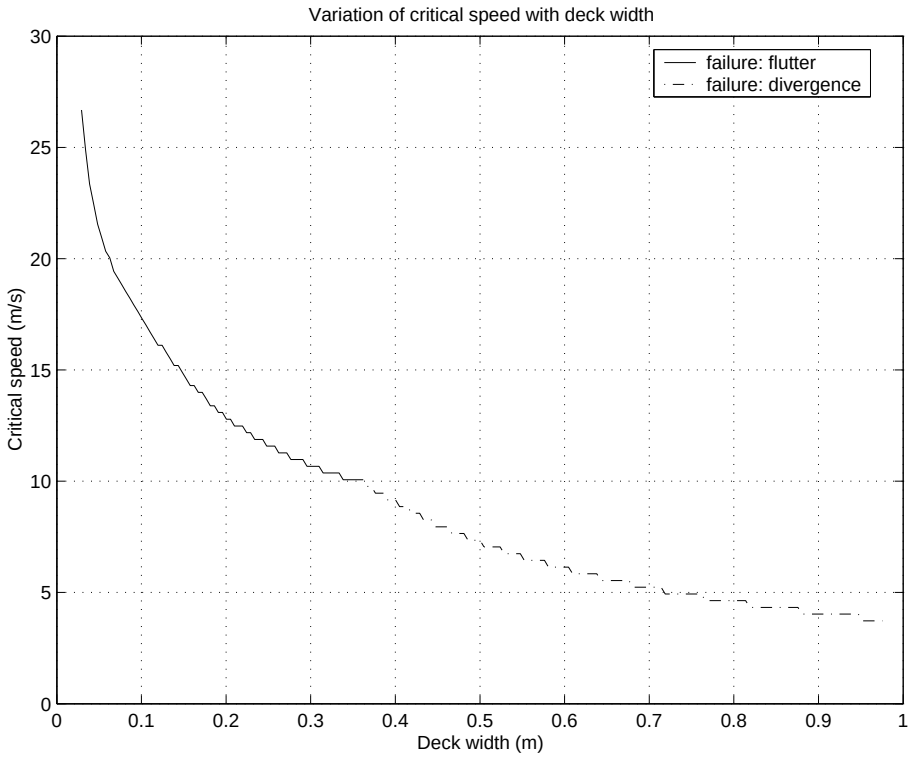

Figure 5.6: Variation of the flutter speed with an increasing deck width

be taken into account that the characteristics parameters of the section like mass, stiffness and damping could also change with deck width; anyway this figure gives some insights of why a twin box deck section can withstand higher wind speeds than a single box section (Richardson (1981)), in view of the fact that the critical speed of a narrow deck section is higher than the one of a wider girder. Also, Figure 5.6 stresses the fact that wider decks are proner to fail by divergence than narrow deck sections.

Chapter 6

State-space model of a bridge with control surfaces

6.1 Antecedents

As commented in section 1.1, there are essentially two main approaches of using control surfaces: contiguous control surfaces located next to the edges of the girder and separated control surfaces positioned below or above the edges of the girder. The latter of these approaches will be the subject of the present chapter. In the following lines an extension of the work of Wilde and Fujino (1998) will be carried out.

6.2 State-space representation of a section deck model of a bridge with control surfaces

Figure 6.1 shows a bridge deck (d) section with two separated control surfaces below the leading and trailing edges of the girder (referred afterwards as wing 1 (w_1) and wing 2 (w_2) respectively), and located at distances e_1 and e_2 from the elastic center of the deck; the coordinate system has its origin at the center of gravity of the bridge deck, as shown in Figure 6.1; the positive

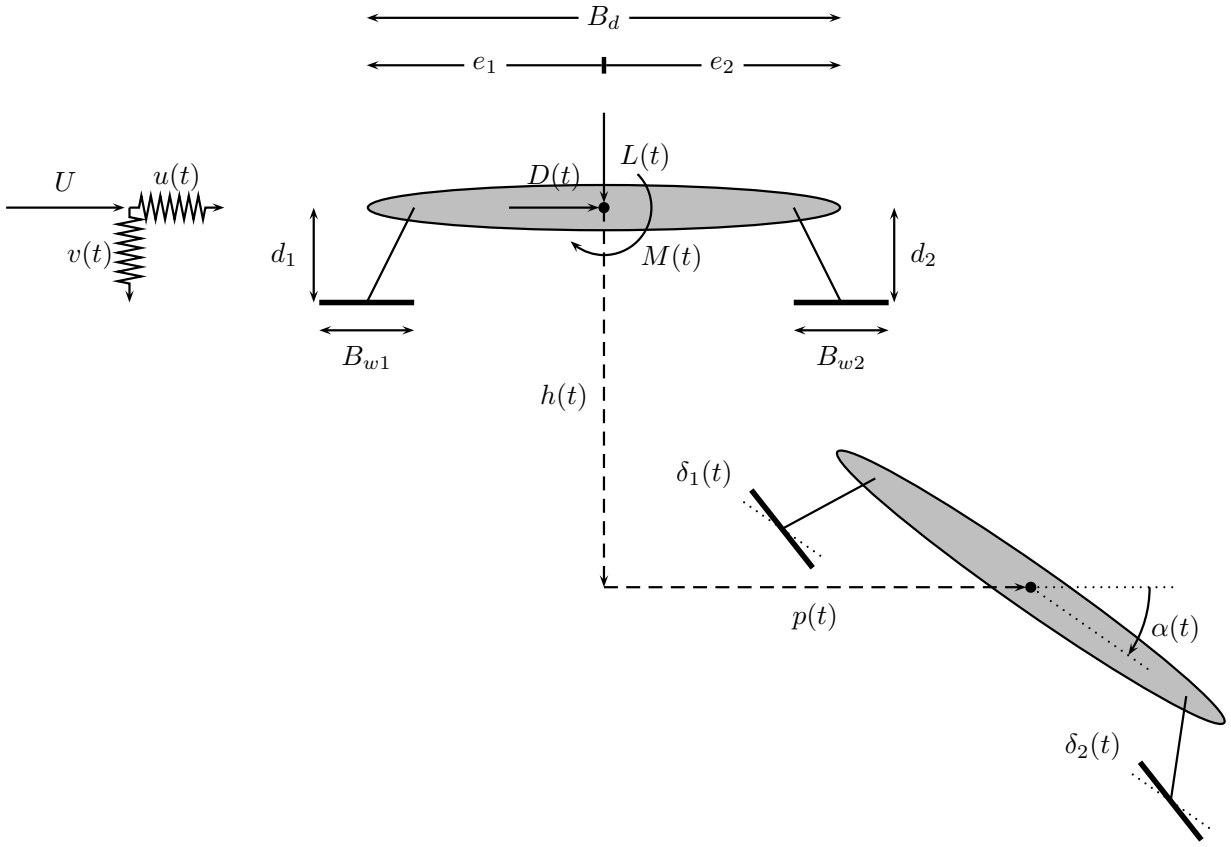

Figure 6.1: Cross section of bridge deck with control surfaces

movements are, downward, windward and clockwise for the vertical, horizontal and torsional movements respectively.

The motion of *an element* of the bride-wind-control surfaces (BWCS) system can be modelled as

$$\mathbf{M}\ddot{\mathbf{q}}(t) + \mathbf{C}\dot{\mathbf{q}}(t) + \mathbf{K}\mathbf{q}(t) = \mathbf{Q}(t) \tag{6.1}$$

where the vector of forces acting on the section is represented by

$$\mathbf{Q}(t) = \mathbf{T}_d^{lg}\mathbf{Q}_{sed}(t) + \mathbf{T}_{w_1}^{lg}\mathbf{Q}_{sew_1}(t) + \mathbf{T}_{w_2}^{lg}\mathbf{Q}_{sew_2}(t) + \mathbf{T}_d^{lg}\mathbf{Q}_{bd}(t) + \mathbf{T}_{w_1}^{lg}\mathbf{Q}_{bw_1}(t) + \mathbf{T}_{w_2}^{lg}\mathbf{Q}_{bw_2}(t) + \mathbf{T}_u^{lg}\mathbf{u}(t) \tag{6.2}$$

Equation (6.1) can also be rewritten in a state-space fashion, yielding,

$$\begin{bmatrix} \dot{\mathbf{q}}(t) \\ \ddot{\mathbf{q}}(t) \end{bmatrix} = \begin{bmatrix} \mathbf{0} & \mathbf{I} \\ -\mathbf{M}^{-1}\mathbf{K} & -\mathbf{M}^{-1}\mathbf{C} \end{bmatrix} \begin{bmatrix} \mathbf{q}(t) \\ \dot{\mathbf{q}}(t) \end{bmatrix} + \begin{bmatrix} \mathbf{0} \\ \mathbf{M}^{-1} \end{bmatrix} \begin{bmatrix} \mathbf{T}_d^{lg} & \mathbf{T}_{w1}^{lg} & \mathbf{T}_{w2}^{lg} \end{bmatrix} \begin{bmatrix} \mathbf{Q}_{sed}(t) \\ \mathbf{Q}_{sew1}(t) \\ \mathbf{Q}_{sew2}(t) \end{bmatrix} + \begin{bmatrix} \mathbf{0} \\ \mathbf{M}^{-1} \end{bmatrix} \begin{bmatrix} \mathbf{T}_d^{lg} & \mathbf{T}_{w1}^{lg} & \mathbf{T}_{w2}^{lg} \end{bmatrix} \begin{bmatrix} \mathbf{Q}_{bd}(t) \\ \mathbf{Q}_{bw1}(t) \\ \mathbf{Q}_{bw2}(t) \end{bmatrix} + \begin{bmatrix} \mathbf{0} \\ \mathbf{M}^{-1} \end{bmatrix} \mathbf{T}_u^{lg}\mathbf{u}(t) \tag{6.3}$$

where, $\mathbf{Q}_{sed}(t), \mathbf{Q}_{sew_1}(t), \mathbf{Q}_{sew_2}(t)$ represent the loads due to self-excited forces in the deck, leading and trailing surfaces, $\mathbf{Q}_{bd}(t), \mathbf{Q}_{bw_1}(t), \mathbf{Q}_{bw_2}(t)$ symbolizes the buffeting forces acting on the same surfaces,

$$\mathbf{u}(t) = \begin{bmatrix} u_1(t) \\ u_2(t) \end{bmatrix} \tag{6.4}$$

represent the torques applied on the leading and trailing surfaces due to the controlled movement of the control surfaces, $\mathbf{T}_d^{lg}$, $\mathbf{T}_{w_1}^{lg}$, $\mathbf{T}_{w_2}^{lg}$, $\mathbf{T}_u^{lg}$, are transformation matrices which will be described in subsection 6.2.1, and

$$\mathbf{q}(t) = \begin{bmatrix} \frac{h(t)}{B_d} & \frac{p(t)}{B_d} & \alpha(t) & \delta_1(t) & \delta_2(t) \end{bmatrix}^{\mathrm{T}} \tag{6.5}$$

symbolizes the motion of the different degrees of freedom of the system: $h(t)$ and $p(t)$ denote, respectively, the vertical and horizontal displacement of the system, $\alpha(t)$ is the torsional movement of the deck, $\delta_1(t)$ and $\delta_2(t)$ represents the variables describing the rotations of the leading and trailing surfaces respectively *relative* to the deck and B_d and stands for the deck width. In addition, $\mathbf{M}$, $\mathbf{C}$ and $\mathbf{K}$, in equation (6.1), represent the mass, damping and stiffness matrices of the system respectively, with entries corresponding to their associate coefficients in their respective degrees of freedom; these matrices will be derived in subsection 6.2.2.

As the considered system is linear, the principle of superposition can be used, and therefore, the contribution of the self-excited forces relative to the deck and control surfaces is added to the forces caused by buffeting and those caused by the control forces. Also, equation (6.1) supposes that the flow around the deck or trailing surfaces is unaffected by the wake created by the upstream members; for these reason, the aerodynamics of the control surfaces and deck are formulated independently.

There are two ways of formulating the state space model of the BWCS system: using Karpel's minimum-state formulation or Roger's rational function approximation; however, before developing the respective formulae, some considerations regarding the forces and displacements acting on the system must be provided.

6.2.1 Relationship between the forces and displacements acting on the bridge-wind-control surfaces system and its components

In equation (6.5) were defined the degrees of freedom of the BWCS system. As it is supposed that the aerodynamics of the control surfaces and deck are formulated independently, then each of these surfaces has its own movements, which are related to the absolute coordinate system $\mathbf{q}(t)$. Thus, the deck movements and the vector of displacements are related by,

$$h_d(t) = B_d \frac{h(t)}{B_d} \tag{6.6}$$

$$p_d(t) = B_d \frac{p(t)}{B_d} \tag{6.7}$$

$$\alpha_d(t) = \alpha(t) \tag{6.8}$$

In the same way, between control surface movements and components of the vector of global displacements the following relationship exists

$$h_{w1}(t) = B_d \frac{h(t)}{B_d} + d_1 \cos\alpha(t) - e_1 \sin\alpha(t) - d_1 \tag{6.9}$$

$$p_{w1}(t) = B_d \frac{p(t)}{B_d} - e_1 \cos\alpha(t) - d_1 \sin\alpha(t) + e_1 \tag{6.10}$$

$$\alpha_{w1}(t) = \alpha(t) + \delta_1(t) \tag{6.11}$$

$$h_{w2}(t) = B_d \frac{h(t)}{B_d} + d_2 \cos\alpha(t) + e_2 \sin\alpha(t) - d_2 \tag{6.12}$$

$$p_{w2}(t) = B_d \frac{p(t)}{B_d} + e_2 \cos\alpha(t) - d_2 \sin\alpha(t) - e_2 \tag{6.13}$$

$$\alpha_{w2}(t) = \alpha(t) + \delta_2(t) \tag{6.14}$$

Linearizing the above equations, i.e. expanding the sine and cosine terms in a MacLaurin series and employing only the first term of it, and setting the result in matrix form, yields,

$$\begin{aligned}
\mathbf{q}_d(t) &= \mathbf{T}_d^{gl}\mathbf{q}(t); \qquad \mathbf{T}_d^{gl} = \begin{bmatrix} 1 & 0 & 0 & 0 & 0 \\ 0 & 1 & 0 & 0 & 0 \\ 0 & 0 & 1 & 0 & 0 \end{bmatrix} \\
\mathbf{q}_{w1}(t) &= \mathbf{T}_{w1}^{gl}\mathbf{q}(t); \quad \mathbf{T}_{w1}^{gl} = \begin{bmatrix} \frac{B_d}{B_{w1}} & 0 & -\frac{e_1}{B_{w1}} & 0 & 0 \\ 0 & \frac{B_d}{B_{w1}} & -\frac{d_1}{B_{w1}} & 0 & 0 \\ 0 & 0 & 1 & 1 & 0 \end{bmatrix} \\
\mathbf{q}_{w2}(t) &= \mathbf{T}_{w2}^{gl}\mathbf{q}(t); \quad \mathbf{T}_{w2}^{gl} = \begin{bmatrix} \frac{B_d}{B_{w2}} & 0 & \frac{e_2}{B_{w2}} & 0 & 0 \\ 0 & \frac{B_d}{B_{w2}} & -\frac{d_2}{B_{w2}} & 0 & 0 \\ 0 & 0 & 1 & 0 & 1 \end{bmatrix}
\end{aligned} \tag{6.15}$$

where,

$$\mathbf{q}_d(t) = \begin{bmatrix} \frac{h_d(t)}{B_d} & \frac{p_d(t)}{B_d} & \alpha_d(t) \end{bmatrix}^{\mathrm{T}} \tag{6.16}$$

$$\mathbf{q}_{w1}(t) = \begin{bmatrix} \frac{h_{w1}(t)}{B_{w1}} & \frac{p_{w1}(t)}{B_{w1}} & \alpha_{w1}(t) \end{bmatrix}^{\mathrm{T}} \tag{6.17}$$

$$\mathbf{q}_{w2}(t) = \begin{bmatrix} \frac{h_{w2}(t)}{B_{w2}} & \frac{p_{w2}(t)}{B_{w2}} & \alpha_{w2}(t) \end{bmatrix}^{\mathrm{T}} \tag{6.18}$$

On the other hand, considering the BWCS system as a whole, the sum of wind-induced forces acting in the same degrees of freedom expressed in equation (6.5) are:

$$L_d(t) = L_{sed}(t) + L_{sew1}(t) + L_{sew2}(t) + L_{bd}(t) + L_{bw1}(t) + L_{bw2}(t) \tag{6.19}$$

$$D_d(t) = D_{sed}(t) + D_{sew1}(t) + D_{sew2}(t) + D_{bd}(t) + D_{bw1}(t) + D_{bw2}(t) \tag{6.20}$$

$$\begin{aligned}
M_d(t) = &- \left(L_{sew1}(t) + L_{bw1}(t)\right)\left(e_1\cos\alpha(t) + d_1\sin\alpha(t)\right) \\
&+ \left(L_{sew2}(t) + L_{bw2}(t)\right)\left(e_2\cos\alpha(t) - d_2\sin\alpha(t)\right) \\
&+ \left(D_{sew1}(t) + D_{bw1}(t)\right)\left(e_1\sin\alpha(t) - d_1\cos\alpha(t)\right) \\
&- \left(D_{sew2}(t) + D_{bw2}(t)\right)\left(e_2\sin\alpha(t) + d_2\cos\alpha(t)\right) \\
&+ M_{sed}(t) + M_{bd}(t) + M_{w1}(t) + M_{w2}(t)
\end{aligned} \tag{6.21}$$

$$M_{w1}(t) = M_{sew1}(t) + M_{bw1}(t) + u_1(t) \tag{6.22}$$

$$M_{w2}(t) = M_{sew2}(t) + M_{bw2}(t) + u_2(t) \tag{6.23}$$

Linearizing the above equations, using the fact that $\sin\alpha(t) \approx \alpha(t)$ and $\cos\alpha(t) \approx 1$ for small

rotations of the control surfaces, and expressing them in matrix form yields,

$$
\begin{aligned}
\mathbf{Q}(t) \;=\; & \begin{bmatrix} 1 & 0 & 0 \\ 0 & 1 & 0 \\ 0 & 0 & 1 \\ 0 & 0 & 0 \\ 0 & 0 & 0 \end{bmatrix} (\mathbf{Q}_{sed}(t) + \mathbf{Q}_{bd}(t)) + \\
& \begin{bmatrix} 1 & 0 & 0 \\ 0 & 1 & 0 \\ -(e_1 + d_1\alpha(t)) & e_1\alpha(t) - d_1 & 1 \\ 0 & 0 & 1 \\ 0 & 0 & 0 \end{bmatrix} (\mathbf{Q}_{sew1}(t) + \mathbf{Q}_{bw1}(t)) + \\
& \begin{bmatrix} 1 & 0 & 0 \\ 0 & 1 & 0 \\ e_2 - d_2\alpha(t) & -(e_2\alpha(t) + d_2) & 1 \\ 0 & 0 & 0 \\ 0 & 0 & 1 \end{bmatrix} (\mathbf{Q}_{sew2}(t) + \mathbf{Q}_{bw2}(t)) + \begin{bmatrix} 0 & 0 \\ 0 & 0 \\ 1 & 1 \\ 1 & 0 \\ 0 & 1 \end{bmatrix} \mathbf{u}(t)
\end{aligned} \tag{6.24}
$$

where,

$$\mathbf{Q}(t) = \begin{bmatrix} L_d(t) & D_d(t) & M_d(t) & M_{w1}(t) & M_{w2}(t) \end{bmatrix}^{\mathrm{T}} \tag{6.25}$$

$$\mathbf{Q}_{sed}(t) = \begin{bmatrix} L_{sed}(t) & D_{sed}(t) & M_{sed}(t) \end{bmatrix}^{\mathrm{T}} \tag{6.26}$$

$$\mathbf{Q}_{sew1}(t) = \begin{bmatrix} L_{sew1}(t) & D_{sew1}(t) & M_{sew1}(t) \end{bmatrix}^{\mathrm{T}} \tag{6.27}$$

$$\mathbf{Q}_{sew2}(t) = \begin{bmatrix} L_{sew2}(t) & D_{sew2}(t) & M_{sew2}(t) \end{bmatrix}^{\mathrm{T}} \tag{6.28}$$

$$\mathbf{Q}_{bd}(t) = \begin{bmatrix} L_{bd}(t) & D_{bd}(t) & M_{bd}(t) \end{bmatrix}^{\mathrm{T}} \tag{6.29}$$

$$\mathbf{Q}_{bw1}(t) = \begin{bmatrix} L_{bw1}(t) & D_{bw1}(t) & M_{bw1}(t) \end{bmatrix}^{\mathrm{T}} \tag{6.30}$$

$$\mathbf{Q}_{bw2}(t) = \begin{bmatrix} L_{bw2}(t) & D_{bw2}(t) & M_{bw2}(t) \end{bmatrix}^{\mathrm{T}} \tag{6.31}$$

The terms $d_1\alpha(t)$ and $d_2\alpha(t)$ in equation (6.24) are despreciable in comparison to e_1 and e_2 respectively, thus they can be neglected; the same applies to $e_1\alpha(t)$ and $e_2\alpha(t)$ as they are small

in comparison to d_1 and d_2. In this way, equation (6.24) can be approximated by,

$$\mathbf{Q}(t) = \mathbf{T}_d^{lg}\left(\mathbf{Q}_{sed}(t) + \mathbf{Q}_{bd}(t)\right) + \mathbf{T}_{w1}^{lg}\left(\mathbf{Q}_{sew1}(t) + \mathbf{Q}_{bw1}(t)\right) + \mathbf{T}_{w2}^{lg}\left(\mathbf{Q}_{sew2}(t) + \mathbf{Q}_{bw2}(t)\right) + \mathbf{T}_u^{lg}\mathbf{u}(t) \tag{6.32}$$

where

$$\mathbf{T}_d^{lg} = \begin{bmatrix} 1 & 0 & 0 \\ 0 & 1 & 0 \\ 0 & 0 & 1 \\ 0 & 0 & 0 \\ 0 & 0 & 0 \end{bmatrix};\quad \mathbf{T}_{w1}^{lg} = \begin{bmatrix} 1 & 0 & 0 \\ 0 & 1 & 0 \\ -e_1 & -d_1 & 1 \\ 0 & 0 & 1 \\ 0 & 0 & 0 \end{bmatrix};\quad \mathbf{T}_{w2}^{lg} = \begin{bmatrix} 1 & 0 & 0 \\ 0 & 1 & 0 \\ e_2 & -d_2 & 1 \\ 0 & 0 & 0 \\ 0 & 0 & 1 \end{bmatrix};\quad \mathbf{T}_u^{lg} = \begin{bmatrix} 0 & 0 \\ 0 & 0 \\ 1 & 1 \\ 1 & 0 \\ 0 & 1 \end{bmatrix} \tag{6.33}$$

6.2.2 State space model using Karpel's minimum state representation

For the present, only the effect self-excited forces will be analyzed; later the influence of the buffeting forces will be taken into account. As stated in chapter 5, the movement of the deck due to self-excited forces alone can be modelled as,

$$\mathbf{M}_d\ddot{\mathbf{q}}_d(t) + \mathbf{C}_d\dot{\mathbf{q}}_d(t) + \mathbf{K}_d\mathbf{q}_d(t) = \mathbf{Q}_{sed}(t) \tag{6.34}$$

where, $\mathbf{M}_d = \mathrm{diag}\left([m_dB_d\ m_dB_d\ J_\alpha]\right)$, $\mathbf{C}_d = \mathrm{diag}\left([c_hB_d\ c_pB_d\ c_\alpha]\right)$, $\mathbf{K}_d = \mathrm{diag}\left([k_hB_d\ k_pB_d\ k_\alpha]\right)$ are the girder mass, damping and stiffness matrices,

$$\mathbf{Q}_{sed}(t) = \mathbf{V}_d\left(\left(\frac{B_d}{\bar{U}}\right)^2\mathbf{A}_{3d}\ddot{\mathbf{q}}_d(t) + \left(\frac{B_d}{\bar{U}}\right)\mathbf{A}_{2d}\dot{\mathbf{q}}_d(t) + \mathbf{A}_{1d}\mathbf{q}_d(t) + \mathbf{G}_d\mathbf{x}_{ad}(t)\right) \tag{6.35}$$

is the vector of self-excited forces acting on the section of the bridge deck and

$$\dot{\mathbf{x}}_{ad}(t) = \frac{\bar{U}}{B_d}\mathbf{E}_d\mathbf{q}_d(t) - \frac{\bar{U}}{B_d}\mathbf{R}_d\mathbf{x}_{ad}(t) \tag{6.36}$$

its corresponding vector of aerodynamic states; also $\mathbf{V}_d$ stands for

$$\mathbf{V}_d = U^2(t)\begin{bmatrix} \frac{1}{2}\rho B_d & 0 & 0 \\ 0 & \frac{1}{2}\rho B_d & 0 \\ 0 & 0 & \frac{1}{2}\rho B_d^2 \end{bmatrix}; \tag{6.37}$$

analogously, the self-excited forces in the control surfaces can be modelled as,

$$\mathbf{Q}_{sewk}(t) = \mathbf{V}_{wk}\left(\left(\frac{B_{wk}}{\bar{U}}\right)^2 \mathbf{A}_{3wk}\ddot{\mathbf{q}}_{wk}(t) + \left(\frac{B_{wk}}{\bar{U}}\right)\mathbf{A}_{2wk}\dot{\mathbf{q}}_{wk}(t) + \mathbf{A}_{1wk}\mathbf{q}_{wk}(t) + \mathbf{G}_{wk}\mathbf{x}_{awk}(t)\right) \tag{6.38}$$

with along with its aerodynamic states vector

$$\dot{\mathbf{x}}_{awk}(t) = \frac{\bar{U}}{B_{wk}}\mathbf{E}_{wk}\mathbf{q}_{wk}(t) - \frac{\bar{U}}{B_{wk}}\mathbf{R}_{wk}\mathbf{x}_{awk}(t) \tag{6.39}$$

for $k = 1, 2$, arranging $\mathbf{V}_{w1}$ and $\mathbf{V}_{w2}$ in a similar way as in (6.37); in this way, the movement of the control surfaces can be stated as the solution of the differential equation,

$$\mathbf{M}_{wk}\ddot{\mathbf{q}}_{wk}(t) + \mathbf{C}_{wk}\dot{\mathbf{q}}_{wk}(t) + \mathbf{K}_{wk}\mathbf{q}_{wk}(t) = \mathbf{Q}_{sewk}(t) \tag{6.40}$$

where, $\mathbf{M}_{wk} = \mathrm{diag}\left([m_{wk}B_{wk}\ m_{wk}B_{wk}\ J_{\delta wk}]\right)$, $\mathbf{C}_{wk} = \mathrm{diag}\left([c_{hwk}B_{wk}\ c_{pwk}B_{wk}\ c_{\delta wk}]\right)$, $\mathbf{K}_{wk} = \mathrm{diag}\left([k_{hwk}B_{wk}\ k_{pwk}B_{wk}\ k_{\delta wk}]\right)$ are the wing mass, damping and stiffness matrices.

Adding equations (6.34) and (6.40) and making use of the relations (6.15) and (6.32) one can obtain,

$$\mathbf{M}\ddot{\mathbf{q}}(t) + \mathbf{C}\dot{\mathbf{q}}(t) + \mathbf{K}\mathbf{q}(t) = \mathbf{T}_d^{lg}\mathbf{Q}_{sed}(t) + \mathbf{T}_{w_1}^{lg}\mathbf{Q}_{sew_1}(t) + \mathbf{T}_{w_2}^{lg}\mathbf{Q}_{sew_2}(t) + \mathbf{T}_u^{lg}\mathbf{u}(t) \tag{6.41}$$

where,

$$\mathbf{M} = [m_dB_d \quad m_dB_d \quad J_\alpha \quad J_{\delta w1} \quad J_{\delta w2}] \tag{6.42}$$

$$\mathbf{C} = [c_dB_d \quad c_dB_d \quad c_\alpha \quad c_{\delta w1} \quad c_{\delta w2}] \tag{6.43}$$

$$\mathbf{K} = [k_dB_d \quad k_dB_d \quad c_\alpha \quad k_{\delta w1} \quad k_{\delta w2}] \tag{6.44}$$

As can be seen, all terms describing the inertial coupling between deck and surfaces are ignored, because the thickness and width of the control surfaces are only a fraction of the dimension of the deck.

Finally, replacing the above formulae into (6.2), the equation of motion of the BWCS system (6.1) can be rewritten in state space form as

$$\dot{\mathbf{y}}(t) = \mathbf{A}(t)\mathbf{y}(t) + \begin{bmatrix} \mathbf{0} \\ \bar{\mathbf{M}}^{-1} \\ \mathbf{0} \\ \mathbf{0} \\ \mathbf{0} \end{bmatrix} \begin{bmatrix} \mathbf{T}_d^{lg} & \mathbf{T}_{w1}^{lg} & \mathbf{T}_{w2}^{lg} \end{bmatrix} \begin{bmatrix} \mathbf{Q}_{bd}(t) \\ \mathbf{Q}_{bw1}(t) \\ \mathbf{Q}_{bw2}(t) \end{bmatrix} + \begin{bmatrix} \mathbf{0} \\ \bar{\mathbf{M}}^{-1} \\ \mathbf{0} \\ \mathbf{0} \\ \mathbf{0} \end{bmatrix} \mathbf{T}_u^{lg}\mathbf{u}(t) \tag{6.45}$$

where,

$$\mathbf{y}(t) = \begin{bmatrix} \mathbf{q}(t) \\ \dot{\mathbf{q}}(t) \\ \mathbf{x}_{ad}(t) \\ \mathbf{x}_{aw1}(t) \\ \mathbf{x}_{aw2}(t) \end{bmatrix}, \tag{6.46}$$

$$\mathbf{A}(t) = \begin{bmatrix} \mathbf{0} & \mathbf{I} & \mathbf{0} & \mathbf{0} & \mathbf{0} \\ -\bar{\mathbf{M}}^{-1}\bar{\mathbf{K}} & -\bar{\mathbf{M}}^{-1}\bar{\mathbf{C}} & U^2(t)\bar{\mathbf{M}}^{-1}\mathbf{T}_d^{lg}\mathbf{V}_d\mathbf{G}_d & U^2(t)\bar{\mathbf{M}}^{-1}\mathbf{T}_{w1}^{lg}\mathbf{V}_{w1}\mathbf{G}_{w1} & U^2(t)\bar{\mathbf{M}}^{-1}\mathbf{T}_{w2}^{lg}\mathbf{V}_{w2}\mathbf{G}_{w2} \\ \frac{\bar{U}}{B_d}\mathbf{E}_d\mathbf{T}_d^{gl} & \mathbf{0} & -\frac{\bar{U}}{B_d}\mathbf{R}_d & \mathbf{0} & \mathbf{0} \\ \frac{\bar{U}}{B_{w1}}\mathbf{E}_{w1}\mathbf{T}_{w1}^{gl} & \mathbf{0} & \mathbf{0} & -\frac{\bar{U}}{B_{w1}}\mathbf{R}_{w1} & \mathbf{0} \\ \frac{\bar{U}}{B_{w2}}\mathbf{E}_{w2}\mathbf{T}_{w2}^{gl} & \mathbf{0} & \mathbf{0} & \mathbf{0} & -\frac{\bar{U}}{B_{w2}}\mathbf{R}_{w2} \end{bmatrix}, \tag{6.47}$$

$$\bar{\mathbf{M}} = \mathbf{M} - U^2(t)\left(\left(\frac{B_d}{U}\right)^2\mathbf{T}_d^{lg}\mathbf{V}_d\mathbf{A}_{3d}\mathbf{T}_d^{gl} - \left(\frac{B_{w1}}{U}\right)^2\mathbf{T}_{w1}^{lg}\mathbf{V}_{w1}\mathbf{A}_{3w1}\mathbf{T}_{w1}^{gl} - \left(\frac{B_{w2}}{U}\right)^2\mathbf{T}_{w2}^{lg}\mathbf{V}_{w2}\mathbf{A}_{3w2}\mathbf{T}_{w2}^{gl}\right), \tag{6.48}$$

$$\bar{\mathbf{C}} = \mathbf{C} - U^2(t)\left(\left(\frac{B_d}{U}\right)\mathbf{T}_d^{lg}\mathbf{V}_d\mathbf{A}_{2d}\mathbf{T}_d^{gl} - \left(\frac{B_{w1}}{U}\right)\mathbf{T}_{w1}^{lg}\mathbf{V}_{w1}\mathbf{A}_{2w1}\mathbf{T}_{w1}^{gl} - \left(\frac{B_{w2}}{U}\right)\mathbf{T}_{w2}^{lg}\mathbf{V}_{w2}\mathbf{A}_{2w2}\mathbf{T}_{w2}^{gl}\right), \tag{6.49}$$

$$\bar{\mathbf{K}} = \mathbf{K} - U^2(t)\left(\mathbf{T}_d^{lg}\mathbf{V}_d\mathbf{A}_{1d}\mathbf{T}_d^{gl} - \mathbf{T}_{w1}^{lg}\mathbf{V}_{w1}\mathbf{A}_{1w1}\mathbf{T}_{w1}^{gl} - \mathbf{T}_{w2}^{lg}\mathbf{V}_{w2}\mathbf{A}_{1w2}\mathbf{T}_{w2}^{gl}\right). \tag{6.50}$$

As can be seen, there are eight structural states, and three pairs of aerodynamic states vectors corresponding to the self-excited aerodynamics of the deck and the control surfaces. It is a good point to remember that the self-excited forces are only dependent on the average wind velocity U; therefore, as can be seen from equations (6.47) to (6.50), the system is linear and time invariant setting $U(t) = \bar{U}$.

6.2.3 State space model using Roger's rational function approximation

Making a reasoning similar to that stated in sections 5.1.1 and 6.2.2, we can arrive at the following state space form using Roger's rational function approximation: in equation (6.45), matrix $\mathbf{A}(t)$ can be expressed as,

$$\mathbf{A}(t) = \begin{bmatrix} \mathbf{A}_{11} & \mathbf{A}_{12} \\ \mathbf{A}_{21} & \mathbf{A}_{22} \end{bmatrix} \tag{6.51}$$

where

$$\mathbf{A}_{11} = \begin{bmatrix} \mathbf{0} & \mathbf{I} \\ -\bar{\mathbf{M}}^{-1}\bar{\mathbf{K}} & -\bar{\mathbf{M}}^{-1}\bar{\mathbf{C}} \end{bmatrix}, \tag{6.52}$$

$$\mathbf{A}_{12} = U^2(t) \begin{bmatrix} \mathbf{0} & \mathbf{0} & \mathbf{0} & \mathbf{0} & \mathbf{0} & \mathbf{0} & \mathbf{0} & \mathbf{0} & \mathbf{0} \\ \bar{\mathbf{M}}^{-1}\mathbf{T}_d^{lg}\mathbf{V}_d & \cdots & \bar{\mathbf{M}}^{-1}\mathbf{T}_d^{lg}\mathbf{V}_d & \bar{\mathbf{M}}^{-1}\mathbf{T}_{w1}^{lg}\mathbf{V}_{w1} & \cdots & \bar{\mathbf{M}}^{-1}\mathbf{T}_{w1}^{lg}\mathbf{V}_{w1} & \bar{\mathbf{M}}^{-1}\mathbf{T}_{w2}^{lg}\mathbf{V}_{w2} & \cdots & \bar{\mathbf{M}}^{-1}\mathbf{T}_{w2}^{lg}\mathbf{V}_{w2} \end{bmatrix}, \tag{6.53}$$

$$\mathbf{A}_{21} = \begin{bmatrix} \mathbf{0} & \mathbf{A}_{4d}\mathbf{T}_d^{gl} \\ \mathbf{0} & \vdots \\ \mathbf{0} & \mathbf{A}_{(3+m_d)\_d}\mathbf{T}_d^{gl} \\ \mathbf{0} & \mathbf{A}_{4w1}\mathbf{T}_{w1}^{gl} \\ \mathbf{0} & \vdots \\ \mathbf{0} & \mathbf{A}_{(3+m_{w1})\_w1}\mathbf{T}_{w1}^{gl} \\ \mathbf{0} & \mathbf{A}_{4w2}\mathbf{T}_{w2}^{gl} \\ \mathbf{0} & \vdots \\ \mathbf{0} & \mathbf{A}_{(3+m_{w2})\_w2}\mathbf{T}_{w2}^{gl} \end{bmatrix} \tag{6.54}$$

and

$$\mathbf{A}_{22} = \begin{bmatrix} -\frac{\bar{U}}{B_d}d_{1d}\mathbf{I} & \mathbf{0} & \mathbf{0} & \mathbf{0} & \mathbf{0} & \mathbf{0} & \mathbf{0} & \mathbf{0} & \mathbf{0} \\ \mathbf{0} & \ddots & \mathbf{0} & \mathbf{0} & \mathbf{0} & \mathbf{0} & \mathbf{0} & \mathbf{0} & \mathbf{0} \\ \mathbf{0} & \mathbf{0} & -\frac{\bar{U}}{B_d}d_{m_d d}\mathbf{I} & \mathbf{0} & \mathbf{0} & \mathbf{0} & \mathbf{0} & \mathbf{0} & \mathbf{0} \\ \mathbf{0} & \mathbf{0} & \mathbf{0} & -\frac{\bar{U}}{B_{w1}}d_{1w1}\mathbf{I} & \mathbf{0} & \mathbf{0} & \mathbf{0} & \mathbf{0} & \mathbf{0} \\ \mathbf{0} & \mathbf{0} & \mathbf{0} & \mathbf{0} & \ddots & \mathbf{0} & \mathbf{0} & \mathbf{0} & \mathbf{0} \\ \mathbf{0} & \mathbf{0} & \mathbf{0} & \mathbf{0} & \mathbf{0} & -\frac{\bar{U}}{B_{w1}}d_{m_{w1}w1}\mathbf{I} & \mathbf{0} & \mathbf{0} & \mathbf{0} \\ \mathbf{0} & \mathbf{0} & \mathbf{0} & \mathbf{0} & \mathbf{0} & \mathbf{0} & -\frac{\bar{U}}{B_{w2}}d_{1w2}\mathbf{I} & \mathbf{0} & \mathbf{0} \\ \mathbf{0} & \mathbf{0} & \mathbf{0} & \mathbf{0} & \mathbf{0} & \mathbf{0} & \mathbf{0} & \ddots & \mathbf{0} \\ \mathbf{0} & \mathbf{0} & \mathbf{0} & \mathbf{0} & \mathbf{0} & \mathbf{0} & \mathbf{0} & \mathbf{0} & -\frac{\bar{U}}{B_{w2}}d_{m_{w2}w2}\mathbf{I} \end{bmatrix} \tag{6.55}$$

using $\bar{\mathbf{M}}$, $\bar{\mathbf{C}}$, and $\bar{\mathbf{K}}$, as defined in equations (6.48), (6.49) and (6.50).

It is expected that the main stabilizing action comes from the vertical forces induced by the wind on the control surfaces, multiplied by the arms e_1 and e_2 resulting in a large stabilizing moment.

6.3 Two-degree-of-freedom deck section model with control surfaces: open loop configuration

To the bridge analyzed in section 5.3 were attached a pair of control surfaces below the deck. The parameters of those surfaces were set to the values shown in Table 6.1; also, the Karpel's

Table 6.1: Structural and geometric parameters of the control surfaces (per unit length)

Parameter	**Value**
Control surface width (B_w)	0.1 B_d
Position of control surfaces from center of deck e	0.5 B_d
Frequency of pitching mode (ω_δ)	37.7 rad/s
Damping of pitching mode (ξ_δ)	70.0 %

minimum state formulation parameters of the wings were set to (Wilde (2003)):

$$\mathbf{a}_1 = \begin{bmatrix} 0.3576 & 4.5450 \\ 0.0894 & 1.1360 \end{bmatrix}; \mathbf{a}_2 = \begin{bmatrix} 4.1880 & 1.5350 \\ 1.0580 & -0.3998 \end{bmatrix};$$
$$\mathbf{g} = \begin{bmatrix} 3.0090 & 0.1818 \\ 0.7563 & 0.0455 \end{bmatrix}; \mathbf{R} = \begin{bmatrix} 0.0320 & 0 \\ 0 & 0.1902 \end{bmatrix}; \mathbf{e} = \begin{bmatrix} -0.6369 \times 10^{-4} & 0.2414 \times 10^{-2} \\ -0.3673 & 1.5540 \end{bmatrix} \tag{6.56}$$

A *deterministic* stability analysis was made for the open loop configuration of the BWCS system. Figure A.2 shows a pole map of this system, and the variation the corresponding damping and frequency parameters of the poles with a growing wind speed. It was seen that in the open loop configuration, the behavior of the bridge does not depend on the values of the frequency and damping of the control surfaces, as will be discussed in the next chapter, these parameters only have influence in the closed loop configuration; also, it was noted that the position of the poles corresponding to the control surface vibration modes remains constant with the mean wind speed variation.

On the other hand, it was found that the critical speed for the aforementioned system is 10.7 m/s. The instability of the system appears because the pitching mode damping becomes negative. Comparing this result with the presented in section 5.3 for the bridge without control surfaces ($U_{cr} = 10.4$ m/s), it can be seen that the control surfaces in an open loop configuration increases the critical wind speed of the system in 3%, which is a desirable feature inasmuch as

the winged bridge does not become unstable for lower wind velocities than the bridge without control surfaces.

Comparing Figures A.1 and A.2, it can be easily seen that the vibration frequencies of the pitching and heaving mode do not change with an increasing mean wind speed; however, the damping of these modes does. So, it can be concluded that the main effect of the attachment of a pair of wings under the bridge wing system is that they impel the increase of the damping of the different modes of vibration of the system.

Figure 6.2 shows the relationship between the control surface width/deck width ratio and the

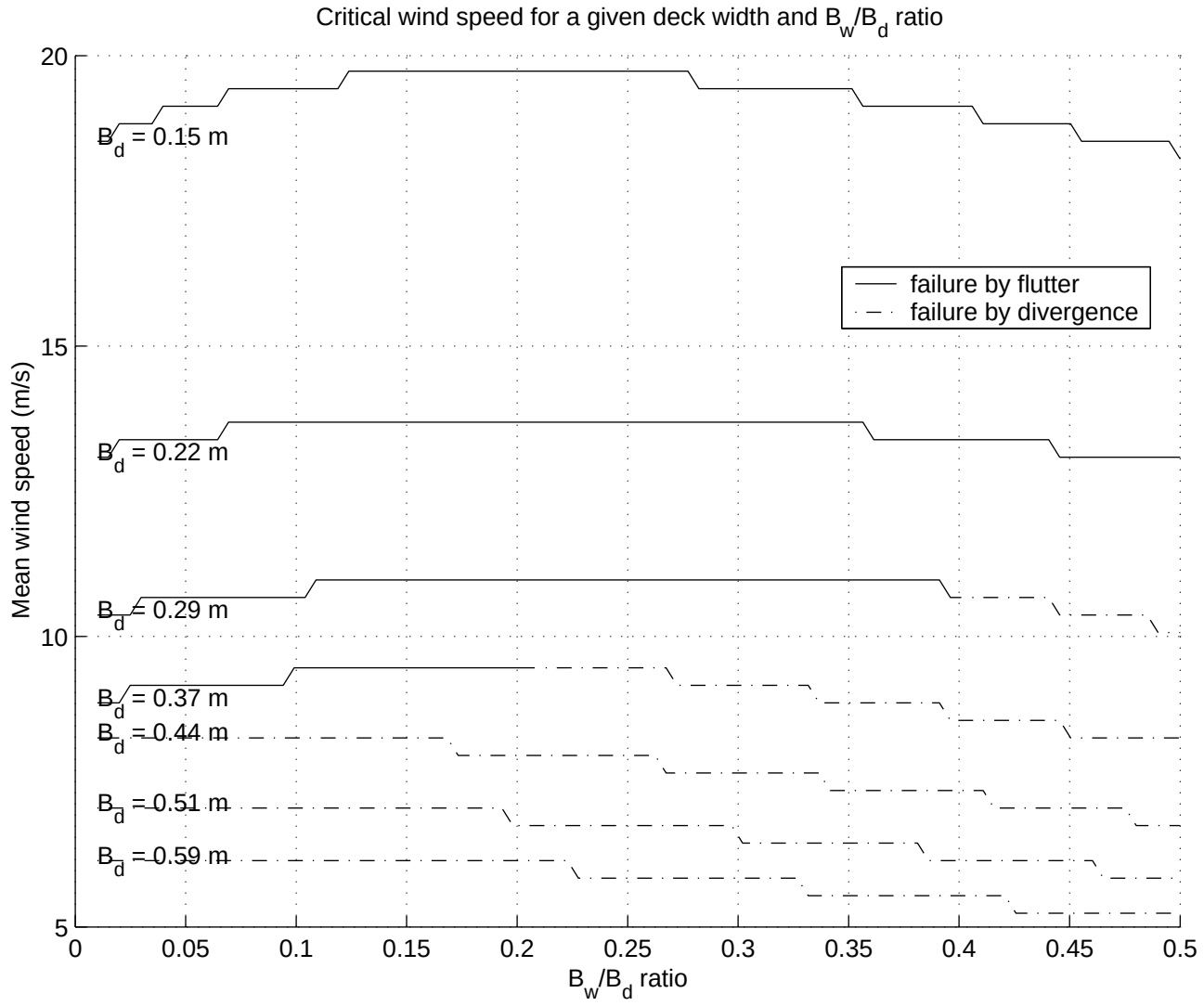

Figure 6.2: Critical wind speed for a given deck width and a B_w/B_d ratio

critical velocity for several deck widths. It can be seen that narrower decks have a higher critical velocity than wider decks. Also it can be seen that the optimal B_w/B_d ratio can be found in the 0.15 to 0.25 range approximately. However, in practice, lower ratios should be preferred inasmuch as broader wings increase the dead load of the bridge, and that the critical wind velocity does not decrement excessively with narrower control surfaces, so the selection of the wing width implies a trade off between cost and performance. It is seen also that wider control surfaces tend to make the bridge prone to fail the bridge by divergence; however this is only a hypothesis inasmuch as the influence of the wake made by the leading wing could have a great influence on this result.

The controlled case, that is the closed loop configuration of the BWCS system, will be discussed in the next chapter.

Chapter 7

Stochastic control of the bridge-wind-control surfaces system

Civil engineering structures cope with a singular set of problems. They are massive systems which require large actuation forces, their modelling is uncertain in both the inherent nature of the structure as well as the external forces that they must withstand. In addition, structures are infinitesimal systems that are not completely observable from sensors located at a single point; even, these sensors maybe contaminated with noise (Housner et al. (1997)).

Stochastic optimal control theory is specially suitable to manage such difficulties, as it can determine the best strategy for controlling a dynamic system in the presence of uncertainty; for example, it can encompass a number of functions like,

- Parameter and system identification.
- Definition of a control scheme for a dynamic system subject to random disturbances, with perhaps noisy observations, in order to achieve some objective.
- Estimation of the states of a dynamic system from noisy and incomplete output measurements.

A brief description of each of the previously mentioned items, with exception of the former, will be given in the following, after Stengel (1986).

7.1 Setup of the problem

Let

$$\dot{\mathbf{x}}(t) = \mathbf{f}\left(\mathbf{x}(t), \mathbf{u}(t), \mathbf{w}(t), \mathbf{p}(t), t\right); \quad \mathbf{x}(t_0) = \mathbf{x_0} \tag{7.1}$$

$$\mathbf{y}(t) = \mathbf{h}\left(\mathbf{x}(t), \mathbf{u}(t), \mathbf{w}(t), \mathbf{p}(t), t\right) \tag{7.2}$$

$$\mathbf{z}(t) = \mathbf{j}\left(\mathbf{y}(t), \mathbf{n}(t), t\right) \tag{7.3}$$

be a set of equations which describe respectively the evolution of the state, output and measurement of a time-varying nonlinear dynamical system, where $\mathbf{x}(t)$ is the n-dimensional state vector, $\mathbf{y}(t)$ is the r-dimensional process output vector, $\mathbf{z}(t)$ is the r-dimensional vector of observations, $\mathbf{p}(t)$ is the l-dimensional vector of system parameters, $\mathbf{u}(t)$ is the n-dimensional controllable inputs vector, $\mathbf{w}(t)$ is the s-dimensional vector of uncontrollable inputs (disturbances) and $\mathbf{n}(t)$ is the r-dimensional measurement noise (sensor noise) vector. It must bear in mind that the dimension of $\mathbf{y}(t)$ and $\mathbf{z}(t)$, depend only on r, the number of sensors.

The time-optimal control problem to be solved is to find a control vector $\mathbf{u}^*(t), t \in [t_0, t_f]$ which drives the state vector from an initial to a final value while minimizing a scalar cost functional, J_0, given by

$$J_0 = \phi\left(\mathbf{x}\left(t_f\right), \mathbf{w}\left(t_f\right), \mathbf{p}\left(t_f\right), t_f\right) + \int_{t_0}^{t_f} \mathcal{L}\left(\mathbf{x}\left(t\right), \mathbf{u}\left(t\right), \mathbf{w}\left(t\right), \mathbf{p}\left(t\right), t\right) \mathrm{d}t \tag{7.4}$$

where $\mathcal{L}()$ is a functional called the *Lagrangian* and $\phi()$ is the *terminal constraint*. Under the premise that the disturbances and measurement noise, and perhaps the parameter variations are stochastic processes, the system response will also be a stochastic process. Hence, the cost function must be given as the expected value of the deterministic cost function (7.4), as

$$J = \mathrm{E}\left[\phi\left(\mathbf{x}\left(t_f\right), \mathbf{w}\left(t_f\right), \mathbf{p}\left(t_f\right), t_f\right) + \int_{t_0}^{t_f} \mathcal{L}\left(\mathbf{x}\left(t\right), \mathbf{u}\left(t\right), \mathbf{w}\left(t\right), \mathbf{p}\left(t\right), t\right) \mathrm{d}t\right] \tag{7.5}$$

Assuming the sensor and disturbance noise to be small zero mean additive and white, and the initial conditions and parameters of the system to be random, then the stochastic optimal control solution, $\mathbf{u}^*(t)$, is found by the solution of the following problem:

Solve:

$$\mathbf{u}^*(t) = \arg\min_{\mathbf{u}(t)} \mathrm{E}\left[\phi\left(\mathbf{x}\left(t_f\right), t_f\right) + \int_{t_0}^{t_f} \mathcal{L}\left(\mathbf{x}\left(t\right), \mathbf{u}\left(t\right), t\right) \mathrm{d}t\right] \tag{7.6}$$

for $t \in [t_0, t_f]$ subject to the stochastic differential constraint,

$$\mathrm{d}\mathbf{x}(t) = \mathbf{f}\left(\mathbf{x}(t), \mathbf{u}(t), t\right) \mathrm{d}t + \mathbf{L}(t)\mathbf{w}(t)\mathrm{d}t \tag{7.7}$$

and to the initial conditions,

$$\mathrm{E}\left[\mathbf{x}(t_0)\right] = \mathbf{x}_0; \quad \mathrm{E}\left[\left(\mathbf{x}(t_0) - \mathbf{x}_0\right)\left(\mathbf{x}(t_0) - \mathbf{x}_0\right)^{\mathrm{T}}\right] = \mathbf{P}_0 \tag{7.8}$$

in the assumption that the effects of disturbances are small, Gaussian, white and additive, with $\mathbf{L}(t)$ defined as in (7.19), and $\mathbf{P}_0$ is the $n \times n$ initial covariance matrix; also,

$$\mathbf{y}(t) = \mathbf{h}\left(\mathbf{x}(t), \mathbf{u}(t), t\right) \tag{7.9}$$

$$\mathbf{z}(t) = \mathbf{j}\left(\mathbf{y}(t), \mathbf{n}(t), t\right) \tag{7.10}$$

and,

$$\mathrm{E}\left[\mathbf{w}(t)\right] = \mathbf{0}; \quad \mathrm{E}\left[\mathbf{w}(t)\mathbf{w}^{\mathrm{T}}(\tau)\right] = \mathbf{W}(t)\delta(t-\tau) \tag{7.11}$$

$$\mathrm{E}\left[\mathbf{n}(t)\right] = \mathbf{0}; \quad \mathrm{E}\left[\mathbf{n}(t)\mathbf{n}^{\mathrm{T}}(\tau)\right] = \mathbf{N}(t)\delta(t-\tau) \tag{7.12}$$

where, $\mathbf{N}(t)$ and $\mathbf{W}(t)$ are respectively the $r \times r$ and $s \times s$ autocorrelation matrices of the measurement and disturbance noise.

It is clear that, if the control $\mathbf{u}(t)$ were known, then the stochastic differential equation (7.7) could be solved employing Itô calculus, leading to a response that is Markovian; the state vector $\mathbf{x}(t)$ could be solved provided that its transition probability density function or its statistical moments can be found within some error induced by closure. Nevertheless, calculation of the optimal control $\mathbf{u}^*(t)$ requires equation (7.6) to be minimized, which itself demands knowledge of the state vector, $\mathbf{x}(t)$, implying some kind of recursive nonlinear estimation and design procedure. As can be seen, stochastic control of nonlinear systems is a difficult task; in this way, the aforementioned problem is usually solved using a neighboring scheme.

7.2 Linear quadratic control in the continuous time case

A neighboring scheme linearizes the state evolution, observation and measurement equations and assumes that the cost function is quadratic in the states and control, leading to the time domain

linear quadratic gaussian (LQG) theory and its frequency domain analog, the H_2 control (Stengel (1986)). The LQG problem can be stated as,

Solve:

$$\mathbf{u}^*(t) = \arg\min_{\mathbf{u}(t)} \frac{1}{2}\mathrm{E}\left[\mathbf{x}^{\mathrm{T}}(t_f)\mathbf{S}(t_f)\mathbf{x}(t_f) + \int_{t_0}^{t_f} \mathbf{x}^{\mathrm{T}}(t)\mathbf{Q}(t)\mathbf{x}(t) + \mathbf{u}^{\mathrm{T}}(t)\mathbf{R}(t)\mathbf{u}(t)\mathrm{d}t\right] \tag{7.13}$$

for $t \in [t_0, t_f]$ subject to the linear dynamic constraint,

$$\mathrm{d}\mathbf{x}(t) = \mathbf{F}(t)\mathbf{x}(t)\mathrm{d}t + \mathbf{G}(t)\mathbf{u}(t)\mathrm{d}t + \mathbf{L}(t)\mathbf{w}(t)\mathrm{d}t \tag{7.14}$$

and to the generalized initial condition,

$$\mathrm{E}\left[\mathbf{x}(t_0)\right] = \mathbf{x}_0; \quad \mathrm{E}\left[\left(\mathbf{x}(t_0) - \mathbf{x}_0\right)\left(\mathbf{x}(t_0) - \mathbf{x}_0\right)^{\mathrm{T}}\right] = \mathbf{P}_0 \tag{7.15}$$

with measurement equation,

$$\mathbf{z}(t) = \mathbf{H}(t)\mathbf{x}(t) + \mathbf{n}(t) \tag{7.16}$$

and, disturbance and measure noises characterized by (7.11) y (7.12) respectively; in this case, $\mathbf{F}(t)$, $\mathbf{G}(t)$, $\mathbf{L}(t)$ and $\mathbf{H}(t)$ are Jacobian matrices defined as,

$$\mathbf{F}(t) = \frac{\partial \mathbf{f}}{\partial \mathbf{x}} \quad (n \times n) \tag{7.17}$$

$$\mathbf{G}(t) = \frac{\partial \mathbf{f}}{\partial \mathbf{u}} \quad (n \times m) \tag{7.18}$$

$$\mathbf{L}(t) = \frac{\partial \mathbf{f}}{\partial \mathbf{w}} \quad (n \times s) \tag{7.19}$$

$$\mathbf{H}(t) = \frac{\partial \mathbf{h}}{\partial \mathbf{x}} \quad (r \times n) \tag{7.20}$$

evaluated along the solution of the deterministic optimal path problem.

It must be taken into account that if the state vector $\mathbf{x}(t)$ is completely measurable, then the optimal solution to the linear quadratic control problem can be solved, for example, by stochastic dynamic programming. However, usually this is not possible in civil engineering structures as the states represented for instance by the velocities and displacements relative to each degree of freedom are either immeasurable (i.e. those associated with actuator dynamics) or never fully accessible. In practice, measurement is usually limited to absolute accelerations and perhaps, relative displacements between structural members in a limited set of points as a result of the cost of the sensors (Housner et al. (1997)). Accordingly, as the states of the system cannot be

directly sensed, they must be estimated. It can be shown that the design of the estimator has nothing to do with the controller design, i.e. the design of the estimator and the one of the controller are completely independent tasks (Stengel (1986), Szidarovszky and Bahill (1998)).

7.2.1 State estimation

As indicated, the state vector estimator $\hat{\mathbf{x}}(t)$ can be used instead of unknown true state of the dynamical system to reach an optimal solution. In continuous time, the optimal estimator is a Kalman-Bucy filter (Kalman (1960), Kalman and Bucy (1961)), which assures that $\hat{\mathbf{x}}(t)$ is a minimum-variance estimator, unbiased in the sense that $\mathrm{E}\left[\hat{\mathbf{x}}(t)\right] = \mathrm{E}\left[\mathbf{x}(t)\right]$ and linear in the observation data $\mathbf{z}(t)$ (Stengel (1986)).

Let

$$\mathbf{e}(t) = \mathbf{x}(t) - \hat{\mathbf{x}}(t) \tag{7.21}$$

be the estimation error, for $t \in [0, t_f]$ setting $t_0 = 0$. The state estimate is characterized by the conditional probability distribution function of $\mathbf{x}(t)$, so that the first and second centralized moments are given by $\hat{\mathbf{x}}(t) = \mathrm{E}\left[\mathbf{x}(t)\right]$ and $\hat{\mathbf{P}}(t) = \mathrm{E}\left[\mathbf{e}(t)\mathbf{e}^{\mathrm{T}}(t)\right]$. If the dynamical system is described by (7.7) to (7.16) and the measurement and disturbance noises are characterized by (7.11) and (7.12) respectively, then the state estimate is given by the solution to

$$\mathrm{d}\hat{\mathbf{x}}(t) = \mathbf{F}(t)\hat{\mathbf{x}}(t)\mathrm{d}t + \mathbf{G}(t)\mathbf{u}(t)\mathrm{d}t + \mathbf{K}(t)\left[\mathbf{z}(t) - \mathbf{H}(t)\hat{\mathbf{x}}(t)\right]\mathrm{d}t; \quad \hat{\mathbf{x}}(0) = \hat{\mathbf{x}}_0 \tag{7.22}$$

where the filter gain is

$$\mathbf{K}(t) = \mathbf{P}(t)\mathbf{H}^{\mathrm{T}}(t)\mathbf{N}^{-1}(t) \tag{7.23}$$

and the state covariance error estimate $\mathbf{P}(t)$ is given by the integration of the Ricatti equation

$$\dot{\hat{\mathbf{P}}}(t) = \mathbf{F}(t)\hat{\mathbf{P}}(t) + \hat{\mathbf{P}}(t)\mathbf{F}^{\mathrm{T}}(t) + \mathbf{L}(t)\mathbf{W}(t)\mathbf{L}^{\mathrm{T}}(t) - \hat{\mathbf{P}}(t)\mathbf{H}^{\mathrm{T}}(t)\mathbf{N}^{-1}(t)\mathbf{H}(t)\hat{\mathbf{P}}(t) \tag{7.24}$$

subject to the initial condition

$$\hat{\mathbf{P}}(0) = \hat{\mathbf{P}}_0 \tag{7.25}$$

As can be seen, the state-estimation error covariance matrix $\mathbf{P}(t)$, for a linear-optimal state estimator is independent of the actual control input.

7.2.2 Stochastic control for linear time varying systems

Given the optimal estimator $\hat{\mathbf{x}}(t)$, it can be demonstrated that the filter residual $\mathbf{z}(t) - \mathbf{H}(t)\hat{\mathbf{x}}(t)$ is a zero mean white noise process with evolutive autocovariance function

$$\mathbf{N}'(t) = \mathbf{N}(t) + \mathbf{H}(t)\mathbf{P}(t)\mathbf{H}^{\mathrm{T}}(t) \tag{7.26}$$

As is commented in Stengel (1986), the filter and control design procedures are dual problems because they are identical in form (compare equations (7.7) and (7.22)). Hence, the optimal control law can be demonstrated to be

$$\mathbf{u}^*(t) = -\mathbf{R}^{-1}(t)\mathbf{G}^{\mathrm{T}}(t)\mathbf{S}(t)\hat{\mathbf{x}}(t) \tag{7.27}$$

where $\mathbf{S}(t)$ is the solution to the Ricatti equation

$$\dot{\mathbf{S}}(t) = -\mathbf{F}^{\mathrm{T}}(t)\mathbf{S}(t) - \mathbf{S}(t)\mathbf{F}(t) - \mathbf{Q}(t) + \mathbf{S}(t)\mathbf{G}(t)\mathbf{R}^{-1}(t)\mathbf{G}^{\mathrm{T}}(t)\mathbf{S}(t) \tag{7.28}$$

with final condition

$$\mathbf{S}(t_f) = \mathbf{S}_f \tag{7.29}$$

One of the great properties of the above approach is that it can guarantee closed-loop asymptotic stability for a great variety of linear systems, including those that are by nature unstable.

7.3 Linear quadratic control in the discrete time case

Controller strategies are usually implemented in hardware working with discrete and digital algorithms; therefore, it is worth to analyze the above described control strategies in the discrete time case. The duality between state estimation and control design procedures also applies for the discrete time linear quadratic controller; thus, an analogous formulation can be developed.

Consider a cost function of the form,

$$J = \frac{1}{2}\mathrm{E}\left[\mathbf{x}_{k_f}^{\mathrm{T}}\mathbf{S}_{k_f}\mathbf{x}_{k_f} + \sum_{k=0}^{k_f-1}\left(\mathbf{x}_k^{\mathrm{T}}\mathbf{Q}_k\mathbf{x}_k + \mathbf{u}_k^{\mathrm{T}}\mathbf{R}_k\mathbf{u}_k\right)\right] \tag{7.30}$$

subject to the linear system constraint,

$$\mathbf{x}_{k+1} = \mathbf{\Phi}_k\mathbf{x}_k + \mathbf{\Gamma}_k\mathbf{u}_k + \mathbf{\Lambda}_k\mathbf{w}_k \tag{7.31}$$

and to the initial condition on the random variable $\mathbf{x}_k$ satisfying

$$\mathrm{E}\left[\mathbf{x}_0\right] = \bar{\mathbf{x}}_0; \quad \mathrm{E}\left[\left(\mathbf{x}_0 - \bar{\mathbf{x}}_0\right)\left(\mathbf{x}_0 - \bar{\mathbf{x}}_0\right)^{\mathrm{T}}\right] = \mathbf{P}_0. \tag{7.32}$$

The system (7.31) can be observed through the noisy measurement equation

$$\mathbf{z}_k = \mathbf{H}_k\mathbf{x}_k + \mathbf{n}_k \tag{7.33}$$

In the above formulation, the disturbance and measurement noises, $\mathbf{w}_k$ and $\mathbf{n}_k$ respectively, are white, Gaussian and additive, and its probabilistic behavior is driven by

$$\mathrm{E}\left[\mathbf{w}_k\right] = \mathbf{0}; \quad \mathrm{E}\left[\mathbf{w}_j\mathbf{w}_k^{\mathrm{T}}\right] = \mathbf{W}_k\delta_{jk} \tag{7.34}$$

$$\mathrm{E}\left[\mathbf{n}_k\right] = \mathbf{0}; \quad \mathrm{E}\left[\mathbf{n}_j\mathbf{n}_k^{\mathrm{T}}\right] = \mathbf{N}_k\delta_{jk} \tag{7.35}$$

The current state $\mathbf{x}_k$ can be estimated from the past information database on control and measurement, that is, from $\mathbf{u}_j$ and $\mathbf{z}_j$ for $j = 0, \ldots, k$. However, a profile of the conditional probability density function of $\mathbf{x}_j$ for $j = 0, \ldots, k$ would be more useful than the control and measurement histories. As the control history is known and the noises affecting the system are a Gaussian sequence, then the state is also a Gaussian sequence; in this way, the state history can be entirely characterized by the knowledge of the state mean and covariance profile estimations, that is, the working information set would be stated as,

$$\Im[0, k] = \{\hat{\mathbf{x}}_j, \mathbf{P}_j | j = 0, \ldots, k\} \tag{7.36}$$

On the other hand, because the dynamic system (7.31) is Markovian and the measurement errors are uncorrelated in time, all the needed information about the past trajectory is contained in the present state and covariance estimates. Then the information set can be reduced to

$$\Im_k = \{\hat{\mathbf{x}}_k, \mathbf{P}_k\} \tag{7.37}$$

which is equivalent to (7.36).

The conditional estimates of actual state are given by the state's mean and covariance before and after measurement updates, and can be estimated and predicted using a Kalman filter. These estimates are as follows (Stengel (1986), Pollock (1999)),

- State prediction:

$$\hat{\mathbf{x}}_k(-) = \mathrm{E}\left[\mathbf{x}_k \,|\Im_{k-1}\right] \tag{7.38}$$

$$\hat{\mathbf{x}}_k(-) = \mathbf{\Phi}_{k-1}\hat{\mathbf{x}}_{k-1}(+) + \mathbf{\Gamma}_{k-1}\mathbf{u}_{k-1} \tag{7.39}$$

- Covariance prediction:

$$\hat{\mathbf{P}}_k(-) = \mathrm{E}\left[(\mathbf{x}_k - \hat{\mathbf{x}}_k(-))(\mathbf{x}_k - \hat{\mathbf{x}}_k(-))^{\mathrm{T}} | \Im_{k-1}\right] \tag{7.40}$$

$$\hat{\mathbf{P}}_k(-) = \mathbf{\Phi}_{k-1}\mathbf{P}_{k-1}(+)\mathbf{\Phi}_{k-1}^{\mathrm{T}} + \mathbf{\Lambda}_{k-1}\mathbf{W}_{k-1}\mathbf{\Lambda}_{k-1}^{\mathrm{T}} \tag{7.41}$$

- State prediction updating:

$$\hat{\mathbf{x}}_k(+) = \mathrm{E}\left[\mathbf{x}_k | \Im_k\right] \tag{7.42}$$

$$\hat{\mathbf{x}}_k(+) = \mathbf{x}_k(-) + \mathbf{K}_k(\mathbf{z}_k - \mathbf{H}_k\hat{\mathbf{x}}_k(-)) \tag{7.43}$$

- Covariance prediction updating

$$\hat{\mathbf{P}}_k(+) = \mathrm{E}\left[(\mathbf{x}_k - \hat{\mathbf{x}}_k(+))(\mathbf{x}_k - \hat{\mathbf{x}}_k(+))^{\mathrm{T}} | \Im_k\right] \tag{7.44}$$

$$\hat{\mathbf{P}}_k(+) = \left[\mathbf{P}_k^{-1}(-) + \mathbf{H}_k^{\mathrm{T}}\mathbf{N}_k^{-1}\mathbf{H}_k\right]^{-1} \tag{7.45}$$

with a filter gain,

$$\mathbf{K}_k = \mathbf{P}_k(-)\mathbf{H}_k^{\mathrm{T}}\left[\mathbf{H}_k\mathbf{P}_k(-)\mathbf{H}_k^{\mathrm{T}} + \mathbf{N}_k\right]^{-1} \tag{7.46}$$

and initial conditions

$$\hat{\mathbf{x}}_0(+) = \bar{\mathbf{x}}_0; \quad \mathbf{P}_0(+) = \mathbf{P}_0 \tag{7.47}$$

As can be seen, the covariance and filter gain computations are unaffected by the control signal $\mathbf{u}_k$, although it influences the propagation of the mean.

On the other hand, the optimal control law is expressed by,

$$\mathbf{u}_k = -\mathbf{C}_k\hat{\mathbf{x}}_k(+) \tag{7.48}$$

with optimal gain matrix,

$$\mathbf{C}_k = \left(\mathbf{R}_k + \mathbf{\Gamma}_k^T\mathbf{S}_{k+1}\mathbf{\Gamma}_k\right)^{-1}\mathbf{\Gamma}_k^{\mathrm{T}}\mathbf{S}_{k+1}\mathbf{\Phi}_k \tag{7.49}$$

where,

$$\mathbf{S}_k = \mathbf{Q}_k + \mathbf{\Phi}_k^{\mathrm{T}}\mathbf{S}_{k+1}\mathbf{\Phi}_k - \mathbf{\Phi}_k^{\mathrm{T}}\mathbf{S}_{k+1}\mathbf{\Gamma}_k\left(\mathbf{R}_k + \mathbf{\Gamma}_k^{\mathrm{T}}\mathbf{S}_{k+1}\mathbf{\Gamma}_k\right)^{-1}\mathbf{\Gamma}_k^{\mathrm{T}}\mathbf{S}_{k+1}\mathbf{\Phi}_k \tag{7.50}$$

subject to the final condition

$$\mathbf{S}_k|_{k=k_f} = \mathbf{S}_{k_f} \tag{7.51}$$

The optimal feedback control law treats the state estimate as if it were the actual state and by the separation principle, the estimation algorithm is independent of the control law.

Finally, combining (7.43) and (7.39), yields,

$$\hat{\mathbf{x}}_k(+) = \Phi_{k-1}\hat{\mathbf{x}}_{k-1}(+) + \mathbf{\Gamma}_{k-1}\mathbf{u}_{k-1} + \mathbf{K}_k\boldsymbol{\varepsilon}_k \tag{7.52}$$

where,

$$\boldsymbol{\varepsilon}_k = \mathbf{z}_k - \mathbf{H}_k\left[\Phi_{k-1}\hat{\mathbf{x}}_{k-1}(+) + \mathbf{\Gamma}_{k-1}\mathbf{u}_{k-1}\right] \tag{7.53}$$

is the optimal filter residual. It can be shown that $\boldsymbol{\varepsilon}_k$, is a zero-mean white random sequence with

$$\mathrm{E}\left[\boldsymbol{\varepsilon}_k\boldsymbol{\varepsilon}_k^{\mathrm{T}}\right] = \mathbf{N}_k + \mathbf{H}_k\mathbf{P}_k(-)\mathbf{H}_k^{\mathrm{T}}, \tag{7.54}$$

so, the filter residual $\boldsymbol{\varepsilon}_k$ has the effect of disturbance input on state estimate propagation.

7.4 Stochastic control for linear time invariant systems

The problem stated in equations (7.13) to (7.20) can be simplified considering a linear and time invariant system and a cost function with constant matrices. However, this assumption still uses time varying optimal control and estimation gain matrices. Notwithstanding, the behavior of the estimation and control gain matrices is almost constant, except in short intervals of time at the onset and end of the trajectory, respectively. Control gains are almost constant up to the final moments of a trajectory, when $\mathbf{x}^{\mathrm{T}}(t_f)\mathbf{S}_f\mathbf{x}(t_f)$ in (7.13) becomes more important than the integral term in the same equation. Conversely, estimation gain shows a transient behaviour at the beginning of the trajectory, when initial conditions may contain more information than the measurements, settling down to almost constant values as the times goes on. Considering the steady behaviour time much larger than transient behaviour time in gain matrices, then the stochastic cost function (7.13) is dominated by its integral terms, and constant control and estimation gains could be considered good approximations of the optimal gain profiles.

7.4.1 Asymptotic stability of the Linear Quadratic Regulator

Consider a feedback controller which minimizes the following quadratic cost function with zero terminal cost,

$$J = \frac{1}{2}\mathrm{E}\left[\int_0^{t_f} \mathbf{x}^{\mathrm{T}}(t)\mathbf{Q}\mathbf{x}(t) + \mathbf{u}^{\mathrm{T}}(t)\mathbf{R}\mathbf{u}(t)\mathrm{d}t\right] \tag{7.55}$$

subject to the linear dynamic system constraint,

$$\mathrm{d}\mathbf{x}(t) = \mathbf{F}\mathbf{x}(t)\mathrm{d}t + \mathbf{G}\mathbf{u}(t)\mathrm{d}t + \mathbf{L}(t)\mathbf{w}(t)\mathrm{d}t; \quad \mathbf{x}(0) = \mathbf{x}_0 \tag{7.56}$$

with measurement equation

$$\mathbf{z}(t) = \mathbf{H}\mathbf{x}(t) + \mathbf{n}(t) \tag{7.57}$$

for $\mathbf{F}$, $\mathbf{G}$, $\mathbf{L}$, $\mathbf{H}$ and $\mathbf{Q} > \mathbf{0}$, $\mathbf{R} > \mathbf{0}$, assumed to be constant matrices. When there is no measurement noise, the minimizing control law becomes

$$\mathbf{u}(t) = -\mathbf{C}(t)\mathbf{x}(t) \tag{7.58}$$

with gain matrix given by,

$$\mathbf{C}(t) = \mathbf{R}^{-1}\mathbf{G}^{\mathrm{T}}\mathbf{S}(t) \tag{7.59}$$

and

$$\dot{\mathbf{S}}(t) = -\mathbf{F}^{\mathrm{T}}\mathbf{S}(t) - \mathbf{S}(t)\mathbf{F} - \mathbf{Q} + \mathbf{S}(t)\mathbf{G}\mathbf{R}^{-1}\mathbf{G}^{\mathrm{T}}\mathbf{S}(t); \quad \mathbf{S}(t_f) = \mathbf{0} \tag{7.60}$$

It can be shown that the gain matrix in (7.59) guarantees global asymptotic stability of the system (Stengel (1986)); thus the closed-loop system defined by

$$\dot{\mathbf{x}}(t) = \mathbf{F}\mathbf{x}(t) - \mathbf{G}\mathbf{C}(t)\mathbf{x}(t) = \left[\mathbf{F} - \mathbf{G}\mathbf{C}(t)\right]\mathbf{x}(t) \tag{7.61}$$

is stable. This result is independent of the stability of the open-loop system.

On the other hand if t_f in (7.60) becomes infinite, then $\mathbf{S}(0)$ turns into a constant as $\mathbf{S}(t)$ is a monotone and bounded function; hence, $\lim_{t_f\to\infty}\dot{\mathbf{S}}(0) = \mathbf{0}$ and (7.60) turns into an *algebraic Ricatti equation*

$$\mathbf{0} = -\mathbf{F}^{\mathrm{T}}\mathbf{S}(0) - \mathbf{S}(0)\mathbf{F} - \mathbf{Q} + \mathbf{S}(0)\mathbf{G}\mathbf{R}^{-1}\mathbf{G}^{\mathrm{T}}\mathbf{S}(0) \tag{7.62}$$

where $\mathbf{S}(0)$ is the solution. This solution is stable with time running in reverse. Replacing $\mathbf{S}(0)$ into (7.59) and setting t_f as infinite in equation (7.55), yields

$$\mathbf{C}(0) = \mathbf{R}^{-1}\mathbf{G}^{\mathrm{T}}\mathbf{S}(0) \tag{7.63}$$

which also assures global asymptotic stability. Then, the feedback control law becomes,

$$\mathbf{u}(t) = -\mathbf{C}(0)\mathbf{x}(t) \tag{7.64}$$

which is referred to as the *linear quadratic regulator* (LQR).

Closed-loop stability of (7.61) is assured if: (a) $[\mathbf{F}, \mathbf{G}]$ is a completely controllable pair (to guarantee that all unstable modes can be controlled); (b) $\mathbf{R}$ is positive definite (guaranteeing the existence of $\mathbf{R}^{-1}$ in (7.59) and (7.63) and assuring that the control has a positive impact on the cost function); (c) $\mathbf{Q}$ is positive definite (assuring that unstable modes are penalized in the cost function and that all motions have a positive effect on J). If the system has naturally stable modes, then it is indispensable only that $[\mathbf{F}, \mathbf{D}]$ is a detectable pair (where $\mathbf{Q} = \mathbf{D}^{\mathrm{T}}\mathbf{D}$) and that $[\mathbf{F}, \mathbf{G}]$ is a stabilizable pair, as the unstable modes can be adequately controlled while the stable modes take care of themselves.

7.4.2 Asymptotic stability of the Kalman-Bucy filter

Because control and estimation are dual problems, stability of the Kalman-Bucy filter is analogue to that of the LQR. In this case, the estimation error is defined as (7.21) where the estimate $\hat{\mathbf{x}}(t)$ is generated by a constant-gain Kalman-Bucy filter,

$$\mathrm{d}\hat{\mathbf{x}}(t) = \mathbf{F}\hat{\mathbf{x}}(t)\mathrm{d}t + \mathbf{G}\mathbf{u}(t)\mathrm{d}t + \mathbf{K}\left[\mathbf{z}(t) - \mathbf{H}\hat{\mathbf{x}}(t)\right]\mathrm{d}t; \quad \hat{\mathbf{x}}(0) = \hat{\mathbf{x}}_0 \tag{7.65}$$

with steady-state filter gain given by

$$\mathbf{K} = \mathbf{P}(\infty)\mathbf{H}^{\mathrm{T}}\mathbf{N}^{-1} \tag{7.66}$$

In the above equation $\mathbf{P}(\infty)$ is the solution of the algebraic Ricatti equation

$$\mathbf{0} = \mathbf{F}\mathbf{P}(\infty) + \mathbf{P}(\infty)\mathbf{F}^{\mathrm{T}} + \mathbf{L}\mathbf{W}\mathbf{L}^{\mathrm{T}} - \mathbf{P}(\infty)\mathbf{H}^{\mathrm{T}}\mathbf{N}^{-1}\mathbf{H}\mathbf{P}(\infty) \tag{7.67}$$

The state and measurement equations take the forms (7.56) and (7.57) respectively, where $[\mathbf{F}, \mathbf{H}]$ is a completely observable par, and $\mathbf{w}(t)$ and $\mathbf{n}(t)$ are zero mean white process with

$$\mathrm{E}\left[\mathbf{w}(t)\mathbf{w}^{\mathrm{T}}(\tau)\right] = \mathbf{W}\delta(t-\tau) \tag{7.68}$$

$$\mathrm{E}\left[\mathbf{n}(t)\mathbf{n}^{\mathrm{T}}(\tau)\right] = \mathbf{N}\delta(t-\tau) \tag{7.69}$$

and $\mathbf{N}$ and $\mathbf{LWL}^{\mathrm{T}}$ assumed to be positive definite matrices.

From equations (7.21), (7.56), (7.57) and (7.65), the estimation-error dynamic is expressed by

$$\mathrm{d}\mathbf{e}(t) = (\mathbf{F} - \mathbf{KH})\mathbf{e}(t)\mathrm{d}t + \mathbf{Lw}(t)\mathrm{d}t - \mathbf{Kn}(t)\mathrm{d}t \tag{7.70}$$

It can be demonstrated that the gain matrix (7.66) guarantees global asymptotic stability of the estimator (7.70) (Stengel (1986)). The stability of the Kalman-Bucy filter is guaranteed if: (a) $[\mathbf{F}, \mathbf{H}]$ is a detectable pair, (b) $[\mathbf{F}, \mathbf{D}]$ is a stabilizable pair (where $\mathbf{LWL}^{\mathrm{T}} = \mathbf{D}^{\mathrm{T}}\mathbf{D}$); (c) $\mathbf{LWL}^{\mathrm{T}}$ is a positive semi-definite matrix and (d) $\mathbf{N}$ is a positive definite matrix.

7.4.3 Asymptotic stability of the stochastic regulator

The continuous time *stochastic regulator* or LQG (*Linear Quadratic Gaussian*) regulator is a closed-loop system consisting of the constant-gain linear quadratic regulator and the constant-gain Kalman-Bucy filter, arranged as in Figure 7.1 The driving equations are

$$\begin{aligned}
\dot{\mathbf{x}}(t) &= \mathbf{Fx}(t) + \mathbf{Gu}(t) + \mathbf{Lw}(t) && (7.71)\\
\mathbf{z}(t) &= \mathbf{Hx}(t) + \mathbf{n}(t) && (7.72)\\
\dot{\hat{\mathbf{x}}}(t) &= \mathbf{F}\hat{\mathbf{x}}(t) + \mathbf{Gu}(t) + \mathbf{K}\left[\mathbf{z}(t) - \mathbf{H}\hat{\mathbf{x}}(t)\right] && (7.73)\\
\mathbf{u}(t) &= -\mathbf{C}\hat{\mathbf{x}}(t) && (7.74)
\end{aligned}$$

with the initial conditions,

$$\mathrm{E}\left[\mathbf{x}(0)\right] = \mathbf{x}_0; \quad \mathrm{E}\left[(\mathbf{x}(0) - \mathbf{x}_0)^{\mathrm{T}}(\mathbf{x}(0) - \mathbf{x}_0)\right] = \mathbf{P}_0 \tag{7.75}$$

the gains,

$$\begin{aligned}
\mathbf{K} &= \mathbf{PH}^{\mathrm{T}}\mathbf{N}^{-1} && (7.76)\\
\mathbf{C} &= \mathbf{R}^{-1}\mathbf{G}^{\mathrm{T}}\mathbf{S} && (7.77)
\end{aligned}$$

and

$$\begin{aligned}
\mathbf{0} &= -\mathbf{F}^{\mathrm{T}}\mathbf{S} - \mathbf{SF} - \mathbf{Q} + \mathbf{SGR}^{-1}\mathbf{G}^{\mathrm{T}}\mathbf{S} && (7.78)\\
\mathbf{0} &= -\mathbf{FP} + \mathbf{PF}^{\mathrm{T}} + \mathbf{LWL}^{\mathrm{T}} - \mathbf{PH}^{\mathrm{T}}\mathbf{N}^{-1}\mathbf{HP} && (7.79)
\end{aligned}$$

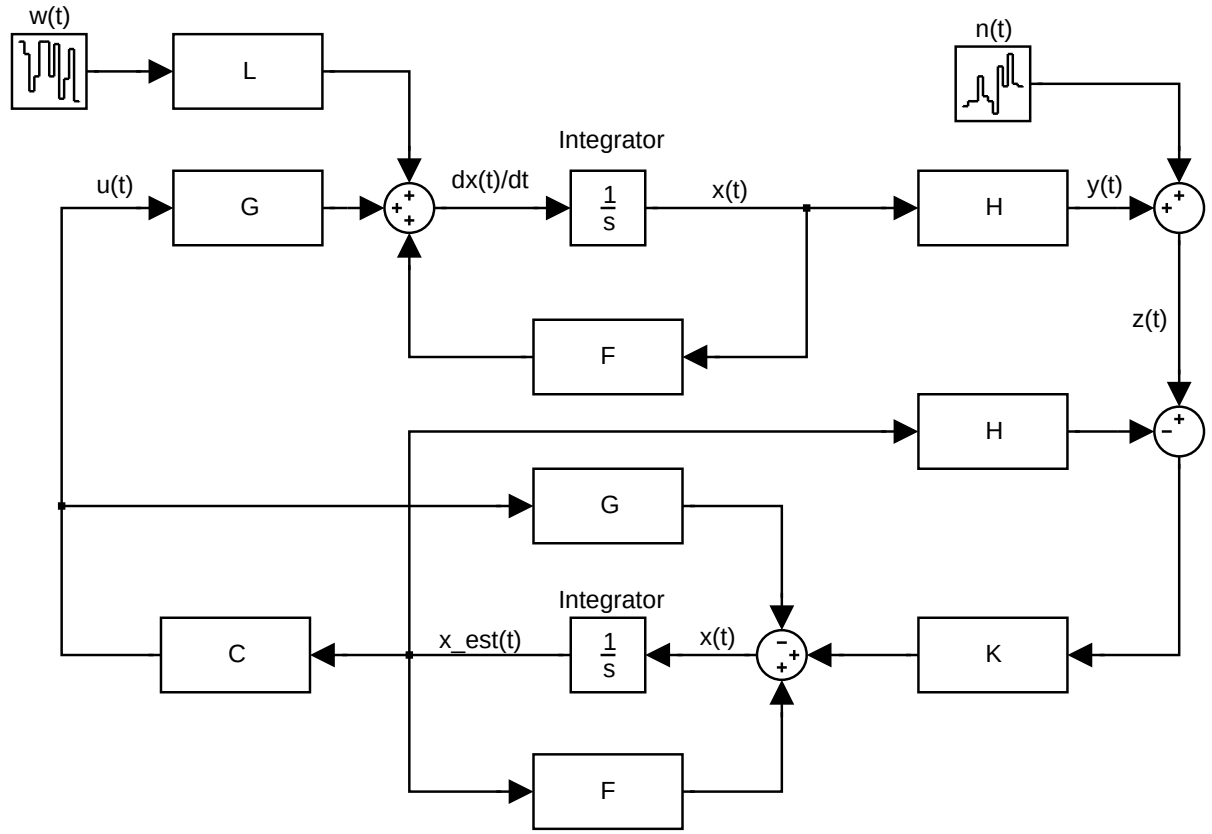

Figure 7.1: Block diagram of the stochastic regulator

Usually, the stability of the closed-loop system is described in terms of the combined state and estimation error dynamics. Using (7.56), (7.21) and (7.70) the total system equation can be expressed as

$$\begin{bmatrix} \mathrm{d}\mathbf{x}(t) \\ \mathrm{d}\mathbf{e}(t) \end{bmatrix} = \begin{bmatrix} \mathbf{F}-\mathbf{GC} & \mathbf{GC} \\ \mathbf{0} & \mathbf{F}-\mathbf{KH} \end{bmatrix} \begin{bmatrix} \mathbf{x}(t) \\ \mathbf{e}(t) \end{bmatrix} \mathrm{d}t + \begin{bmatrix} \mathbf{L} & \mathbf{0} \\ \mathbf{L} & -\mathbf{K} \end{bmatrix} \begin{bmatrix} \mathbf{w}(t) \\ \mathbf{n}(t) \end{bmatrix} \mathrm{d}t \tag{7.80}$$

Finally, it can be shown (Stengel (1986)) that the stability of the total system is described by the separately evaluated stability of the LQR and the Kalman-Bucy filter.

7.5 Control design problem statement

The winged bridge of section 6.3 was controlled using a stochastic regulator algorithm inasmuch as it is supposed that there exists noise in the sensor devices, in the form of an additive white noise

applied to the observation equation and that the system is subjected to buffeting forces, which can be understood as a disturbance to the self-excited system. The aerodynamic coefficients given in Table 7.1 are supposed to relate the wind turbulence and the buffeting forces acting on deck and control surfaces (c.f. equations (5.19),(5.20) and (5.21)).

Table 7.1: Aerodynamic lift, drag and moment coefficients of deck and control surfaces

Parameter	**Value**	**Parameter**	**Value**
C_L	0.0942	C'_L	1.9050
C_D	0.3230	C'_D	0.0000
C_M	0.0104	C'_M	0.2717

To apply the stochastic regulator, the disturbances of the system must be modelled as Gaussian white noises. This can be accomplished modelling the horizontal and vertical wind fluctuations ($u(t)$ and $v(t)$ respectively) as a filtered white noise using an autoregressive (AR) model estimated via Yule-Walker method (Papoulis (1991)). As the simulation was carried out on a digital computer, a sampled realization of the both wind fluctuations, $u[n]$ and $v[n]$ respectively, was simulated for a sampling time of $T = 0.05$ seconds taking into account that a 20 Hz (125.66 rad/s) sampling frequency is large enough to assure that all the main participating modes of the BWCS system become excited (c.f. Tables 5.1 and 6.1). In the case of the vertical wind fluctuation, it can be modelled from the Simiu and Scanlan spectrum (c.f. page 16) and the AR model

$$v[n] + a_1 v[n-1] + \cdots + a_N v[n-N] = \sqrt{\text{var}(w)}w[n] \tag{7.81}$$

which models adequately the wind fluctuation signal; this equation has a transfer function

$$L(z) = \frac{\sqrt{\text{var}(w)}}{1 + a_1 z^{-1} + \cdots + a_N z^{-N}} \tag{7.82}$$

where $L(z)$ is the *innovations filter* of $v[n]$, N is the order of the AR model and var(w) represents the variance estimate of the zero-mean unit-variance Gaussian white noise input of (7.82), $w[n]$. An analogous formulation can be derived for the horizontal wind spectrum, assuming that both vertical and horizontal spectrums are by no means correlated.

The coefficients of (7.81) were calculated as follows: from the power spectral density of the process, the autocorrelation function was estimated using the inverse Fourier transform; then the Levinson-Durbin recursion algorithm was used to solve the resulting set of Yule-Walker equations

(c.f. section 3.2); finally, the filter (7.82) was recasted into a discrete state space form and then into a continuous one (writing it in a "formal" way), as sketched in section 3.2:

$$\dot{\mathbf{y}}_{\text{fluc}}(t) = \mathbf{A}_{\text{fluc}}(t)\mathbf{y}_{\text{fluc}}(t) + \mathbf{B}_{\text{fluc}}(t)\mathbf{w}(t) \tag{7.83}$$

$$\boldsymbol{\eta}(t) = \mathbf{D}_{\text{fluc}}(t)\mathbf{y}_{\text{fluc}}(t) + \mathbf{F}_{\text{fluc}}(t)\mathbf{w}(t) \tag{7.84}$$

where

$$\boldsymbol{\eta} = \begin{bmatrix} \frac{u(t)}{\bar{U}} \\ \frac{v(t)}{\bar{U}} \end{bmatrix} \tag{7.85}$$

It must bear in mind that the aforementioned AR model is dependent on the average wind velocity; so for a given mean wind speed, the filter is linear and time invariant. Also it must be said that an 8 degree AR model was employed for both vertical, and horizontal wind fluctuation models.

On the other side, the BWCS model can be represented as explained in section 6.2,

$$\dot{\mathbf{y}}_{\text{bwsc}}(t) = \mathbf{A}_{\text{bwcs}}(t)\mathbf{y}_{\text{bwcs}}(t) + \mathbf{B}_{\text{buf}}(t)\boldsymbol{\eta}(t) + \mathbf{B}_{\text{cs}}(t)\mathbf{u}(t) \tag{7.86}$$

$$\mathbf{u}_{\text{bwcs}}(t) = \mathbf{D}_{\text{fluc}}\mathbf{y}_{\text{bwcs}}(t) \tag{7.87}$$

where,

$$\mathbf{B}_{\text{buf}}(t) = \bar{U}^2 \begin{bmatrix} \mathbf{0} \\ \bar{\mathbf{M}}^{-1} \\ \mathbf{0} \\ \mathbf{0} \\ \mathbf{0} \end{bmatrix} \begin{bmatrix} \mathbf{T}_d^{lg}\mathbf{v}_d & \mathbf{T}_{w1}^{lg}\mathbf{v}_{w1} & \mathbf{T}_{w2}^{lg}\mathbf{v}_{w2} \end{bmatrix} \begin{bmatrix} \mathbf{a}_{bud} & \mathbf{a}_{bvd} \\ \mathbf{a}_{buw1} & \mathbf{a}_{bvw1} \\ \mathbf{a}_{buw2} & \mathbf{a}_{bvw2} \end{bmatrix} \tag{7.88}$$

Equations (7.84) and (7.87) can be melded in one,

$$\begin{bmatrix} \dot{\mathbf{y}}_{\text{bwcs}}(t) \\ \dot{\mathbf{y}}_{\text{fluc}}(t) \end{bmatrix} = \begin{bmatrix} \mathbf{A}_{\text{bwcs}}(t) & \mathbf{B}_{\text{buf}}(t)\mathbf{D}_{\text{fluc}} \\ \mathbf{0} & \mathbf{A}_{\text{fluc}}(t) \end{bmatrix} \begin{bmatrix} \mathbf{y}_{\text{bwcs}}(t) \\ \mathbf{y}_{\text{fluc}}(t) \end{bmatrix} + \begin{bmatrix} \mathbf{B}_{\text{cs}}(t) \\ \mathbf{0} \end{bmatrix} \mathbf{u}(t) + \begin{bmatrix} \mathbf{B}_{\text{buf}}(t)\mathbf{F}_{\text{fluc}}(t) \\ \mathbf{B}_{\text{fluc}}(t) \end{bmatrix} \mathbf{w}(t) \tag{7.89}$$

with a corresponding observation equation,

$$\mathbf{z}(t) = \begin{bmatrix} \mathbf{D}_{\text{bwcs}} & \mathbf{0} \end{bmatrix} \begin{bmatrix} \mathbf{y}_{\text{bwcs}}(t) \\ \mathbf{y}_{\text{fluc}}(t) \end{bmatrix} + \mathbf{n}(t) \tag{7.90}$$

Observe that, both equations have the forms (7.71) and (7.72) respectively.

There are a number of different topics concerning the design, constraints, implementation and evaluation of the control algorithm. In the following, a detailed examination of those topics will be carried on.

7.5.1 Evaluation criteria and control strategy constraints

The required control algorithm must furnish the system stability on the selected wind design range, having a good performance over it; in this way, some requirements and constraints should be considered:

- The control surfaces algorithm must assure in low wind speed cases serviceability issues in the structure; in high wind velocities the structural safety is of maximum concern. This is achieved by minimization of the bridge girder vibrations.

- The aerodynamic/aeroelastic behaviour of the bridge and flaps discussed previously has been done for small displacements and rotations. In this way, for large displacements, the behaviour of the system cannot be adequately modelled. Therefore, assuming that the bridge deck dragging and heaving displacements are small, flap and deck pitching must be constrained to lay in the range $|\alpha_{w,d}| < 15°$ (Ostenfeld and Larsen (1992)). This restriction also must be imposed to avoid flow separation around control surfaces.

- Shear and moments forces evaluated in the bridge deck connection and along the deck must be preserved between acceptable bounds.

- The deviation of the tension in the hangers and main cable from the nominal pretension must be kept as small as possible. That is, the tension in the cables should neither approach zero nor surpass a service maximum load. This criterion is selected to reduce the likelihood of failure and the unseating of the cables (Dyke et al. (2000),Dyke et al. (2003)). In this way, the tension in cables should remain within a recommend range of $0.2T_f$ to $0.7T_f$ where T_f is the cable tension failure load.

The former two items are the only ones considered in this work, as the others are only taken into account when a complete bridge model is considered.

7.5.2 Control system design

For a given mean wind velocity $\bar{U}$, the system (7.89) is linear and time invariant. On the other side, the stochastic regulator estimates two gain matrices: one corresponding to the linear quadratic regulator and other corresponding to the Kalman filter; these two matrices show a good performance of the controller in a neighborhood of $\bar{U}$. However, for lower or greater wind velocities the performance of the corresponding stochastic regulator may be poor or, even, could destabilize the system. Therefore, the basic idea of the control algorithm is that for a set of m wind speeds

$$\left\{\bar{U}_1, \bar{U}_2, \ldots, \bar{U}_m | \bar{U}_i < \bar{U}_{i+1}, i = 1, \ldots, m-1\right\}, \tag{7.91}$$

covering the wind design range, a corresponding set of gains should be computed. So, for a given wind speed $\bar{U} \in \left[\bar{U}_1, \bar{U}_m\right]$, the respective gain matrices are calculated by interpolation, approximating in this way a wind-speed variant gain, which is not exactly the same at the selected operating points, but is close in the sense of the picked performance index. As was studied in section 6.3, the critical wind velocity of the winged bridge in open loop configuration is 10.7 m/s; in this work, the control algorithm was designed such that it guarantees the stability of the bridge in the range of velocities from 5 m/s up to approximately twice the uncontrolled bridge critical velocity, that is, 21 m/s. So, it is very important to analyze the performance of the control strategy for the different stochastic regulators in $\left[\bar{U}_1, \bar{U}_m\right]$, taking in mind several aspects like sensor and actuator dynamics, selection of the cost function and selection of the parameters of the control surfaces. These issues will be addressed in the following.

Position of the sensors and control devices

Generally sensors and actuators should be positioned such that all major participating modes (i.e. those which should be controlled) are observable and controllable. Also, it is very important to take into account that locations of both sensors and actuators close to or on a modal point should be avoided. So a careful study of the positioning of these devices must be carried out (Soong (1990)). In this study, the analysis of the position of those sensors and actuators was not made, inasmuch as, it is only important when a full model bridge is considered.

Sensors

There are two types of sensors installed on the bridge: motion sensors and wind velocity sensors. Motion sensors are positioned in the nodes of the finite deck-elements of the bridge model and flaps along the span. They measure deck-dragging, -heaving and -pitching velocity and displacement and the rotation angle and torsional velocity of the control surfaces[1]. Each of the measured responses is affected by a zero mean additive Gaussian white noise $\mathbf{n}(t)$, which represents the noise in the sensor devices.

On the other hand, wind velocity sensors in the vertical and horizontal directions were located in the middle of each bridge deck or control surface finite element; it was be assumed that these sensors give perfect measurements.

Both type of sensors, movement and wind velocity, have a sampling rate of 20 Hz, following the criterion stated in page 72. As can be seen this frequency is greater than two times the maximum bridge frequency we are interested in controlling (obeying Nyquist sampling theorem). This is to avoid aliasing in recorded signals.

Finally, it is important to note that sensor devices-structure interaction are in this study neglected. That is, sensor measures are supposed not to be affected by deck vibration. In the following an almost-free noise sensor channel will be assumed for the simulations. Section 7.5.3 deals with noise in the measurement signals.

Control devices

The control system employs actuators placed in the nodes of the finite element model on both the main and side spans; each one of these actuators is considered to have a maximum capacity; so, in a real implementation, the model should have a saturator corresponding to the maximum load given by the actuators. However, in the present study, the actuator dynamics, the maximum moment capacity of the actuators and the actuator-structure interaction is neglected. In this way, they are considered to be ideal.

[1]It must be taken into account that it is desirable to have a sensor for velocity, as the differentiation of a displacement noisy measure is a bad estimate of the wind velocity inasmuch as noise effects would increase.

Control algorithm

As stated before, it is assumed in this study that the sensor gives perfect observations affected by additive Gaussian white noise, that ideal control devices are employed, and that there are external disturbances acting on the system. In this way, the state can be estimated using a Kalman filter.

As it is assumed that the control algorithm would be implemented in a digital equipment, the sensor signals must be discretized and digitalized before show them to the control algorithm, also the control signals must be made analogue, before apply them to the control device. So a discrete-time control algorithm must be employed along with A/D and D/A converters, assuming that the digital implementation works in 16 or 32 bits of precision. In this manner, the controller in its final form should be converted to a discrete time fashion, using a zero-order hold on the inputs transformation (MATLAB's `c2d` command (Chen (1999))) such that the controller has the same sampling time as the sensors, that is, $T = 0.05$ seconds.

Figure 7.2 shows block diagram representation of the control system.

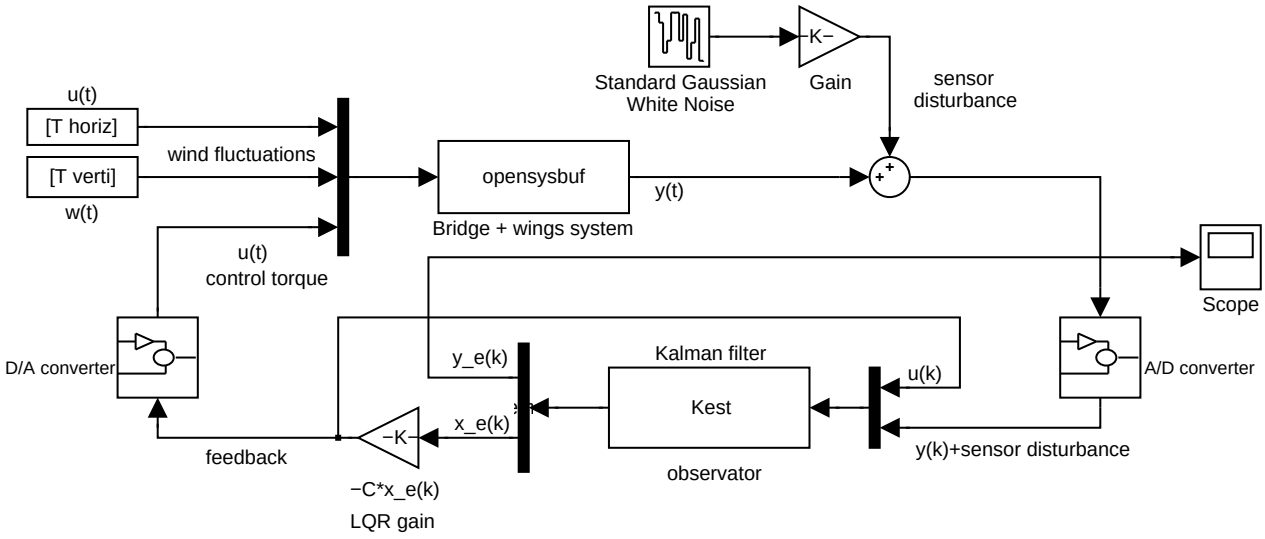

Figure 7.2: Block diagram representation of the control system

Selection of the cost function

As was seen previously the basic idea of the optimal control is to minimize a criterion and in this way improve the efficiency of the control algorithm; in the case of the stochastic regulator for a linear time invariant system, equation (7.55) represents the mentioned cost function: its weighting matrices $\mathbf{Q}$ and $\mathbf{R}$, were chosen such that the total energy corresponding to the winged bridge and the control forces were as small as possible. The total energy of the bridge is given by the sum of the kinetic and the elastic energy stored in the structure. In this way, matrices $\mathbf{Q}$ and $\mathbf{R}$ were selected such that

$$\mathbf{x}^{\mathrm{T}}(t)\mathbf{Q}\mathbf{x}(t) = \beta(\bar{U})\left(\frac{1}{2}\dot{\mathbf{x}}_d^{\mathrm{T}}(t)\mathbf{M}_d\dot{\mathbf{x}}_d(t) + \frac{1}{2}\mathbf{x}_d^{\mathrm{T}}(t)\mathbf{K}_d\mathbf{x}_d(t)\right) \tag{7.92}$$

and

$$\mathbf{R} = \mathbf{I} \tag{7.93}$$

where $\beta(\bar{U}) > 0$ stands for a weighting parameter dependent on the mean wind speed which must be tuned. In this case, when $\beta(\bar{U})$ is large, the movement of the bridge is minimized regardless of the control forces employed. The converse happens when $\beta(\bar{U})$ approaches zero. It must bear in mind that the minimization of the total energy attempts towards the fulfillment of the first evaluation criterion stated in section 7.5.1, while the minimization of the control forces tries to accomplish the second evaluation criterion; accordingly, a compromise between the control forces and the bridge total energy must be performed.

Figure 7.3 (left) shows the influence of the variation of the weighting parameter $\beta(\bar{U})$ and the change of wind speed in the increase of the critical velocity for the winged bridge whose parameters appear in Table 6.1, while Figure 7.3 (right) shows the variation of these parameters and its effect on the maximum absolute rotation of the deck or control surfaces. The last figure was made in the following way: a realization of the wind fluctuation was input to the winged bridge system in a closed loop configuration, subsequently, the time history of the rotations of the deck and control surfaces was analyzed for a maximum absolute value. It must be said that an more appropriate analysis can be done using excursion probabilities (Soong and Grigoriu (1993)) using a method for calculating probabilities of structural failure like the one stated in Hurtado and Alvarez (2001) and Hurtado and Alvarez (2003), however, this analysis will not be addressed in this thesis.

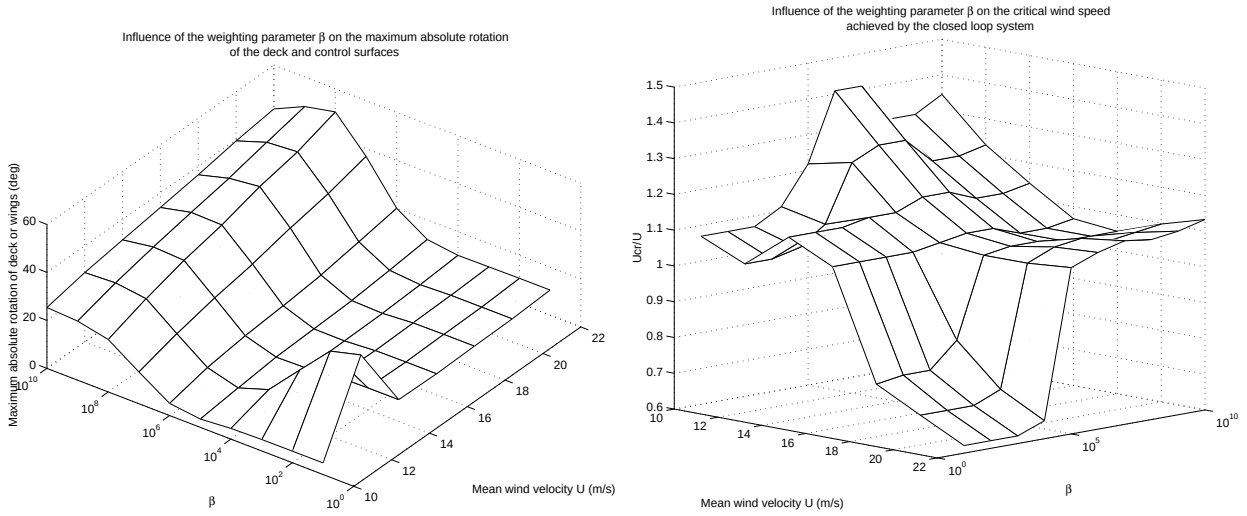

Figure 7.3: Influence of the variation of the weighting parameter β and the mean wind velocity on the maximum absolute rotation of the deck and control surfaces (left) and on the critical wind speed/mean wind speed ratio (right) for the controlled bridge

In the the present study, $\beta(\bar{U})$ was set to 3×10^5 for all wind velocities since from Figure 7.3 it can be observed that for this value of $\beta(\bar{U})$ the performance criteria stated in section 7.5.1, are accomplished inasmuch as the the critical wind speed is maximized while the deck vibrations are minimized and the maximum rotation of the control surfaces and deck remains bounded for an increasing velocity. An unexpected behavior was observed in Figure 7.3 (left) inasmuch as for a low value of $\beta(\bar{U})$ (between 1 and 1000) and low velocities (10-14 m/s) the maximum absolute value of the flaps rotation was very high, making its use infeasible in these ranges.

Selection of the damping and stiffness parameters of the control surfaces

The design process involves the selection of the different structural parameters, such that the bridge will have an adequate behaviour during its lasting life. In this way, the choice of the stiffness and damping parameters of the wings attached to the deck was carried out. Figure 7.4 shows the influence of these parameters on the critical wind speed of the bridge. It can be easily seen that the most important parameter in the design of the wings is the damping since for larger damping ratios the structure can withstand higher wind speeds.

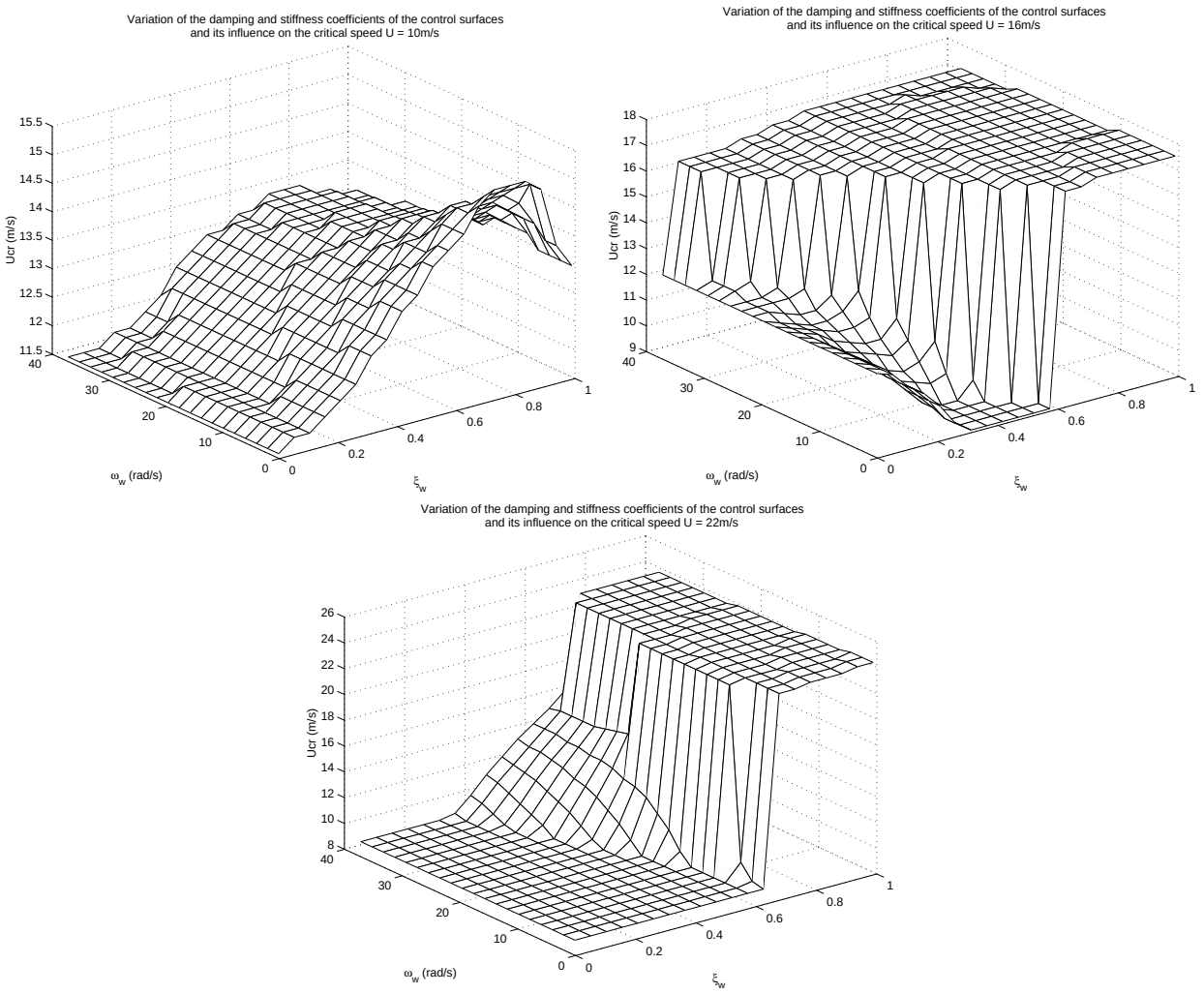

Figure 7.4: Influence of the variation of the damping and stiffness parameters of the control surfaces on the critical speed of the closed loop bridge-wind-control surfaces system for $\bar{U} = 10$, 16 and 21 m/s

7.5.3 Evaluation of the control strategy

A desirable requirement in control systems is that the system must be observable and controllable. In the case of the bridge-wind-control surfaces model, the controllability was checked. From linear system theory, it is well know that a system is controllable if the matrix

$$\left[\begin{array}{cccccc} \mathbf{A} & \mathbf{AB} & \mathbf{A}^2\mathbf{B} & \cdots & \mathbf{A}^{n-1}\mathbf{B} \end{array} \right] \tag{7.94}$$

has a rank n where n is the dimension of the corresponding state space vector. Then for the BWCS system in the open loop configuration to be controllable, the matrix (7.94) must have a

rank of 14. However, its rank is 8. As the system was not controllable, then the "stabilizability" of it was checked. It could be observed that all modes with a nonzero imaginary part were controllable: it means that the fluttering can be alleviated by the control algorithm; also, it was observed that the noncontrollable modes take care of themselves.

Figure A.6 shows a pole map of the closed-loop system for an increasing wind velocity and a stochastic regulator design speed of $\bar{U} = 21$ m/s. As can be seen, the closed loop system critical velocity is 22.5 m/s, corresponding to flutter. In this way, the flutter wind speed of the deck with flaps is 118 % higher compared to the deck without control surfaces and 110 % higher compared to the open loop system. It is interesting to note that the controller made for a design speed of $\bar{U}$ = 21 m/s perfectly controls the wind over the desired interval, however, as was discussed before, it is better to calculate a set of gains corresponding to the set of velocities (7.91), inasmuch as the system dynamic properties vary considerably with the mean wind velocity, so this unique control law may not be efficient for the whole range of wind speeds.

In the following, the behavior of the controlled bridge will be analyzed for different wind speeds, comparing it with the one of the bridge without control surfaces and the winged bridge in open loop configuration.

Behavior of the system controlled by an LQR algorithm without buffeting forces

Figure 7.5 shows a time history plot of the variation of the rotations of the wings and the heaving and pitching deck displacements of the winged bridge in closed loop configuration controlled by an LQR algorithm in the presence of no buffeting forces, no noise in the sensors and an average wind speed of 12 m/s. The controller must stabilize the bridge given that the initial displacements of the bridge are $h_d = 1/B_d$ and $\alpha_d = 0.1$ radians. It was observed that this controller can quickly stabilize the bridge for all velocity ranges. However for very high wind velocities the criteria stated in section 7.5.1 are not fulfilled. On the other hand, Figure 7.6 presents the variation of the control force with time. Both figures suggest that the optimal control law occurs when the leading wing moves in the opposite direction and the trailing wing rotates in the same direction with respect to the deck motion, also that both movements have a slight phase lead with respect to the deck rotation. This phase lead is very important because the aeroelastic forces controlling the bridge and induced by the wings begin to counteract the deck vibration in the same instant

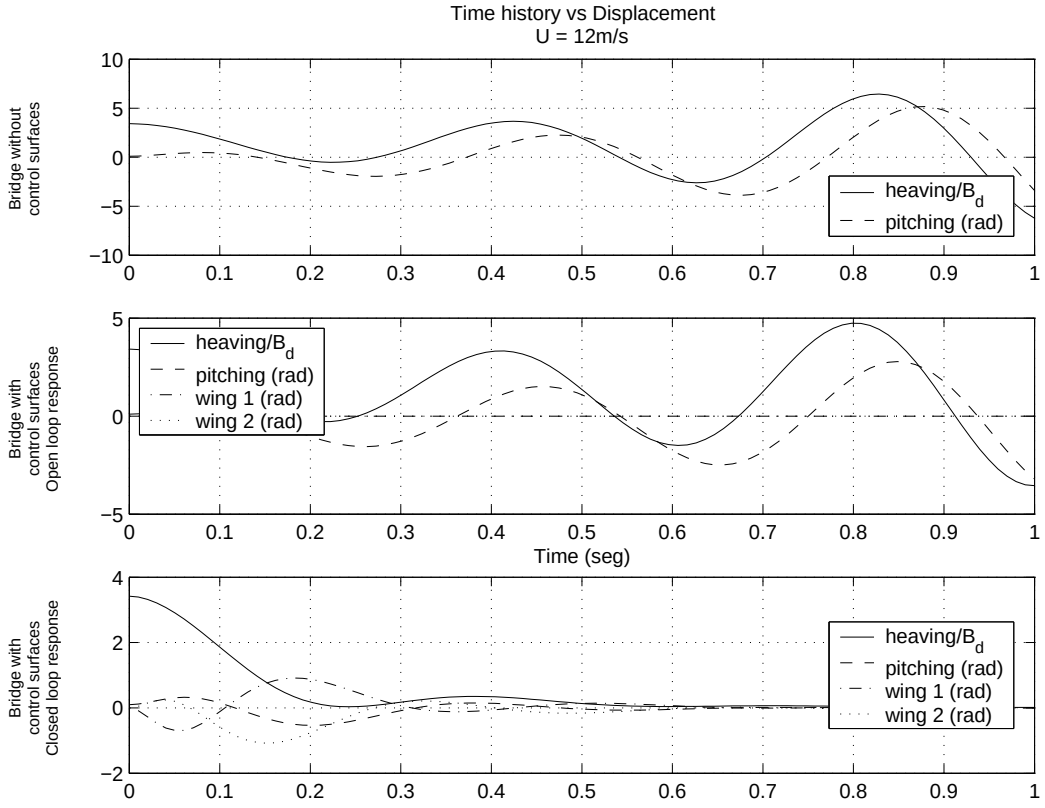

Figure 7.5: Variation of the deck heaving and pitching and rotations of the control surfaces for a BWCS system controlled by an LQR algorithm in the presence of no buffeting forces, for $\bar{U} =$ 12 m/s

the movement of the deck begins. This is in agreement with the investigations of Cobo del Arco and Aparicio (1998) and Huynh and Thoft-Christensen (2001). Figure 7.5 also shows an example of the fluttering in the deck without flaps and the winged bridge in the open loop case. Observe that flutter is characterized by an increasing oscillating movement of the deck displacements.

Variation of the damping and stiffness parameters of the bridge-wind-control surfaces system for an increasing wind speed

Each pole can be related to a pair of damping and stiffness coefficients by means of equation (5.60). Appendix A shows various pole maps of the BWCS system for several design conditions, along with the damping and stiffness parameters related to these eigenvalues. It can be easily seen that for a mean wind speed less than 10 m/s, the frequencies of the controlled bridge are almost the same as the uncontrolled one, nevertheless, the attachment of the controlled surfaces

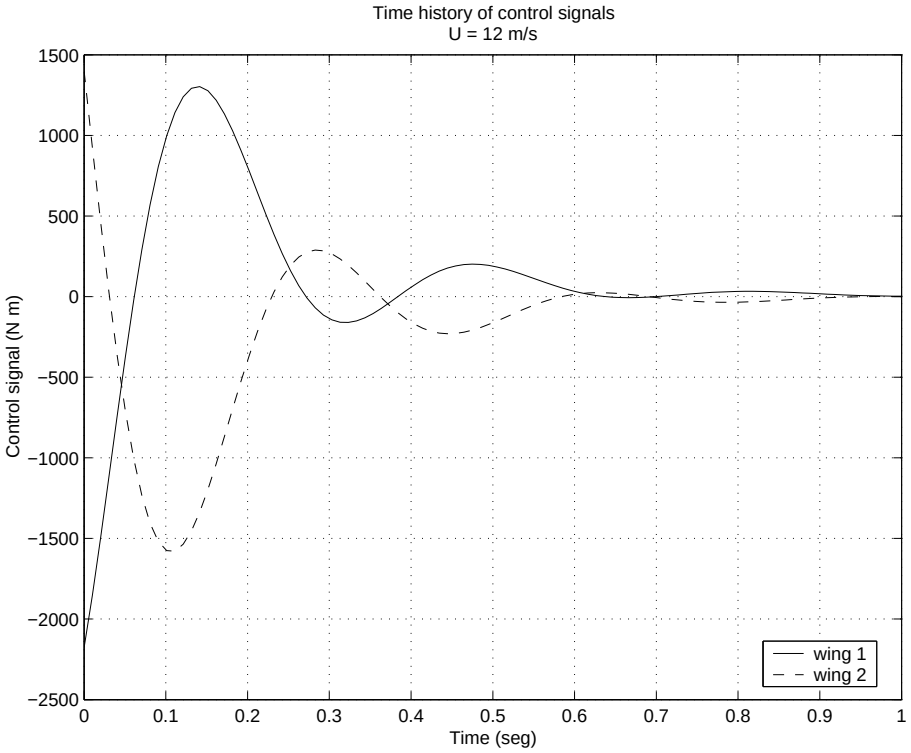

Figure 7.6: Variation of the control signal for a bridge wind control surface system controlled by an LQR algorithm in the presence of no buffeting forces, for $\bar{U} = 12$ m/s

to the deck has the effect of increasing the damping of the different vibration modes of the system; this damping increases up to the design speed of the controller; then, for greater velocities the damping suddenly falls until the failure of the system occurs, inasmuch as at least one of the poles moves to the right semi-plane. Relating the pole map of the variable gain stochastic regulator (Figure A.8) with the ones corresponding to the stochastic regulators designed for $\bar{U} = 10$, 16 and 21 m/s (Figures A.4, A.5 and A.6 respectively), one can see that this controller increases substantially the damping and stiffness of the vibration modes of the bridge. The variable gain LQR also shares this property. In all cases, the controlled bridge failed due to fluttering.

It is worth remembering that in all the BWCS systems in closed loop configuration showed in appendix A the coupling among vibration modes occurs. This is a typical phenomenon present in long span bridges which is desirable to avoid (Katsuchi et al. (1999)). Maybe choosing a different combination of matrices $\mathbf{Q}$ and $\mathbf{R}$, the veering of the eigenvalues loci can be forced, since the strong coupling between modes are the main source of the negative damping that leads to flutter (Chen et al. (2000)).

Finally, it was observed that the vibration modes corresponding to the control surfaces remain almost constant until the failure of the bridge.

Behavior of the system controlled by the stochastic regulator including self-excited and buffeting forces

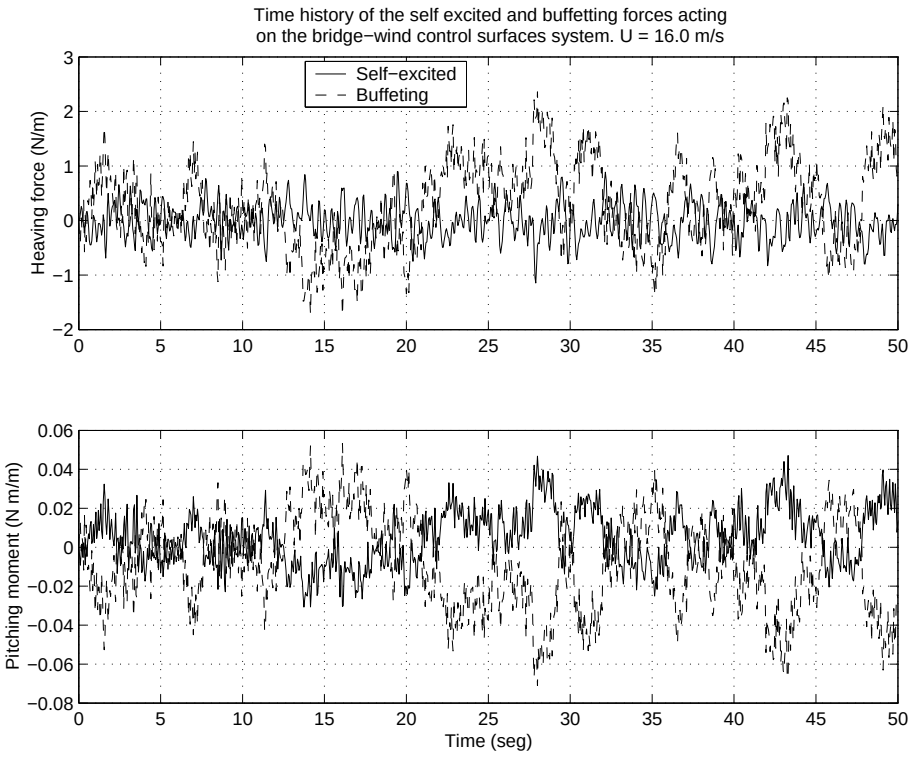

Figure 7.7: Time history of the self-excited and buffeting forces acting on the BWCS system for $\bar{U} = 16$ m/s

Figure 7.7 shows that the buffeting forces acting on the BWCS system are greater than self-excited forces; as in the employed stochastic regulator strategy the buffeting forces are treated as disturbances to the system, one can foretell that such large turbulence-induced forces are a serviceability problem to cope with. Bucher and Lin (1988, 1989) stated that these forces due to turbulence in the flow can have a stabilizing or destabilizing effect in bridges. For the present case, they destabilize the structure, as is discussed in detail in Chapter 8. From Figures 7.8 and 7.9 one can note that the these turbulence-induced disturbances can be controlled by the use of control surfaces for low speed cases. However, in turbulent winds, although buffeting heaving vibrations can be stabilized over a wide range of wind velocities, they cannot become enclosed

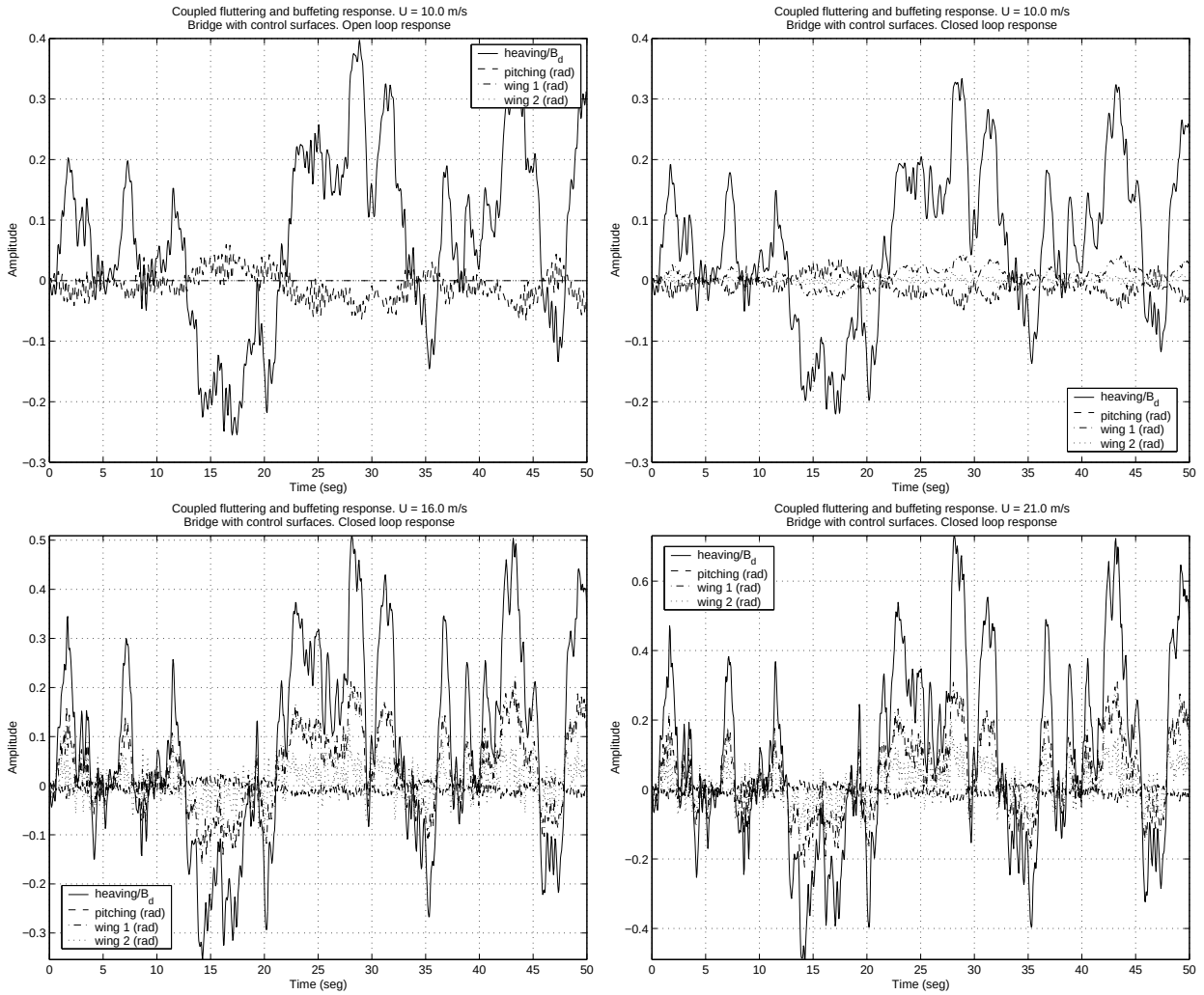

Figure 7.8: Time history of the displacements of in the different degrees of freedom for a , for $\bar{U} = 10$, 16 and 21 m/s

into safe bounds. This is serious drawback that can limit the use of separated wings as a mean of controlling wind-induced vibrations. This figure also shows that the control surfaces effectively manages the torsional vibrations of the bridge; thereby one can conclude that the main stabilizing action comes from the torque induced by the lifting forces over the control surfaces.

Figure 7.7 shows the variation of the control torque with time for $\bar{U} = 16$ m/s; in this case the leading wing has the greater impact on the deck vibrations control. This phenomenon is explained in the following lines. From the aerodynamic coefficients in Table 7.1, it should be noted that the vertical wind fluctuation has the greater influence on the bridge response to buffeting. Given that all coefficients in Table 7.1 are positive, equations (5.19) and (5.21) highlight the fact that

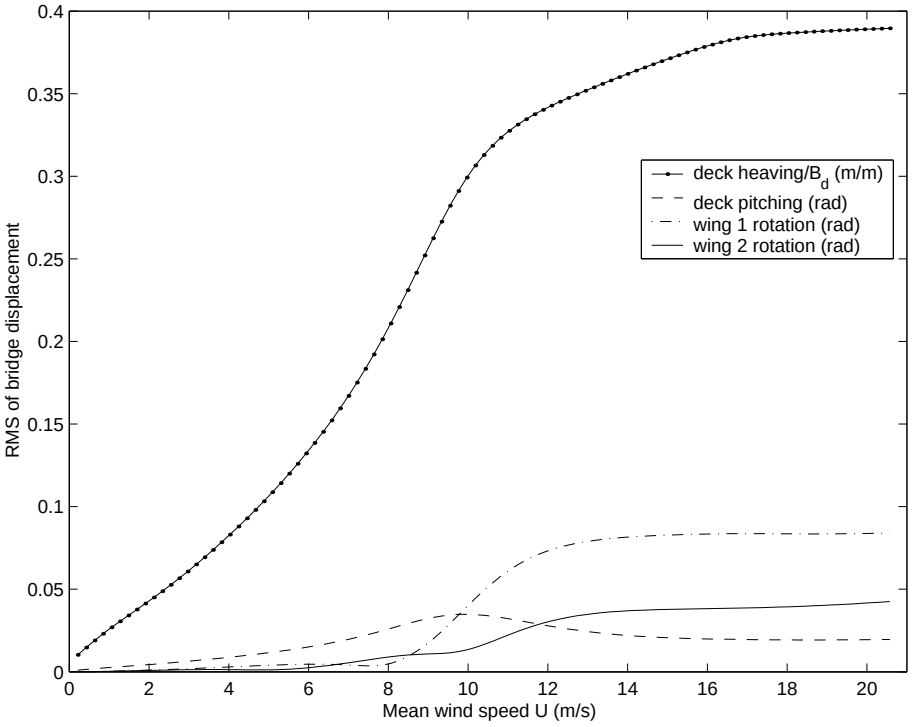

Figure 7.9: Root mean square of the BWCS in closed loop configuration displacement for an increasing wind speed

when the vertical wind fluctuation around the mean is positive (downward direction), a positive lift force and a negative torque (counterclockwise direction) act on the BWCS system. The control system is entrusted to rotate the wings to generate the balancing forces; in this way, both wings rotate in a positive direction (clockwise) to generate the equilibrium lift forces; however, the trailing control surface rotates in a lesser degree, such that a positive torque is generated by the pair of wings to cancel the buffeting twisting force out. The converse rotations happen when the vertical wind fluctuation is negative (however, the leading control surface still has the largest rotation). This is a notable difference of the BWCS system behaviour compared to the one taken over when there are no buffeting forces (steady wind flow). Therefore, it can be concluded that the leading control surface plays the most important role in the control system.

The performance of the control system in the heaving mode for highly turbulent winds, can be improved if wider wings are employed, since the buffeting forces in the vertical direction are proportional to the width of the surface. However, this is not an efficient solution, inasmuch as it would increase the dead load of the bridge and the construction costs.

Frequency response the controlled system

The frequency response is a representation of the system response to sinusoidal inputs at different frequencies. Figure 7.10 shows the Bode plot of the magnitude of the transfer function matrix $\mathbf{H}(j\omega)$ of the open and close loop winged systems between the buffeting forces and the deck displacements for different mean wind speeds. This matrix is given by, (Szidarovszky and Bahill (1998)),

$$\mathbf{H}(j\omega) = \mathbf{D}\left(j\omega\mathbf{I} - \mathbf{A}\right)^{-1}\mathbf{B} \tag{7.95}$$

provided that, $U(t) = \bar{U}$. Also, Figure 7.11 shows the power spectral density of the pitching and heaving deck displacement response for different wind speeds in turbulent flow. It can be observed that the vertical wind fluctuation has a greater influence on the heaving and pitching response of the winged bridge; also, the frequency response of both the open and closed loop cases is almost the same for low wind speeds; in this case, the system vibrates almost in the same frequency of the corresponding vibration mode; however, for greater wind speeds, it can be concluded that the controlled surfaces smooths the frequency response, so that there are not large peaks of response; furthermore, the pitching mode in high velocities has a component corresponding to the vibration of the control surfaces. Finally, it can be said that the buffeting component drives the bridge to move with lower pitching vibration frequencies.

Influence of the noise on the sensors

To study the influence of the noise in the system velocity and displacement $\mathbf{n}(t)$, its covariance $\mathrm{E}[n_i(t)n_j(t)] = \sigma_i^2\delta_{ij}$ should be changed modelling different signal-noise ratios (SNRs). In this way, the study begins with high ratios (for example 40 decibels), which model almost noise-free transmission channels, decreasing the relation up to 3 decibels to analyze the performance when noisy sensed signals are employed. Then σ_i, can be calculated from the relationship,

$$\text{SNR (dB)} = 20\log_{10}\left(\frac{\text{RMS}\left([\mathbf{D}_{\text{bwcs}}\mathbf{y}_{\text{bwcs}}]_i\right)}{\sigma_i}\right) \tag{7.96}$$

where RMS stands for the root mean square measure of the signal.

Two situations were modelled: one in which the SNR was approximately 3 dB and other for 36 dB. It was observed that noisy measurements do not make the bridge unstable, indeed the

critical velocity of the bridge grew up: for example, for a design speed of 16 m/s, in the 36 dB case the critical velocity was $U_{cr} = 18.0$ m/s while in the 3 dB situation was $U_{cr} = 17.5$ m/s. This behavior was not expected. However, both the variance of the displacement response and the variance of the control force increases for the noisy case, in the 36 dB case the standard deviations of the rotations for the leading and trailing control surfaces were 116.7 and 46.1 N m respectively, while in the 3 dB case were 140.7 and 81.9. In this way, the response of the trailing wing notably increased. Noise in the sensors is not desirable, inasmuch as the control system requires higher control forces, with stronger 0 to 40 rad/seg components, as can be depicted from Figure 7.12.

A robustness analysis of the controlled BWCS system including a controller delay study was not performed, in view of the fact that the classical phase and gain margin concepts cannot be directly applied to MIMO systems. In this case, some special techniques of μ-analysis should be applied, as described in Field et al. (1996).

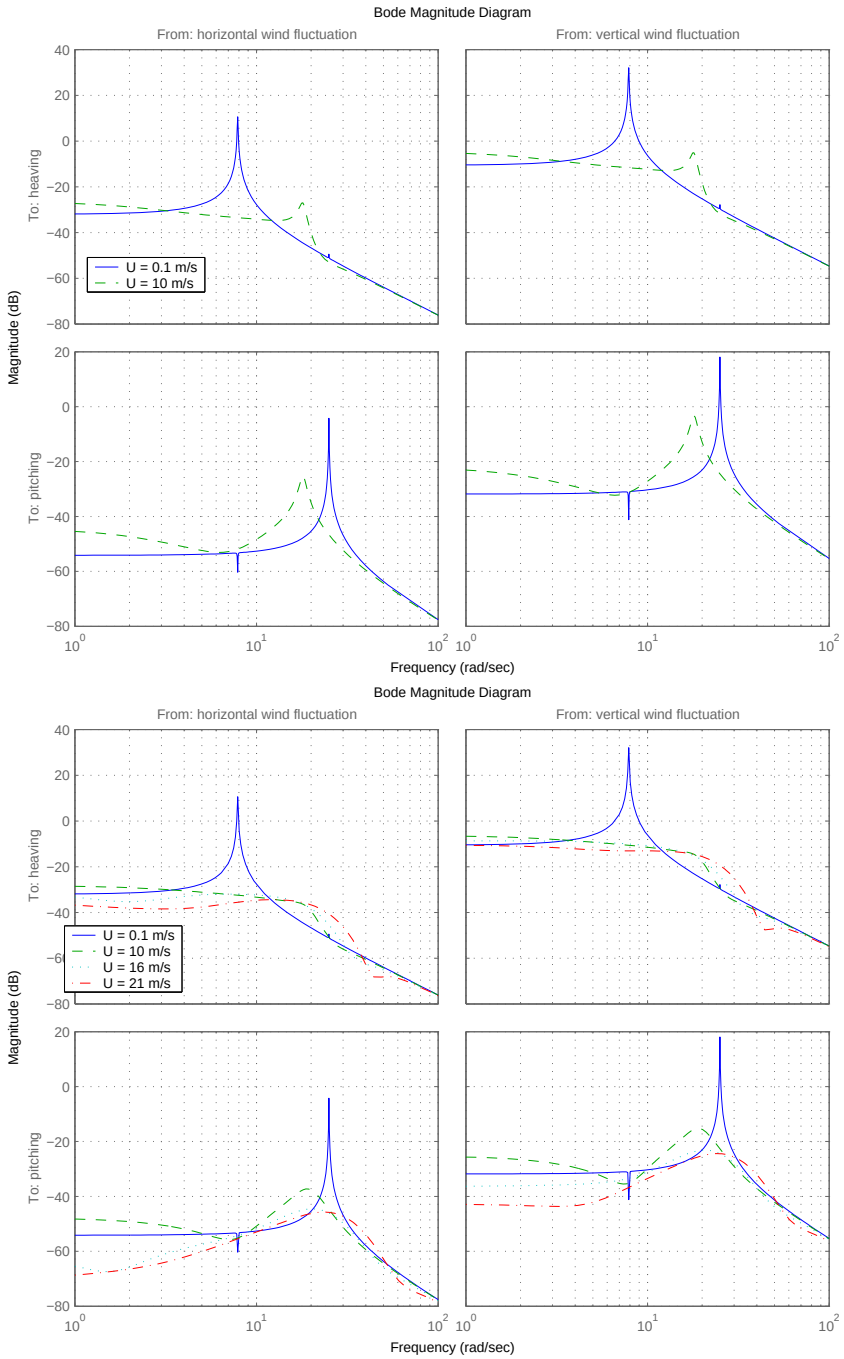

Figure 7.10: Bode magnitude plot of the winged bridge in the open (top) and closed loop (bottom) cases between the buffeting forces and the deck displacements for different wind speeds

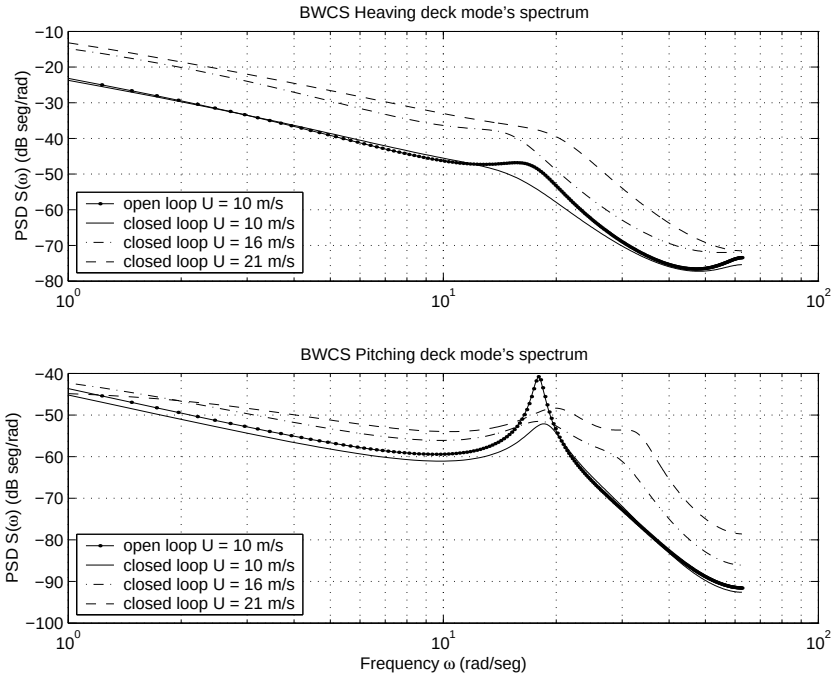

Figure 7.11: Power spectral density of the heaving and pitching deck displacement responses of the winged bridge in the open and closed loop cases for different wind speeds

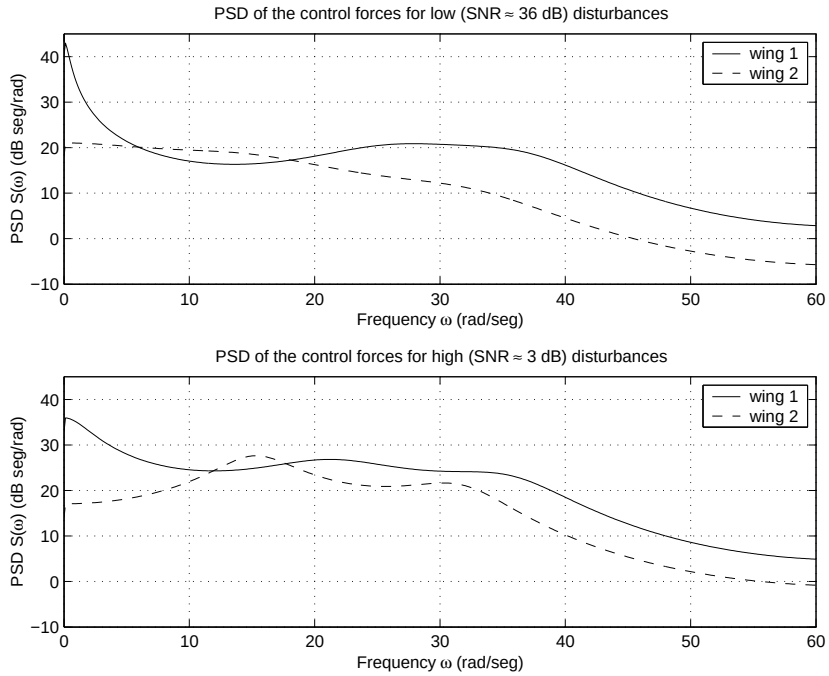

Figure 7.12: Power spectral density of the control force for noise and almost free noise sensor signals, for a stochastic regulator designer for $\bar{U} = 16$ m/s

Chapter 8

Random parametric excitation formulation and parametric stochastic stability analysis

> "*Equilibrium is only an instant of perfection, stability is more: it is the permanent likelihood that the equilibrium is not far.*"
>
> *Harm van Veen.*
> *The Tao of Kite Flying*

It was studied in earlier chapters that the state space representations (5.40) and (6.45) are dependent on wind velocity $U(t)$; in turn, mass, damping and stiffness aerodynamic matrices are functions of wind speed. As the oscillatory motion of the structure depends on the variation of such time-dependent parameters the induced vibration of the bridge is said to be *parametric*. In this case the wind is called a *parametric excitation*. As wind excites the bridge, some average quantity of energy flows into it. This energy is dissipated by the damping of the system; however, when wind velocity is greater than the critical velocity, the damping of the system becomes negative and the amplitude of the response increases. This is kind of instability is referred to as *parametric instability*.

Bridge parametric instability has been addressed by several authors. For example, Lin and Ariaratnam (1980) investigated the effect of wind turbulence in the stochastic stability of bridges

using a one-torsional-vibration-mode-modelled bridge; they concluded that turbulence has a destabilizing effect. Later Bucher and Lin (1988, 1989) regarded Lin and Ariaratnam (1980) study as incomplete inasmuch as they demonstrated that turbulence propels energy transfer between the different modes of vibration of the bridge, from the least stable modes to the more stable ones; in this way, turbulence could have also a stabilizing effect on the bridge if there is a favorable aerodynamic coupling between modes, as was experimentally demonstrated by Huston (1986). Lin (1996) discusses some outstanding problems present in bridges an analyzes them from a stochastic dynamics point viewpoint. On the other hand, nobody has aimed the problem of the bridge-wind-control surface (BWCS) system parametric stability. In this way, the purpose of this chapter is to explore in this uncharted field.

This chapter is distributed as follows: firstly, the deterministic and the stochastic stability concepts will be briefly reviewed, following with the formulation of the random parametric excitation (RPE) of the bridge systems, and finishing with the applications of the concepts to analyze the BW and BWCS systems parametric instability regions.

8.1 Deterministic stability concept

In the following lines a succinct review of the concept of deterministic stability will be carried on after Szidarovszky and Bahill (1998), Ogata (1997) and Chen (1999).

8.1.1 Elements of Lyapunov stability theory

Lyapunov stability theory is important because is the most general method for determining the stability of a system. In 1892, A. M. Lyapunov made public two methods for determining the stability of systems represented by ordinary differential equations. These methods were identified as the first one and the second one. The first method is composed of all procedures in which the explicit solution of the differential equations representing the system is used. On the other hand, the second method does not require the explicit solutions of the differential equations modelling the system. This is a great advantage because solving those differential equations is, in general, a very difficult task. In the following, the second method of Lyapunov will be succinctly explained.

The second method of Lyapunov

Let, $\dot{\mathbf{x}}(t) = \mathbf{f}(\mathbf{x}(t), t)$ for $\mathbf{x}(t) \in \mathcal{R}^n$ represent a dynamical system where the functions f_i, $i = 1, \ldots, n$ satisfy the *Lipschitz condition*,

$$|f_i(\mathbf{x}(t), t) - f_i(\mathbf{y}(s), s)| \leq K \|\mathbf{x}(t) - \mathbf{y}(s)\| \tag{8.1}$$

for all $t, s \in [t_0, t_f]$, provided a positive constant K. Let $\hat{\mathbf{x}}$ be an *equilibrium point* of the system, that is, $\mathbf{f}(\hat{\mathbf{x}}(t)) = \mathbf{0}$ for all $t \in [t_0, t_f]$. The stability of a trajectory $\mathbf{x}$ around an equilibrium solution $\hat{\mathbf{x}}$ can be expressed according to the Lyapunov definitions of stability:

Lyapunov stability: a trajectory around an equilibrium point is said to be *stable* if, given any $\varepsilon > 0$, there exists $\delta > 0$ such that $\|\mathbf{x}(t_0) - \hat{\mathbf{x}}(t_0)\| < \delta$ implies $\sup_{t \geq t_0} \|\mathbf{x}(t) - \hat{\mathbf{x}}(t)\| < \varepsilon$. The real number δ depends on ε, and, in general depends also on t_0. If δ does no depends on t_0 it is said that the equilibria state is *uniformly stable*.

Asymptotic Lyapunov stability: a trajectory around an equilibrium point is said to be *asymptotically stable* if, it is *stable* and if there exist a $\Delta > 0$ such that $\|\mathbf{x}(t_0) - \hat{\mathbf{x}}(t_0)\| < \Delta$ implies that $\lim_{t \to \infty} \|\mathbf{x}(t) - \hat{\mathbf{x}}(t)\| = 0$

Also we say that an equilibrium point $\hat{\mathbf{x}}$ is *global asymptotically stable* if, it is stable and all trajectories converge to it as $t \to \infty$. This definition suggests indirectly that this point is the only equilibrium point of the system and that all trajectories stay bounded for $t > 0$. This is in general a very useful characteristic, always present in linear time invariant systems.

The concept of Lyapunov functions

It is well know from classical mechanical theory that the energy of a mechanical system subjected to friction always converges to a minimum if there are not additional sources of power. Lyapunov used this principle, by means of the Lyapunov functions, to define the stability of a system. In this way, the Lyapunov functions can be interpreted as the generalization of the energy function of any system. Let $V(\mathbf{x}(t), t)$ be a continuous scalar function of the state variables with continuous partial derivatives. Its time derivative along any trajectory is given by

$$\dot{V}(\mathbf{x}(t), t) = \frac{\partial V}{\partial t} + \frac{\partial V}{\partial \mathbf{x}(t)} \mathbf{f}(\mathbf{x}(t), t) \tag{8.2}$$

Let $\mathcal{S}$ be an open connected set containing the equilibrium point $\hat{\mathbf{x}}$. The function V is said to be a *Lyapunov function* if both V and its time derivative $\dot{V}$ satisfy the following conditions:

1. $V(\mathbf{x}(t), t) > V(\hat{\mathbf{x}}(t), t)$ for all $\mathbf{x}(t) \neq \hat{\mathbf{x}}(t)$.
2. If $\mathcal{S}$ is unbounded, then $\lim_{\|\mathbf{x}(t)\| \to \infty} V(\mathbf{x}(t), t) = \infty$
3. $\dot{V}(\mathbf{x}(t), t) \leq 0$ for all $\mathbf{x}(t) \in \mathcal{S}$.
4. $\dot{V}(\mathbf{x}(t), t)$ does not vanish identically along any trajectory in $\mathcal{S}$ other than $\mathbf{x}(t) = \hat{\mathbf{x}}(t)$.

It can be demonstrated that if there exists a Lyapunov function corresponding to a given system, then the system is uniformly asymptotically stable around the point $\hat{\mathbf{x}}$. The above conditions can be relaxed, leading to the semi-negative-definiteness of $\dot{V}$ in $\mathcal{S}$; in this case, it is said that $\hat{\mathbf{x}}$ is a stable equilibrium point of the system.

8.1.2 Stability of linear time invariant systems

It is well known in linear system theory (Szidarovszky and Bahill (1998)), that a linear time invariant system of the form

$$\dot{\mathbf{x}}(t) = \mathbf{A}\mathbf{x}(t) \tag{8.3}$$

is stable if and only if all eigenvalues of matrix $\mathbf{A}$ have real negative parts, that is, the zeros of the characteristic polynomial $|\lambda\mathbf{I} - \mathbf{A}|$ must have negative real parts in order (8.3) to be stable.

8.1.3 Deterministic stability analysis of the bridge-wind and bridge-wind-control surfaces systems

The BW system state space equation is expressed by equation (5.40), whereas for the BWCS system, it is expressed by (6.45). The deterministic stability of the bridge can be studied by neglecting the buffeting forces, that is, by setting the buffeting force $\mathbf{Q}_b(t)$ to zero in the respective equations, so the deterministic versions of the systems will have the form (8.3); thus, to take into account the buffeting forces into self-excited vibrations, the flutter derivatives are measured in turbulent flow, making $U(t)$ in the aforementioned equations equal to the mean wind speed,

i.e. $U(t) = \bar{U}$. In this situation, matrix $\mathbf{A}$ is dependent on average wind speed. Increasing the mean wind speed $\bar{U}$ from zero, there will be found a velocity for which the bridge will become unstable, known as the *critical wind speed* U_c, that is, there will be a wind velocity for which the real part of an eigenvalue of $\mathbf{A}$ becomes nonnegative as discussed in past chapters.

The deterministic stability of the BW system and the BWCS systems will not be repeated here in view of the fact that it was analyzed in sections 5.3, 6.3 and 7.5.3 respectively.

8.2 Parametric stochastic stability concept

Let

$$\dot{\mathbf{X}}(t) = \mathbf{f}(\mathbf{X}(t), t) + \mathbf{G}(\mathbf{X}(t), t)\boldsymbol{\xi}(t); \quad \mathbf{X}(t_0) = \mathbf{X}_0 \tag{8.4}$$

represent a dynamical system, where $\mathbf{X}(t) \in \mathcal{R}^n$ and $\boldsymbol{\xi}(t)$ is a random noise vector. It is said that (8.4) is a parametrically excited system if $\mathbf{G}(\mathbf{X}(t), t)$ explicitly depends on $\mathbf{X}(t)$. The parametric stochastic stability analysis supplies a criterion for the study of the behaviour of dynamic systems subjected to RPE. In this way, the stability of the system are expressed in terms of the convergence and divergence of the statistical properties of excitation and system physical parameters.

The stochastic stability of an equilibrium point $\hat{\mathbf{X}}$ of equation 8.4 can be analyzed in terms of the following stability modes: stability in the moments, stability in probability, almost sure stability, Lyapunov stability in the moments, among others. In the following lines a review of some of the different stability modes will be carried on according to Ibrahim (1985).

8.2.1 Almost sure stability or stability with probability one

An equilibrium point $\hat{\mathbf{X}}(t)$ is said to be *almost sure stable* or that *is stable with probability one* if, there exists a $\delta > 0$ such that $\left\|\mathbf{X}(t_0) - \hat{\mathbf{X}}(t)\right\| < \delta$ implies

$$\mathrm{P}\left[\lim_{\left\|\mathbf{X}(t_0)-\hat{\mathbf{X}}(t_0)\right\|\to 0} \sup_{t\geq t_0} \left\|\mathbf{X}(t) - \hat{\mathbf{X}}(t)\right\| = 0\right] = 1 \tag{8.5}$$

Also, $\hat{\mathbf{X}}(t)$ is said to be *asymptotically almost sure stable* if, it is almost sure stable and if there exist a $\Delta > 0$ such that $\left\|\mathbf{X}(t_0) - \hat{\mathbf{X}}(t)\right\| < \Delta$ implies that

$$\lim_{T\to\infty} \mathrm{P}\left[\sup_{t\geq T}\left\|\mathbf{X}(t) - \hat{\mathbf{X}}(t)\right\| = 0\right] = 1 \tag{8.6}$$

8.2.2 Lyapunov stability in the moments

An equilibrium point $\hat{\mathbf{X}}(t)$ is said to be *Lyapunov stable in the k-th moment* if, there exists a $\delta > 0$ such that $\left\|\mathbf{X}(t_0) - \hat{\mathbf{X}}(t)\right\| < \delta$ implies

$$\lim_{\left\|\mathbf{X}(t_0)-\hat{\mathbf{X}}(t_0)\right\|\to 0} \mathrm{E}\left[\left\|\mathbf{X}(t) - \hat{\mathbf{X}}(t)\right\|^k\right] = 0 \tag{8.7}$$

for $t \geq t_0$. Also, $\hat{\mathbf{X}}(t)$ is said to be *Lyapunov asymptotically stable in the k-th moment* if, it is Lyapunov stable in the k-th moment and if there exist a $\Delta > 0$ such that $\left\|\mathbf{X}(t_0) - \hat{\mathbf{X}}(t)\right\| < \Delta$ implies that

$$\lim_{t\to\infty} \mathrm{E}\left[\left\|\mathbf{X}(t) - \hat{\mathbf{X}}(t)\right\|^k\right] = 0 \tag{8.8}$$

8.2.3 Stability in the moments

An equilibrium point $\hat{\mathbf{X}}$ is said to be *stable in the k-th moment* if, provided any $\varepsilon > 0$, there exists a $\delta > 0$ such that $\left\|\mathbf{X}(t_0) - \hat{\mathbf{X}}(t_0)\right\| < \delta$ implies

$$\mathrm{E}\left[\sup_{t\geq t_0}\left\|\mathbf{X}(t) - \hat{\mathbf{X}}(t)\right\|_k^k\right] < \varepsilon \tag{8.9}$$

where $\|\cdot\|_k$ stands for the *Minkowski norm*, that is

$$\|\mathbf{y}\|_k = \sqrt[k]{\sum_{i=1}^{n} |y_i|^k}; \quad \mathbf{y} \in \mathcal{R}^n \tag{8.10}$$

Also, $\hat{\mathbf{X}}$ is said to be *asymptotically stable in the k-th moment* if, it is stable in the k-th moment and

$$\lim_{T\to\infty} \mathrm{E}\left[\sup_{t\geq T}\left\|\mathbf{X}(t) - \hat{\mathbf{X}}(t)\right\|_k^k\right] = 0 \tag{8.11}$$

An equilibrium point $\hat{\mathbf{X}}$ is said to be *exponentially stable in the k-th moment* if, given any $\alpha > 0$ and $\beta > 0$, there exists $\delta > 0$ such that $\left\|\mathbf{X}(t_0) - \hat{\mathbf{X}}(t_0)\right\|^k < \delta$ implies

$$\mathrm{E}\left[\left\|\mathbf{X}(t) - \hat{\mathbf{X}}(t)\right\|^k\right] < \beta \left\|\mathbf{X}(t_0) - \hat{\mathbf{X}}(t_0)\right\|^k \exp\left(-\alpha(t - t_0)\right) \tag{8.12}$$

for $t \geq t_0$.

A system is said to be *stable in the moments* if its response moments of all orders are stable. However, stability in the moments not always provides an adequate criterion of the system response stability, as is shown in Ibrahim (1985). It is a good point to annotate that stability in the moments implies almost sure stability (Ibrahim (1985)).

Stability in the first and second order statistical moments

From a practical point of view, first and second order statistical moments are the only ones taken into account, in view of the fact that as the order of the statistical moments increases the region of stability narrows, making their use excessively restrictive for engineering applications; also, it can be shown that, given a linear system representation, with a state vector represented as a Markov vector process, the stability in the second moments implies almost sure stability (Ibrahim (1985)).

Consider the system (8.4), with $\boldsymbol{\xi}(t)$ representing a zero mean stationary Gaussian process. If $\boldsymbol{\xi}(t)$ has a correlation time[1] much smaller than the relaxation time of the system[2], then the excitation can be regarded as a wide band process and can be approximated by a white noise, and in this manner, the state space vector may be considered a Markov diffusion vector process (Soong and Grigoriu (1993)). Replacing $\boldsymbol{\xi}(t)$ for a zero mean Gaussian white noise with spectral density $\mathbf{S}$ then (8.4) can be converted into an equivalent *Itô stochastic differential equation*,

$$\mathrm{d}\mathbf{X}(t) = \mathbf{m}(\mathbf{X}(t), t)\mathrm{d}t + \boldsymbol{\Sigma}(\mathbf{X}(t), t)\mathrm{d}\mathbf{B}(t); \quad \mathbf{X}(t_0) = \mathbf{X}_0 \tag{8.14}$$

[1]The *correlation time*, τ_c, of a component of stationary process $X(t)$ is defined as,

$$\tau_c = \frac{1}{R_X(0)} \int_0^\infty |R_X(\tau)| \, \mathrm{d}\tau \tag{8.13}$$

It is seen that for a stationary stochastic process free of armonics, the autocorrelation exists only in a time interval where $|t_2 - t_1| < \tau_c$.

[2]The *relaxation time* or *constant time of a system* is a measure of the time the system requires to return to equilibrium (or assume a new equilibrium) after a sudden change in applied forces, constraints, boundary conditions, etc.

where $\mathbf{B}(t)$ stands for a Wiener process with $\mathrm{E}[\mathrm{d}\mathbf{B}(t)] = \mathbf{0}$, $\mathrm{E}[\mathrm{d}\mathbf{B}(t)\mathrm{d}\mathbf{B}^{\mathrm{T}}(t)] = 2\mathbf{S}\mathrm{d}t$, and whose drift vector $\mathbf{m}$ and diffusion matrix $\boldsymbol{\Sigma}\boldsymbol{\Sigma}^{\mathrm{T}}$, can be found after applying the *Wong-Zakai convergence theorem* (Wong and Zakai (1965)) to (8.4),

$$m_j = f_j + \frac{1}{2} S_{kr} \frac{\partial g_{jk}}{\partial X_l} g_{lr} \tag{8.15}$$

$$\sigma_{jl}\sigma_{kl} = S_{rs} g_{jr} g_{ks} \tag{8.16}$$

where use is made of the Einstein's summation convention for the common indexes.

Equation (8.14) is a special case of (8.4) which can be solved by application of Itô calculus. An equation of the form (8.4), in which the input cannot be approximated by a Gaussian white noise, can also be set in the form (8.14) modelling the excitation $\boldsymbol{\xi}(t)$ as a *filtered Gaussian white noise* (that is, the output of a dynamic system fed by a Gaussian white noise),

$$\mathrm{d}\boldsymbol{\xi}(t) = \mathbf{g}(\boldsymbol{\xi}(t), t)\mathrm{d}t + \mathrm{d}\mathbf{B}(t) \tag{8.17}$$

so, the vector $\begin{bmatrix}\mathbf{X}^{\mathrm{T}}(t) & \boldsymbol{\xi}^{\mathrm{T}}(t)\end{bmatrix}^{\mathrm{T}}$ satisfies a differential equation with white noise as input, resembling (8.14).

The *Itô stochastic differential rule* says that for any function ψ dependent on time and on the diffusion process $\mathbf{X}(t)$ as defined in (8.14) (i.e. $\psi \equiv \psi(\mathbf{X}(t), t)$),

$$\mathrm{d}\psi = \left(\frac{\partial \psi}{\partial t} + m_j \frac{\partial \psi}{\partial x_j} + \frac{1}{2} \sigma_{jl}\sigma_{kl} \frac{\partial^2 \psi}{\partial x_j \partial x_k} \right) \mathrm{d}t + \sigma_{jk} \frac{\partial \psi}{\partial x_j} \mathrm{d}B_k \tag{8.18}$$

The first moment equation of the diffusion process $\mathbf{X}(t)$, $\boldsymbol{\mu}(t)$ can be found using the Itô stochastic differential rule, setting $\psi = x_m$ and taking expectations of (8.14), that is,

$$\dot{\boldsymbol{\mu}}(t) = \mathrm{E}\left[\mathbf{m}(t)\right] \tag{8.19}$$

whereas, the second moment equation $\mathbf{Z}(t) = \mathrm{E}\left[\mathbf{X}(t)\mathbf{X}^{\mathrm{T}}(t)\right]$ can be found by substituting $\psi = x_m x_n$ into (8.18), and applying the expectation operator, taking in mind that for a Wiener process $\mathrm{E}[\mathrm{d}\mathbf{B}(t)] = \mathbf{0}$,

$$\dot{\mathbf{Z}}(t) = \mathrm{E}\left[\mathbf{m}(t)\mathbf{X}^{\mathrm{T}}(t)\right] + \mathrm{E}\left[\mathbf{X}(t)\mathbf{m}^{\mathrm{T}}(t)\right] + \mathrm{E}\left[\boldsymbol{\Sigma}(t)\boldsymbol{\Sigma}^{\mathrm{T}}(t)\right] \tag{8.20}$$

Finally, the stability of the first and second moment differential equations, (8.19) and (8.20) respectively, must be found.

8.2.4 RPE formulation of the BW and BWCS systems

A stochastic stability analysis begins from a random parametric formulation of the system. In the following a RPE formulation of the BW system using Karpel's formulation will be developed. This study will be made only for a section of the bridge, without admittance function correction of the buffeting forces, since a full study using the spatial correlations of the wind field would render the formulation extremely complicated.

As was seen in chapter 5, the BW system is modelled by linear equations (5.5), (5.46) and (5.27) and driven by Gaussian processes $u(t)$ and $v(t)$. From the aforementioned equations, it follows that

$$\begin{aligned}\mathbf{M}\ddot{\mathbf{q}}(t)+\mathbf{C}\dot{\mathbf{q}}(t)+\mathbf{K}\mathbf{q}(t) &= U^2(t)\mathbf{V}_d\left(\mathbf{A}_1\mathbf{q}(t)+\left(\frac{B_d}{\bar{U}}\right)\mathbf{A}_2\dot{\mathbf{q}}(t)+\mathbf{G}\mathbf{x}_a(t)\right)\\ &\quad+\bar{U}^2\mathbf{V}_d\left(\mathbf{A}_{bu}\frac{u(t)}{\bar{U}}+\mathbf{A}_{bw}\frac{v(t)}{\bar{U}}\right)\end{aligned} \tag{8.21}$$

where the vector of aerodynamic states $\mathbf{x}_a(t)$, satisfies the differential equation (5.49),

$$\dot{\mathbf{x}}_a(t)=\frac{\bar{U}}{B_d}\mathbf{E}\mathbf{q}(t)-\frac{\bar{U}}{B_d}\mathbf{R}\mathbf{x}_a(t) \tag{8.22}$$

In this case, as the instantaneous velocity $U(t)$ is employed, flutter derivatives should be measured in laminar flow (Bucher and Lin (1988, 1989); Cai et al. (1999)).

Considering that $U(t)=\bar{U}+u(t)$ and $U^2(t)\approx\bar{U}^2(1+2\frac{u(t)}{\bar{U}})$, equation (8.21) can be recasted as

$$\begin{aligned}\mathbf{M}_{\text{det}}\ddot{\mathbf{q}}(t)+\mathbf{C}_{\text{det}}\dot{\mathbf{q}}(t)+\mathbf{K}_{\text{det}}\mathbf{q}(t) &= 2\left(\frac{u(t)}{\bar{U}}\right)\bar{U}B_d\mathbf{V}_d\mathbf{A}_2\dot{\mathbf{q}}(t)+2\left(\frac{u(t)}{\bar{U}}\right)\bar{U}^2\mathbf{V}_d\mathbf{A}_1\mathbf{q}(t)\\ &\quad+\left(1+2\frac{u(t)}{\bar{U}}\right)\bar{U}^2\mathbf{V}_d\mathbf{G}\mathbf{x}_a(t)\\ &\quad+\bar{U}^2\mathbf{V}_d\left(\mathbf{A}_{bu}\frac{u(t)}{\bar{U}}+\mathbf{A}_{bw}\frac{w(t)}{\bar{U}}\right)\end{aligned} \tag{8.23}$$

with, $\mathbf{M}_{\text{det}}=\mathbf{M}$, $\mathbf{C}_{\text{det}}=\mathbf{C}-\bar{U}B_d\mathbf{V}_d\mathbf{A}_2$ and $\mathbf{K}_{\text{det}}=\mathbf{K}-\bar{U}^2\mathbf{V}_d\mathbf{A}_1$. Observe that the added aeroelastic mass is neglected, following the reasons stated in page 37. Rearranging the terms of equation (8.23) the random parametric representation form is obtained,

$$\dot{\mathbf{Y}}(t)=\mathbf{A}_{\text{det}}\mathbf{Y}(t)+\left[\tilde{\mathbf{B}}\mathbf{Y}(t)\boldsymbol{\delta}+\mathbf{B}_{\text{buf}}\right]\boldsymbol{\eta}(t) \tag{8.24}$$

where $\boldsymbol{\delta} = [1 \quad 0]$, $\boldsymbol{\eta}(t) = \left[\begin{array}{cc} u(t)/\bar{U} & v(t)/\bar{U} \end{array} \right]^{\mathrm{T}}$, $\mathbf{Y}(t) = \left[\begin{array}{ccc} \mathbf{q}^{\mathrm{T}}(t) & \dot{\mathbf{q}}^{\mathrm{T}}(t) & \mathbf{x}_a{}^{\mathrm{T}}(t) \end{array} \right]^{\mathrm{T}}$,

$$\mathbf{A}_{\mathrm{det}} = \begin{bmatrix} \mathbf{0} & \mathbf{I} & \mathbf{0} \\ -\mathbf{M}_{\mathrm{det}}^{-1}\mathbf{K}_{\mathrm{det}} & -\mathbf{M}_{\mathrm{det}}^{-1}\mathbf{C}_{\mathrm{det}} & \bar{U}^2\mathbf{M}_{\mathrm{det}}^{-1}\mathbf{V}_d\mathbf{G} \\ \frac{\bar{U}}{B_d}\mathbf{E} & \mathbf{0} & -\frac{\bar{U}}{B_d}\mathbf{R} \end{bmatrix}, \tag{8.25}$$

$$\tilde{\mathbf{B}} = \begin{bmatrix} \mathbf{0} & \mathbf{0} & \mathbf{0} \\ 2\bar{U}^2\mathbf{M}_{\mathrm{det}}^{-1}\mathbf{V}_d\mathbf{A}_1 & 2\bar{U}B_d\mathbf{M}_{\mathrm{det}}^{-1}\mathbf{V}_d\mathbf{A}_2 & 2\bar{U}^2\mathbf{M}_{\mathrm{det}}^{-1}\mathbf{V}_d\mathbf{G} \\ \mathbf{0} & \mathbf{0} & \mathbf{0} \end{bmatrix}, \tag{8.26}$$

and,

$$\mathbf{B}_{\mathrm{buf}} = \begin{bmatrix} \mathbf{0} & \mathbf{0} \\ \bar{U}^2\mathbf{M}_{\mathrm{det}}^{-1}\mathbf{V}_d\mathbf{A}_{bu} & \bar{U}^2\mathbf{M}_{\mathrm{det}}^{-1}\mathbf{V}_d\mathbf{A}_{bw} \\ \mathbf{0} & \mathbf{0} \end{bmatrix} \tag{8.27}$$

Using Roger's RFA and following the same steps as above, yields the following matrices,

$$\mathbf{A}_{\mathrm{det}} = \begin{bmatrix} \mathbf{0} & \mathbf{I} & \mathbf{0} & \cdots & \mathbf{0} \\ -\mathbf{M}_{\mathrm{det}}^{-1}\mathbf{K}_{\mathrm{det}} & -\mathbf{M}_{\mathrm{det}}^{-1}\mathbf{C}_{\mathrm{det}} & \bar{U}^2\mathbf{M}_{\mathrm{det}}^{-1}\mathbf{V}_d & \cdots & \bar{U}^2\mathbf{M}_{\mathrm{det}}^{-1}\mathbf{V}_d \\ \mathbf{0} & \mathbf{A}_4 & -\frac{\bar{U}}{B_d}d_1\mathbf{I} & \cdots & \mathbf{0} \\ \vdots & \vdots & \vdots & \ddots & \vdots \\ \mathbf{0} & \mathbf{A}_{3+m} & \mathbf{0} & \cdots & -\frac{\bar{U}}{B_d}d_m\mathbf{I} \end{bmatrix}, \tag{8.28}$$

$$\tilde{\mathbf{B}} = \begin{bmatrix} \mathbf{0} & \mathbf{0} & \mathbf{0} & \cdots & \mathbf{0} \\ 2\bar{U}^2\mathbf{M}_{\mathrm{det}}^{-1}\mathbf{V}_d\mathbf{A}_1 & 2\bar{U}B_d\mathbf{M}_{\mathrm{det}}^{-1}\mathbf{V}_d\mathbf{A}_2 & 2\bar{U}^2\mathbf{M}_{\mathrm{det}}^{-1}\mathbf{V}_d & \cdots & 2\bar{U}^2\mathbf{M}_{\mathrm{det}}^{-1}\mathbf{V}_d \\ \mathbf{0} & \mathbf{0} & \mathbf{0} & \cdots & \mathbf{0} \\ \vdots & \vdots & \vdots & \ddots & \vdots \\ \mathbf{0} & \mathbf{0} & \mathbf{0} & \cdots & \mathbf{0} \end{bmatrix} \tag{8.29}$$

Using the same steps outlined above, the RPE formulation of the BWCS system can be deduced. In this case, the parametric equation of motion turns to

$$\dot{\mathbf{Y}}(t) = \mathbf{A}_{\mathrm{det}}\mathbf{Y}(t) + \left[\tilde{\mathbf{B}}\mathbf{Y}(t)\boldsymbol{\delta} + \mathbf{B}_{\mathrm{buf}}\right]\boldsymbol{\eta}(t) + \mathbf{B}_{\mathrm{cs}}\mathbf{u}(t) \tag{8.30}$$

Using Karpel's minimum state formulation, it yields,

$$\mathbf{Y}(t) = \left[\begin{array}{ccccc} \mathbf{q}^{\mathrm{T}}(t) & \dot{\mathbf{q}}^{\mathrm{T}}(t) & \mathbf{x}_{ad}^{\mathrm{T}}(t) & \mathbf{x}_{aw1}^{\mathrm{T}}(t) & \mathbf{x}_{aw2}^{\mathrm{T}}(t) \end{array} \right]^{\mathrm{T}}, \tag{8.31}$$

$$\mathbf{A}_{\text{det}} = \begin{bmatrix} \mathbf{0} & \mathbf{I} & \mathbf{0} & \mathbf{0} & \mathbf{0} \\ -\mathbf{M}_{\text{det}}^{-1}\mathbf{K}_{\text{det}} & -\mathbf{M}_{\text{det}}^{-1}\mathbf{C}_{\text{det}} & \bar{U}^2\mathbf{M}_{\text{det}}^{-1}\mathbf{T}_d^{lg}\mathbf{V}_d\mathbf{G}_d & \bar{U}^2\mathbf{M}_{\text{det}}^{-1}\mathbf{T}_{w1}^{lg}\mathbf{V}_{w1}\mathbf{G}_{w1} & \bar{U}^2\mathbf{M}_{\text{det}}^{-1}\mathbf{T}_{w2}^{lg}\mathbf{V}_{w2}\mathbf{G}_{w2} \\ \frac{\bar{U}}{B_d}\mathbf{E}_d\mathbf{T}_d^{gl} & \mathbf{0} & -\frac{\bar{U}}{B_d}\mathbf{R}_d & \mathbf{0} & \mathbf{0} \\ \frac{\bar{U}}{B_{w1}}\mathbf{E}_{w1}\mathbf{T}_{w1}^{gl} & \mathbf{0} & \mathbf{0} & -\frac{\bar{U}}{B_{w1}}\mathbf{R}_{w1} & \mathbf{0} \\ \frac{\bar{U}}{B_{w2}}\mathbf{E}_{w2}\mathbf{T}_{w2}^{gl} & \mathbf{0} & \mathbf{0} & \mathbf{0} & -\frac{\bar{U}}{B_{w2}}\mathbf{R}_{w2} \end{bmatrix}, \tag{8.32}$$

$$\tilde{\mathbf{B}} = \begin{bmatrix} \mathbf{0} & \mathbf{0} & \mathbf{0} & \mathbf{0} & \mathbf{0} \\ 2\bar{U}^2\mathbf{M}_{\text{det}}^{-1}\mathbf{K}_p & 2\bar{U}\mathbf{M}_{\text{det}}^{-1}\mathbf{C}_p & 2\bar{U}^2\mathbf{M}_{\text{det}}^{-1}\mathbf{T}_d^{lg}\mathbf{V}_d\mathbf{G}_d & 2\bar{U}^2\mathbf{M}_{\text{det}}^{-1}\mathbf{T}_{w1}^{lg}\mathbf{V}_{w1}\mathbf{G}_{w1} & 2\bar{U}^2\mathbf{M}_{\text{det}}^{-1}\mathbf{T}_{w2}^{lg}\mathbf{V}_{w2}\mathbf{G}_{w2} \\ \mathbf{0} & \mathbf{0} & \mathbf{0} & \mathbf{0} & \mathbf{0} \\ \mathbf{0} & \mathbf{0} & \mathbf{0} & \mathbf{0} & \mathbf{0} \\ \mathbf{0} & \mathbf{0} & \mathbf{0} & \mathbf{0} & \mathbf{0} \end{bmatrix}, \tag{8.33}$$

$$\mathbf{M}_{\text{det}} = \mathbf{M}, \quad \mathbf{C}_{\text{det}} = \mathbf{C} - \bar{U}\mathbf{C}_{\text{p}}, \quad \mathbf{K}_{\text{det}} = \mathbf{K} - \bar{U}^2\mathbf{K}_{\text{p}}, \tag{8.34}$$

$$\mathbf{C}_{\text{p}} = B_d\mathbf{T}_d^{lg}\mathbf{V}_d\mathbf{A}_{2d}\mathbf{T}_d^{gl} - B_{w1}\mathbf{T}_{w1}^{lg}\mathbf{V}_{w1}\mathbf{A}_{2w1}\mathbf{T}_{w1}^{gl} - B_{w2}\mathbf{T}_{w2}^{lg}\mathbf{V}_{w2}\mathbf{A}_{2w2}\mathbf{T}_{w2}^{gl}, \tag{8.35}$$

$$\mathbf{K}_{\text{p}} = \mathbf{T}_d^{lg}\mathbf{V}_d\mathbf{A}_{1d}\mathbf{T}_d^{gl} - \mathbf{T}_{w1}^{lg}\mathbf{V}_{w1}\mathbf{A}_{1w1}\mathbf{T}_{w1}^{gl} - \mathbf{T}_{w2}^{lg}\mathbf{V}_{w2}\mathbf{A}_{1w2}\mathbf{T}_{w2}^{gl} \tag{8.36}$$

and,

$$\mathbf{B}_{\text{buf}} = \begin{bmatrix} \mathbf{0} & \mathbf{0} \\ \bar{U}^2\mathbf{M}_{\text{det}}^{-1}\left(\mathbf{V}_d\mathbf{A}_{bud} + \mathbf{V}_{w1}\mathbf{A}_{buw1} + \mathbf{V}_{w2}\mathbf{A}_{buw2}\right) & \bar{U}^2\mathbf{M}_{\text{det}}^{-1}\left(\mathbf{V}_d\mathbf{A}_{bwd} + \mathbf{V}_{w1}\mathbf{A}_{bww1} + \mathbf{V}_{w2}\mathbf{A}_{bww2}\right) \\ \mathbf{0} & \mathbf{0} \\ \mathbf{0} & \mathbf{0} \\ \mathbf{0} & \mathbf{0} \end{bmatrix} \tag{8.37}$$

It is easy to see that the case $\boldsymbol{\delta} = [\mathbf{0} \quad \mathbf{0}]$, correspond to the determinist variant (non-parametrically excited version) of the BW and BWCS state space representations in laminar flow. (equations (5.51), (5.42) and (5.44)). So, subindex "det" is employed to highlight this fact. The reader must be aware that $\mathbf{A}_{\text{det}}$ does not have buffeting force terms. Note also that the equation of motion in the RPE formulation depends of both the external buffeting forces and the parametric random self-excited forces.

8.2.5 Stochastic stability analysis of the BW and BWCS systems

To simplify the mathematical treatment of the stochastic stability analysis of (8.14), the wind fluctuation vector $\boldsymbol{\eta}(t)$ can be replaced by a white noise excitation in view of the Wong-Zakai convergence theorem. In this way, the buffeting component is modelled as a weakly stationary

wide band random process so that the bridge response is modelled as a diffusion Markov process. Inserting (8.24) into equations (8.15) and (8.16) yields respectively the drift vector,

$$m_j(t) = \left(A_{\mathrm{det}ji} + \frac{1}{2} S_{\eta_1\eta_1} \tilde{B}_{jl} \tilde{B}_{li} \right) y_i(t) + \frac{1}{2} S_{1r} \tilde{B}_{jl} B_{\mathrm{buf}lr} \tag{8.38}$$

and diffusion matrix,

$$\sigma_{jl}(t)\sigma_{kl}(t) = \left[\tilde{B}_{ji} y_i(t) \delta_{1r} + B_{\mathrm{buf}jr} \right] S_{rk} \left[\tilde{B}_{kl} y_l(t) \delta_{1s} + B_{\mathrm{buf}ks} \right] \tag{8.39}$$

or recasting them in a matrix fashion, we obtain respectively,

$$\mathbf{m}(t) = \mathbf{F}\mathbf{Y}(t) + \frac{1}{2} \tilde{\mathbf{B}} \mathbf{B}_{\mathrm{buf}} \mathbf{S}^{\mathrm{T}}_{\boldsymbol{\eta}\boldsymbol{\eta}} \boldsymbol{\delta}^{\mathrm{T}} \tag{8.40}$$

and,

$$\boldsymbol{\Sigma}(t)\boldsymbol{\Sigma}^{\mathrm{T}}(t) = \left[\tilde{\mathbf{B}} \mathbf{Y}(t) \boldsymbol{\delta} + \mathbf{B}_{\mathrm{buf}} \right] \mathbf{S}_{\boldsymbol{\eta}\boldsymbol{\eta}} \left[\tilde{\mathbf{B}} \mathbf{Y}(t) \boldsymbol{\delta} + \mathbf{B}_{\mathrm{buf}} \right]^{\mathrm{T}} \tag{8.41}$$

where,

$$\mathbf{F} = \mathbf{A}_{\mathrm{det}} + \frac{1}{2} S_{\eta_1\eta_1} \tilde{\mathbf{B}} \tilde{\mathbf{B}} \tag{8.42}$$

and

$$\mathbf{S}_{\boldsymbol{\eta}\boldsymbol{\eta}} = \begin{bmatrix} S_{\eta_1\eta_1} & S_{\eta_1\eta_2} \\ S_{\eta_2\eta_1} & S_{\eta_2\eta_2} \end{bmatrix} \tag{8.43}$$

stands for the white noise power spectral density of the normalized wind fluctuations process $\boldsymbol{\eta}(t)$. Observe also that the case $\mathbf{S} = \mathbf{0}$ corresponds to the non parametrically excited version of the BWCS system representation.

The first and second statistic moments of the diffusion process $\mathbf{X}(t)$, can be found taking advantage of the Itô stochastic differential rule for $\psi = y_i$ and $\psi = y_i y_j$ respectively, and applying expectations bearing in mind that for the Wiener process $\mathbf{B}(t)$, $\mathrm{E}[\mathrm{d}\mathbf{B}(t)] = \mathbf{0}$, so that

$$\dot{\boldsymbol{\mu}}(t) = \mathbf{F}\boldsymbol{\mu}(t) + \frac{1}{2} \tilde{\mathbf{B}} \mathbf{B}_{\mathrm{buf}} \mathbf{S}^{\mathrm{T}}_{\boldsymbol{\eta}\boldsymbol{\eta}} \boldsymbol{\delta}^{\mathrm{T}} \tag{8.44}$$

$$\frac{\mathrm{d}}{\mathrm{d}t} \mathrm{E}\left[\mathbf{Y}(t)\mathbf{Y}^{\mathrm{T}}(t) \right] = \mathrm{E}\left[\mathbf{m}\mathbf{Y}^{\mathrm{T}}(t) \right] + \mathrm{E}\left[\mathbf{Y}(t)\mathbf{m}^{\mathrm{T}} \right] + \mathrm{E}\left[\boldsymbol{\Sigma}(t)\boldsymbol{\Sigma}^{\mathrm{T}}(t) \right] \tag{8.45}$$

As,

$$\mathrm{E}\left[\boldsymbol{\Sigma}(t)\boldsymbol{\Sigma}^{\mathrm{T}}(t) \right] = S_{\eta_1\eta_1} \tilde{\mathbf{B}} \mathrm{E}\left[\mathbf{Y}(t)\mathbf{Y}^{\mathrm{T}}(t) \right] \tilde{\mathbf{B}}^{\mathrm{T}} + \tilde{\mathbf{B}} \boldsymbol{\mu}(t) \boldsymbol{\delta} \mathbf{S}_{\boldsymbol{\eta}\boldsymbol{\eta}} \mathbf{B}^{\mathrm{T}}_{\mathrm{buf}} + \mathbf{B}_{\mathrm{buf}} \mathbf{S}_{\boldsymbol{\eta}\boldsymbol{\eta}} \boldsymbol{\delta}^{\mathrm{T}} \boldsymbol{\mu}^{\mathrm{T}}(t) \tilde{\mathbf{B}}^{\mathrm{T}} + \mathbf{B}_{\mathrm{buf}} \mathbf{S}_{\boldsymbol{\eta}\boldsymbol{\eta}} \mathbf{B}^{\mathrm{T}}_{\mathrm{buf}} \tag{8.46}$$

and denoting $\mathbf{Z}(t) = \mathrm{E}\left[\mathbf{Y}(t)\mathbf{Y}^{\mathrm{T}}(t)\right]$, gives,

$$\dot{\mathbf{Z}}(t) = \mathbf{F}\mathbf{Z}(t) + \mathbf{Z}(t)\mathbf{F}^{\mathrm{T}} + S_{\eta_1\eta_1}\tilde{\mathbf{B}}\mathbf{Z}(t)\tilde{\mathbf{B}}^{\mathrm{T}} + \mathbf{P}(t) \tag{8.47}$$

where,

$$\begin{aligned}\mathbf{P}(t) &= \frac{1}{2}\tilde{\mathbf{B}}\mathbf{B}_{\mathrm{buf}}\mathbf{S}^{\mathrm{T}}_{\boldsymbol{\eta\eta}}\boldsymbol{\delta}^{\mathrm{T}}\boldsymbol{\mu}^{\mathrm{T}}(t) + \frac{1}{2}\boldsymbol{\mu}(t)\boldsymbol{\delta}\mathbf{S}_{\boldsymbol{\eta\eta}}\mathbf{B}^{\mathrm{T}}_{\mathrm{buf}}\tilde{\mathbf{B}}^{\mathrm{T}} + \tilde{\mathbf{B}}\boldsymbol{\mu}(t)\boldsymbol{\delta}\mathbf{S}_{\boldsymbol{\eta\eta}}\mathbf{B}^{\mathrm{T}}_{\mathrm{buf}} + \\ &\quad \mathbf{B}_{\mathrm{buf}}\mathbf{S}_{\boldsymbol{\eta\eta}}\boldsymbol{\delta}^{\mathrm{T}}\boldsymbol{\mu}^{\mathrm{T}}(t)\tilde{\mathbf{B}}^{\mathrm{T}} + \mathbf{B}_{\mathrm{buf}}\mathbf{S}_{\boldsymbol{\eta\eta}}\mathbf{B}^{\mathrm{T}}_{\mathrm{buf}}\end{aligned} \tag{8.48}$$

Matrix $\mathbf{Z}(t)$ in (8.47) is symmetric, so its upper triangular part can be unfolded in terms of a new vector $\mathbf{v}(t)$, thus formula (8.47) becomes

$$\dot{\mathbf{v}}(t) = \mathbf{H}\mathbf{v}(t) + \mathbf{Q}(t) \tag{8.49}$$

As mentioned before, given that equations (5.5), (5.46) and (5.27) are linear and that the input vector $\boldsymbol{\eta}(t)$ is a stationary Gaussian vector process, the buffeting response is also a stationary Gaussian process, implying that the statistical moments are independent of time; therefore the time derivative of the first and second statistical moments is equal to zero, so, from (8.45) and (8.49) results,

$$\boldsymbol{\mu} = -\frac{1}{2}\mathbf{F}^{-1}\tilde{\mathbf{B}}\tilde{\mathbf{B}}_{\mathrm{buf}}\mathbf{S}^{\mathrm{T}}_{\boldsymbol{\eta\eta}}\boldsymbol{\delta} \tag{8.50}$$

$$\mathbf{v} = -\mathbf{H}^{-1}\mathbf{Q} \tag{8.51}$$

According to Lin (1979), the stochastic stability approach, must be interpreted as moment stability: if the real part of an eigenvalue of $\mathbf{F}$ becomes positive, then the first moment becomes unstable; in the same manner, if the real part of an eigenvalue of $\mathbf{H}$ becomes greater than zero, then the second moment also becomes unstable. So, an analogous critical velocity is defined in the sense of the first or second moments.

This analysis can be easily adjusted to manage the RPE formulation of the BWCS system in open and closed loop configuration, as follows: in the open loop configuration $\mathbf{u}(t)$ in equation (8.30) is set to zero, as there are no control forces; in the closed loop configuration, assuming that the system is managed by a variable gain LQR control law, equation (8.30) turns to

$$\dot{\mathbf{Y}}(t) = \left(\mathbf{A}_{\mathrm{det}} - \mathbf{B}_{\mathrm{cs}}\mathbf{C}_{\mathrm{LQR}}\right)\mathbf{Y}(t) + \left[\tilde{\mathbf{B}}\mathbf{Y}(t)\boldsymbol{\delta} + \mathbf{B}_{\mathrm{buf}}\right]\boldsymbol{\eta}(t) \tag{8.52}$$

so that, a study similar to the above sketched is carried out. An study in closed loop configuration using also the state estimated by the Kalman filter was not done in as much as the RPE formulation renders very complicated.

8.3 Charts of the stochastic moment stability/instability boundaries

A chart of the stochastic stability/instability boundaries forecasted by first and second moments was made for a varying wind speed and a varying white noise intensity, using the same systems analyzed in past chapters. It must bear in mind that an RPE stability analysis involves the use of flutter derivatives measured in laminar flow. This is not the case in the present section. Figures 8.1 and 8.2 show the critical speed for a varying wind intensity, predicted by the first and

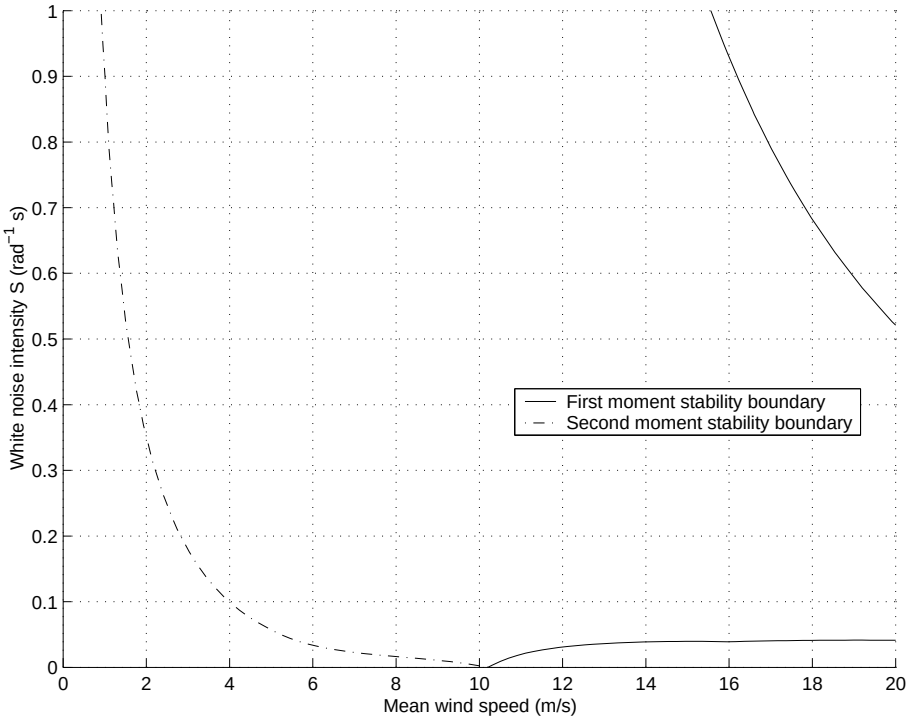

Figure 8.1: Stochastic stability chart for the bridge-wind system

second moments for the BW system and BWCS systems in open and closed loop configurations respectively. Each point in the stability chart represents a condition in which, for a given white noise intensity and a given mean wind speed, the matrices $\mathbf{F}$ and $\mathbf{H}$ have an eigenvalue with zero real part; in this way, the critical velocity is defined in the sense of the first or second moments. Figures 8.1 and 8.2 also show that, the critical velocity given by the second moment is more conservative than the corresponding to the first moment; in other words, the first stability moment gives a higher critical velocity than the second one, indeed, in the present case the

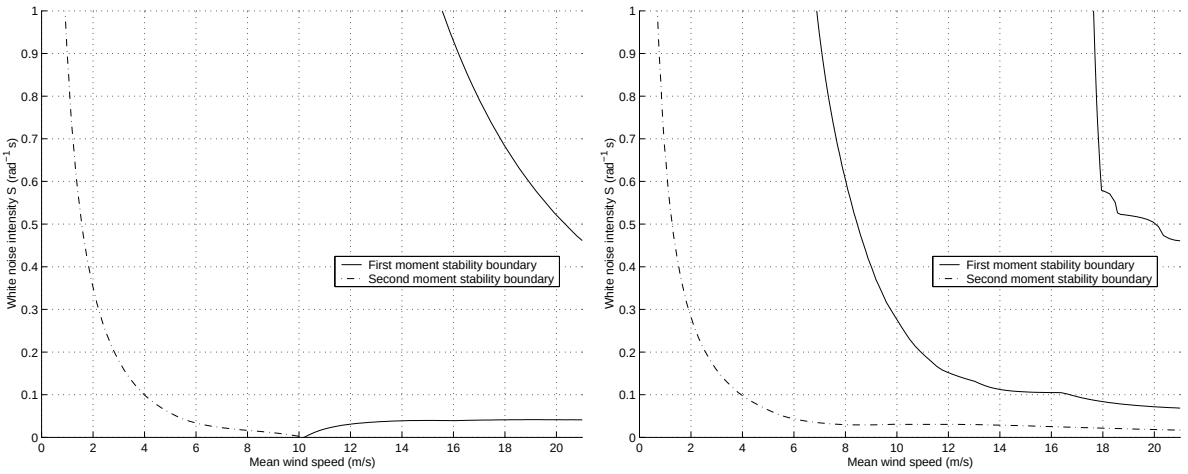

Figure 8.2: Stochastic stability chart for the BWCS system in open (left) and closed (right) loop configuration

critical flutter velocity in the first moment is higher than the deterministic critical velocity of the bridge.

In chapter 3 was explained that Kaimal's spectrum (equation (3.26)) models the longitudinal wind velocity fluctuations $u(t)$. This power spectral density can be modified to model wind fluctuations $\eta_1(t) = u(t)/\bar{U}$ yielding,

$$S_{\eta_1\eta_1}(z,\omega) = \frac{200z}{\bar{U}(z)\left(1+50\frac{\omega z}{2\pi\bar{U}(z)}\right)^{5/3}}\left(\frac{u_*}{\bar{U}(z)}\right)^2 \tag{8.53}$$

In this way, the white noise intensity of the RPE formulation was approximated by $S \equiv S(z,0)$, as Bucher and Lin (1988) suggested. Using a height above the ground of $z = 96$ m (0.64 m for the 1:150 scaled version of the Akashi Kaikyo bridge), a ground surface roughness corresponding to a snow surface ($z_0 = 0.05$ m), from equation (3.28) it follows that $u_*/\bar{U} = 0.053$. Simiu and Scanlan (1996) relates this term to the so called *turbulence intensity*

$$I(t) = \frac{\sigma_u}{\bar{U}} \tag{8.54}$$

by the expression

$$I(t) = \sqrt{\beta}\frac{u_*}{\bar{U}} \tag{8.55}$$

where σ_u^2 denotes the variance of the wind fluctuation. It is commonly assumed that β is varies with the ground surface roughness length z_0, and is independent of z. Table 8.1, presents different values of β. In the present example $\beta = 6.5$; therefore, the turbulence intensity is equal to 0.135,

Table 8.1: Values of β corresponding to various roughness lengths (Simiu and Scanlan (1996))

Description	z_0 (cm)	β
Snow surface	0.5	6.5
High grass	7	6.0
Palmetto[a]	30	5.25
Pine forest[b]	100	4.85
Centers of large cities	250	4.00

[a]Type of small palm-tree with fan-shaped leaves.
[b]Mean height of trees: 15 m; one tree per 10 m^2

which is a realistic value. Replacing the above defined terms into (8.53), it follows that, the white noise intensity S is dependent on the mean wind speed, that is, $S = 0.358/\bar{U}$ approximately. Figure 8.3, shows that the stability boundaries of the first and second moments are influenced by

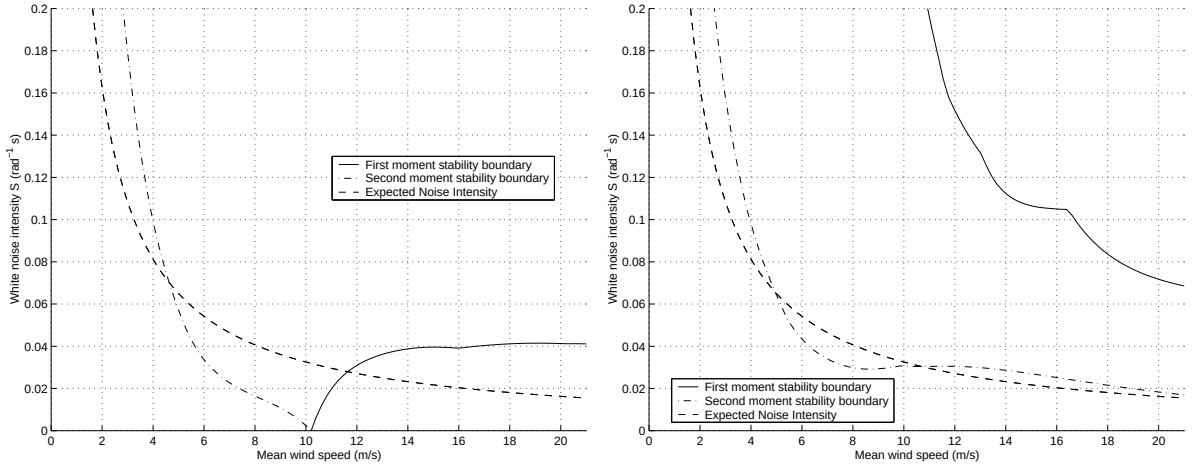

Figure 8.3: Stochastic stability/instability chart and variation of the white noise intensity for the BW system (left) and BWCS system in closed loop configuration (right)

the mean wind velocity $\bar{U}$, the spectral density of the fluctuations S and the bridge aeroelastic and structural parameters; also, it demonstrates that the second moment in the analyzed bridge is unstable for both the BW and BWCS systems, when a RPE analysis is made. From this fact, one can deduce that the present analysis was carried out on a bridge section prone to buffeting induced vibrations, since the second moment becomes unstable in the range between 5 and 10.7 m/s approximately. This result also highlights the fact that the control surfaces could not be as good as expected in the reduction of the vibrations induced by buffeting; therefore, an additional analysis should be made on a section which could become stabilized by turbulence,

since the turbulent component of the wind may reduce or increase the flutter velocity in some cases (Bucher and Lin (1988)), depending on the aeroelastic parameters for a specific bridge.

Chapter 9

Final considerations, summary and future work

Along the present study it was analyzed how the use of separated control surfaces beneath the bridge's deck can be useful to counteract the vibrations induced by wind on the bridge deck, stressing on the analysis of coupled buffeting and self-excited forces. This research differs from previous investigations in that neither nobody has addressed the analysis of the BWCS as a parametrically excited system, nor the influence of the buffeting forces has been taken into consideration.

Several suppositions where made along the present research: the deck was modelled using Theodorsen theory; both the girder and the control surfaces shared the drag-, lift- and moment-aerodynamic coefficients; the bridge was represented using only two degrees of freedom; the random parametric excitation stability analysis was performed using the same flutter derivatives employed in the deterministic analysis. This factors have a great influence in the results below presented. In this way, it is advisable to repeat the analysis on a set of bridges with different aerodynamic/aeroelastic and structural parameters as the ones here employed. In the following a brief description of the principal results found in this work will be made.

The equation modelling the motion of the BWCS system was expressed in a state-space fashion, in contraposition with the traditional iterative frequency approaches extensively used in bridge engineering, making it very suitable for straightforward use of the concepts of control theory.

This state space model assumes that the wake generated by the leading wing and the deck have no interaction within them and the trailing surface. This strong hypothesis requires further study in a wind tunnel test or a computer simulation using computational fluid dynamics techniques.

A comparison of the behaviour of the bridge without control surfaces and the winged bridge in open loop configuration showed for the analyzed model that, the behaviour of the latter does not depend on the values of the frequency and damping of the control surfaces, however, these parameters do drastically affect the performance of the BWCS system in closed loop configuration as they especially impel the increase of the damping of the different vibration modes of the system. It was seen that the most important parameter in the design of the control system is the damping of the control surfaces, since, for highly damped wings the structure can withstand higher wind speeds.

It was found that the critical wind velocity for the uncontrolled BWCS system is a little greater than the one corresponding to the bridge without control surfaces. This is a nice feature inasmuch as the behaviour of the winged bridge does not deteriorate with the use of control surfaces, in fact, it improves.

The variation of the control surfaces/bridge deck width ratio was carried out, demonstrating that the best performance was achieved for the relation from 0.15 to 0.25. However, it was discussed that lower ratios could be preferred inasmuch as the performance of the BWCS system does not deteriorate excessively and that lower ratios imply smaller dead loads on the controlled structure. In contrast, it was shown that higher ratios make the bridge prone to fail by divergence, however, this is only an hypothesis since, in the present case, the wake should have a big influence on the behavior of the controlled bridge, so that, for high ratios the wake analysis is mandatory.

The BWCS was controlled using a variable gain stochastic regulator made up of a LQR optimal gain and a Kalman filter. The last one deals with the noise present in the sensors and the buffeting forces affecting the system. In this case, the buffeting forces were modelled as a filtered Gaussian white noise using an autoregressive model, and the noise in the sensors was assumed to be Gaussian, zero mean, white and additive. This algorithm was employed to stabilize the bridge in the range of velocities from 5 m/s up to 21 m/s, approximately twice the critical wind speed of the BW system. Although a single stochastic regulator designed for a 21 m/s wind speed could stabilize the bridge for all wind velocities in the working range, it was observed that the

variable gain stochastic regulator noticeable increases the stiffness and damping of the vibration modes of the bridge in the range of design. The use of the variable gain regulator was made inasmuch as the system formulation changes with an increasing wind speed. This is not the best strategy to use when a system is sensible to weak and/or rapidly varying inputs, however, it was demonstrated that the BWCS is not the case.

The optimal control force in the presence of steady flow occurs when the leading and trailing control surfaces twist respectively in the opposite and same direction with respect to the deck rotation; also both movements have a slight phase lead with respect to the deck rotation. This phase lead is very important because the aeroelastic forces controlling the bridge and induced by the wings begin to counteract the deck vibration in the same instant the movement of the girder begins.

In the design of the stochastic regulator, it was observed that the BWCS system in open loop configuration is not controllable but stabilizable; in this case, it was ensured that the uncontrollable modes take care of themselves. On the other hand, the optimal control involved used as performance criteria the minimization of both the total energy of the bridge and the rotation of the control surfaces.

The main result of this thesis it that control surfaces attached below the bridge deck although are an outstanding mechanism to deal with self-excited vibrations; nevertheless, it is not as good as one can expect facing up to high buffeting forces, inasmuch as the heaving displacements by them induced are very large and despite the fact that they can be stabilized, they may not become enclosed into serviceability bounds; on the other side, the pitching vibrations can be adequately stabilized, even in high turbulent winds. In this way, one can conclude that the main stabilizing action comes from the torque induced by the lifting forces over the control surfaces. The serviceability bounds should be checked up making the analysis of the accelerations on the girder and tension in the hangers and main cables of a full model bridge.

It was noted that the leading wing has the greater influence on the deck vibrations control, as it was concluded that the vertical wind fluctuation is the main source of the buffeting vibrations. In the present case, when the vertical wind fluctuation around the mean is positive (downward direction), a positive lift force and a negative torque (counterclockwise direction) act on the BWCS system. The control system reacts rotating both wings in a positive (clockwise) direction

to generate the equilibrium forces; however the trailing control surface rotates in a lesser degree, such that a positive torque is generated by the pair of wings to cancel the buffeting twisting force out. The converse rotations happen when the vertical wind fluctuation is negative, however, in this case, the leading control surface still has the largest rotation.

It was commented that if wider wings are employed, the buffeting heaving vibration could be dissipated in a higher degree, however, this is not an efficient solution, in view of the fact that it would lead to the increase of both the dead load of the controlled system and the construction costs.

It was also demonstrated that the control system is robust against noisy measurements; they do not make unstable the bridge, in fact, noise in the measurements made the critical velocity of the bridge to grow up, this is a behaviour which was not expected; however the noise in the sensors spur the actuators to apply to the structure highly varying control torques, since the variance of the displacement response increases.

The random parametric analysis revealed that the present study was performed on a bridge section prone to buffeting induced vibrations. This result highlights the fact that the control surfaces could not be as good as expected in the reduction of the vibrations induced by buffeting; therefore, an additional analysis should be made on a section which could become stabilized by turbulence, since the turbulent component of the wind may reduce or increase the flutter velocity in some cases, as stated by Bucher and Lin (1988), depending on the aeroelastic parameters for a specific bridge.

Many opportunities of future work are available:

Since high buffeting forces are random in nature, the evaluation criteria stated in section 7.5.1 should be assessed from a probabilistic viewpoint by the use of excursion probabilities as a modification of the methods stated in Hurtado and Alvarez (2001) and Hurtado and Alvarez (2003).

A simulation on a full bridge model should be carried out because there are several aspect that must be understood, like the performance of the wings installed only on a section of the central span and the interaction between the control system and towers and the cables; also the full bridge model will be subjected to a wind field not to a single realization of the wind speed

fluctuations. In addition, an analysis of the saturation of the actuators and the influence of the zero-order-hold in the frequency response of the BWCS system must be carried on.

As depicted from the RPE analysis, the bridge in consideration was prone to buffeting vibrations. An analysis of the control surfaces system should be performed on bridges with different aerodynamic/aeroelastic behaviors. In fact, it is desirable to observe the performance of the control system in a bridge which could be stabilized by buffeting forces.

Also, a nonlinear optimization techniques like evolutionary algorithms could be employed for choosing better $\mathbf{Q}$ and $\mathbf{R}$ matrices subject to the fulfillment of the performance criteria stated in section 7.5.1. This optimization should have additional restrictions like the desirable veering of the eigenvalue loci to avoid the unwanted coupling between vibration modes.

A robustness analysis of the controlled BWCS system including a controller delay should be performed, following the μ-analysis techniques described in Field et al. (1996).

Further research about other methods of bridge wind-induced vibration control should be carried on since the present method maybe infeasible due to high construction and maintenance costs, inasmuch as emergency control systems must be installed to take on the control of the wings in the case the principal control fails. For example, the study of flaps attached next to the girder (as an extension of the idea of time changing fairings) must be considered, since this control system actively changes the bridge aerodynamic properties, so better performance could be obtained.

Appendix

Appendix A

Pole maps

In the following pole maps for different configurations of the bridge and bridge-wind-control surfaces system in open loop and closed loop configuration are shown.

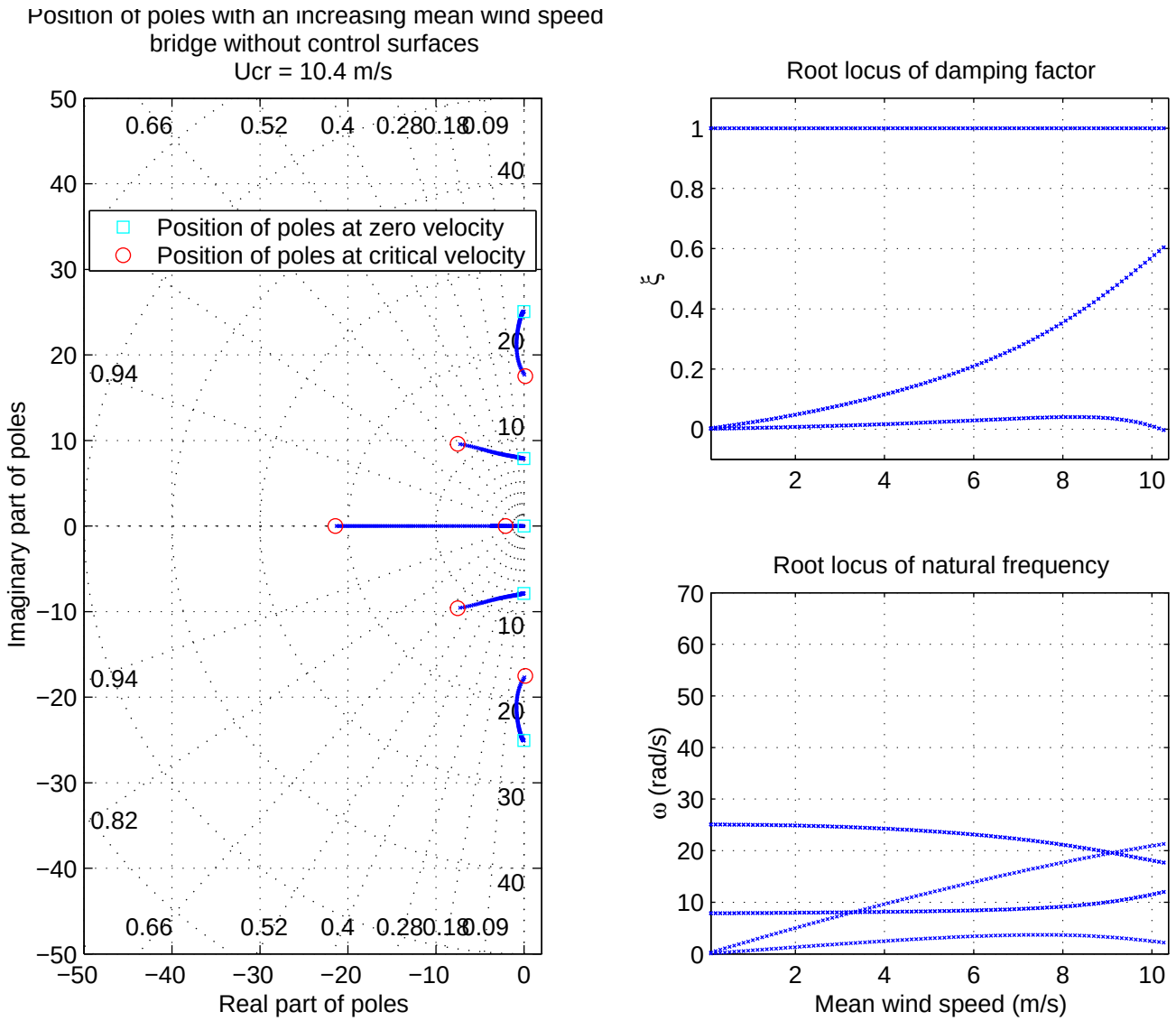

Figure A.1: Pole map for the bridge without control surfaces

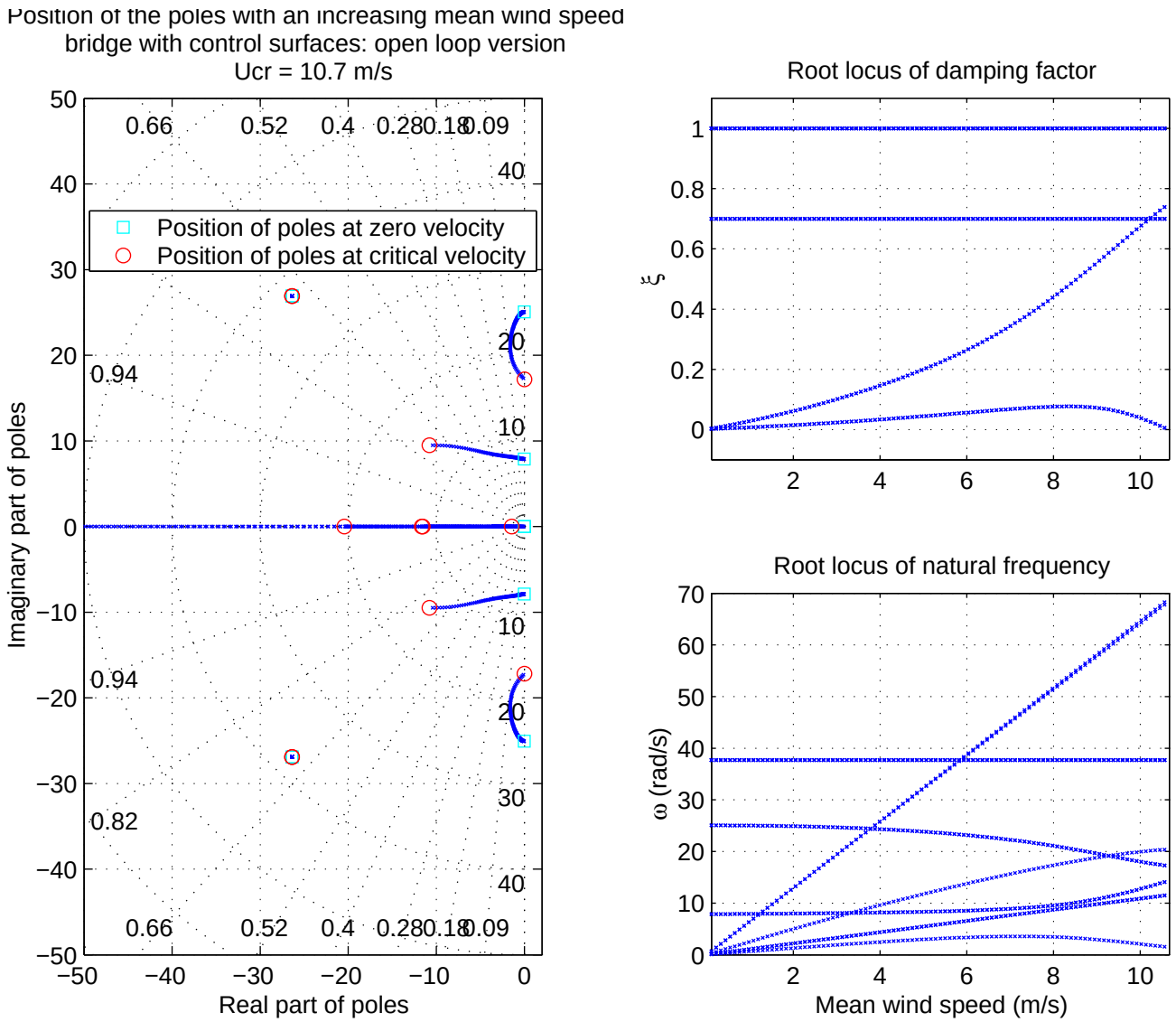

Figure A.2: Pole map for the BWCS in an open loop configuration

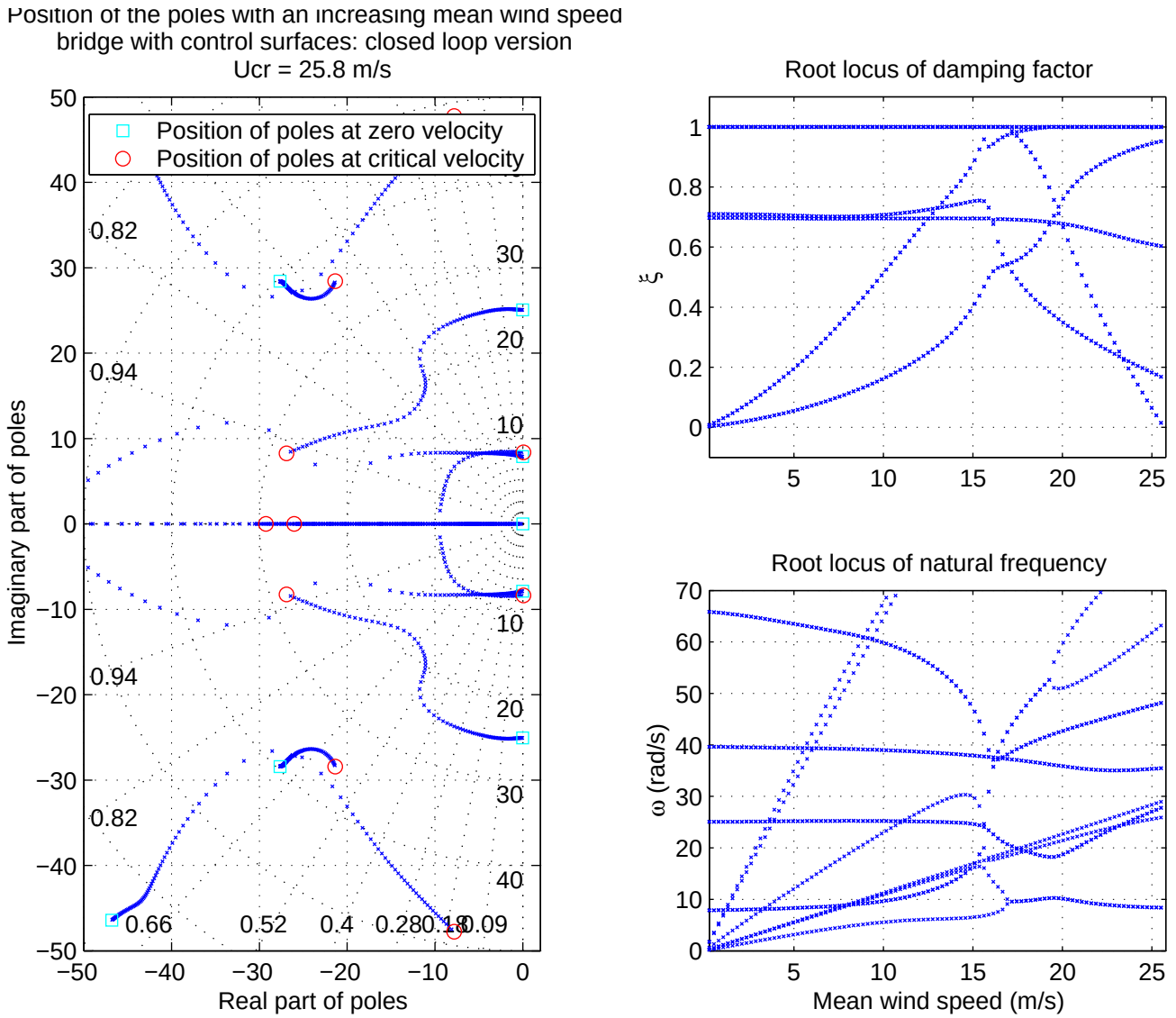

Figure A.3: Pole map for the BWCS in a closed loop configuration controlled by a LQR algorithm designed for $\bar{U} = 16$ m/s

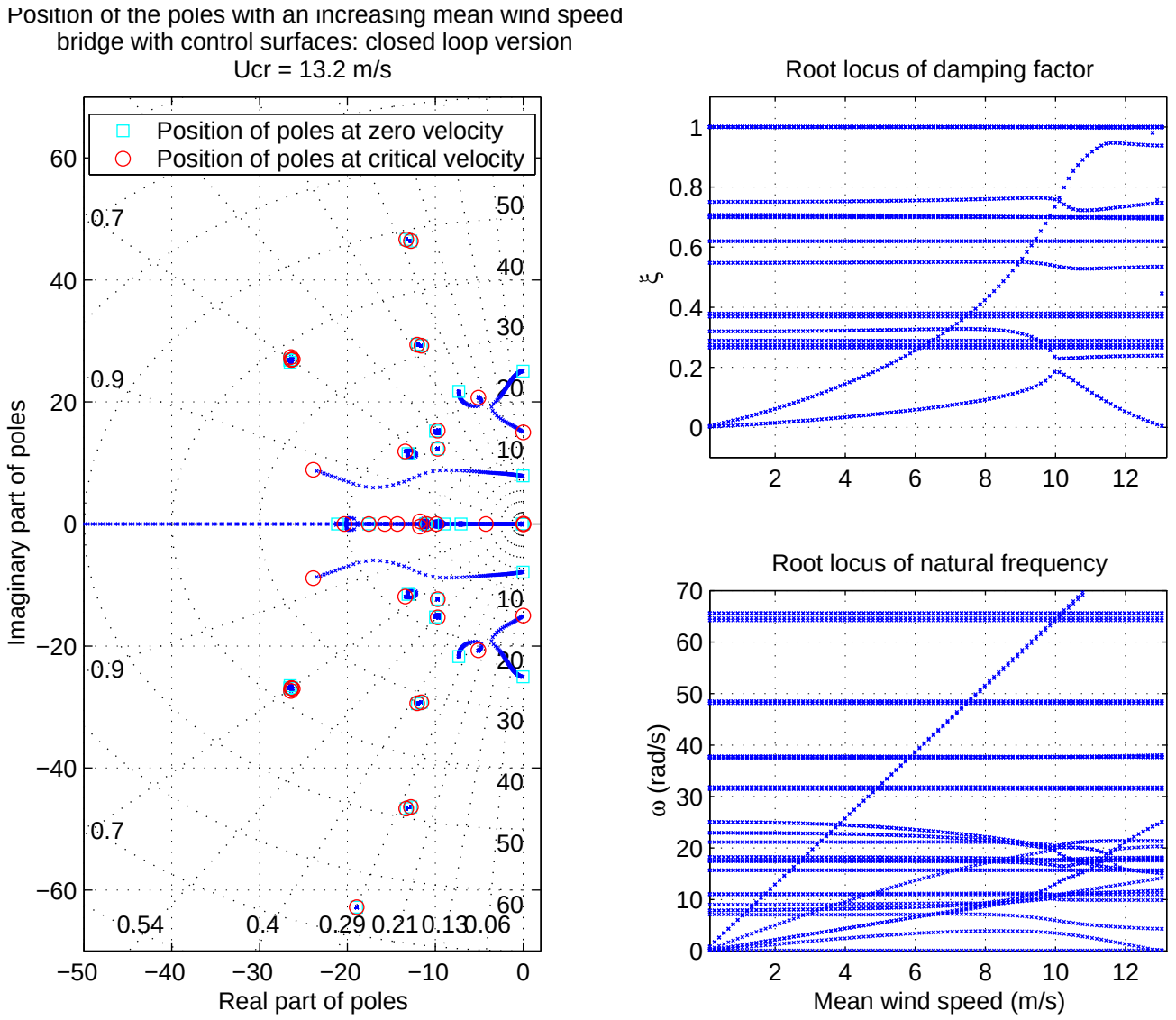

Figure A.4: Pole map for the BWCS in a closed loop configuration controlled by a stochastic regulator designed in for $\bar{U} = 10$ m/s

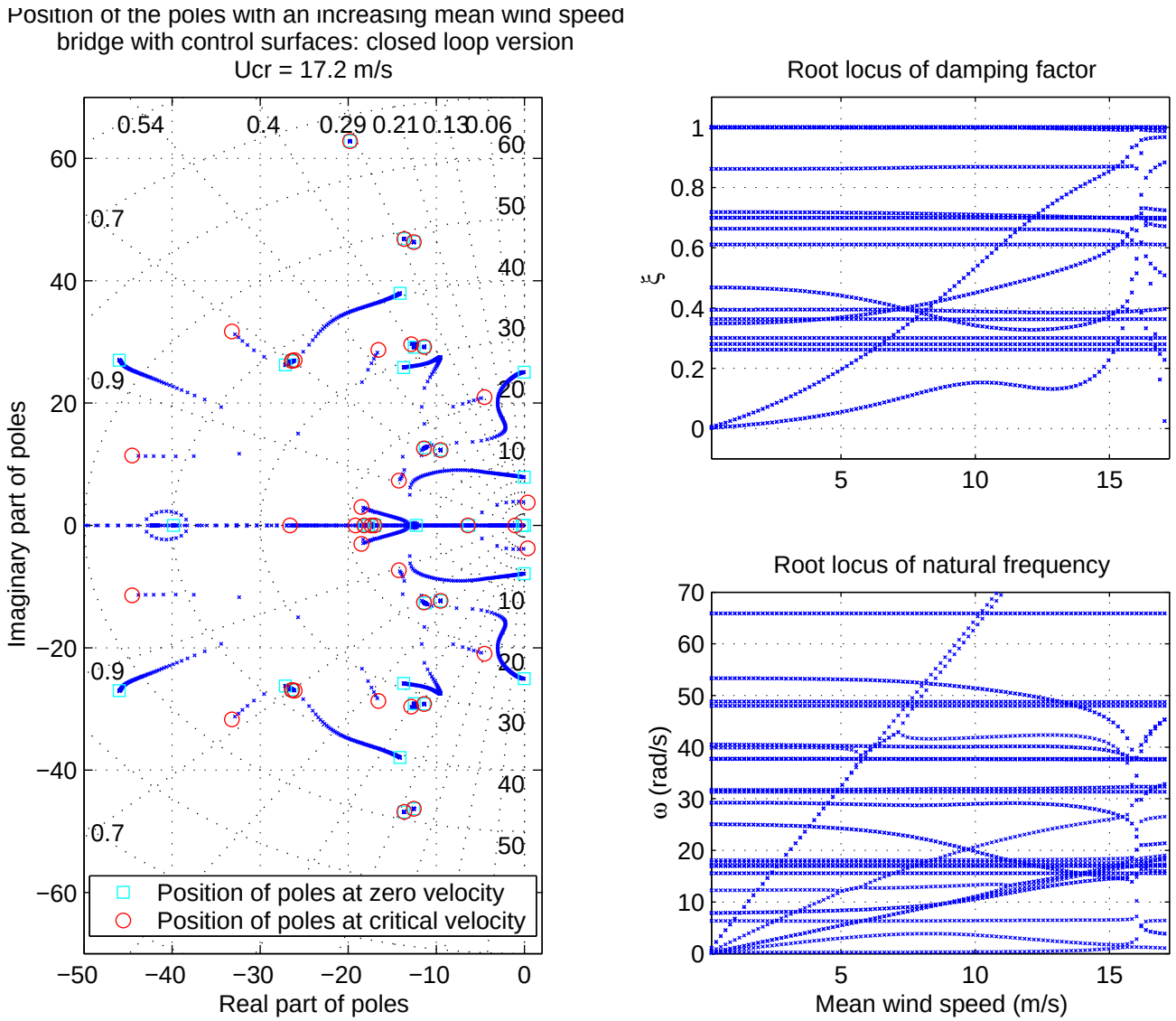

Figure A.5: Pole map for the BWCS in a closed loop configuration controlled by a stochastic regulator designed for $\bar{U} = 16$ m/s

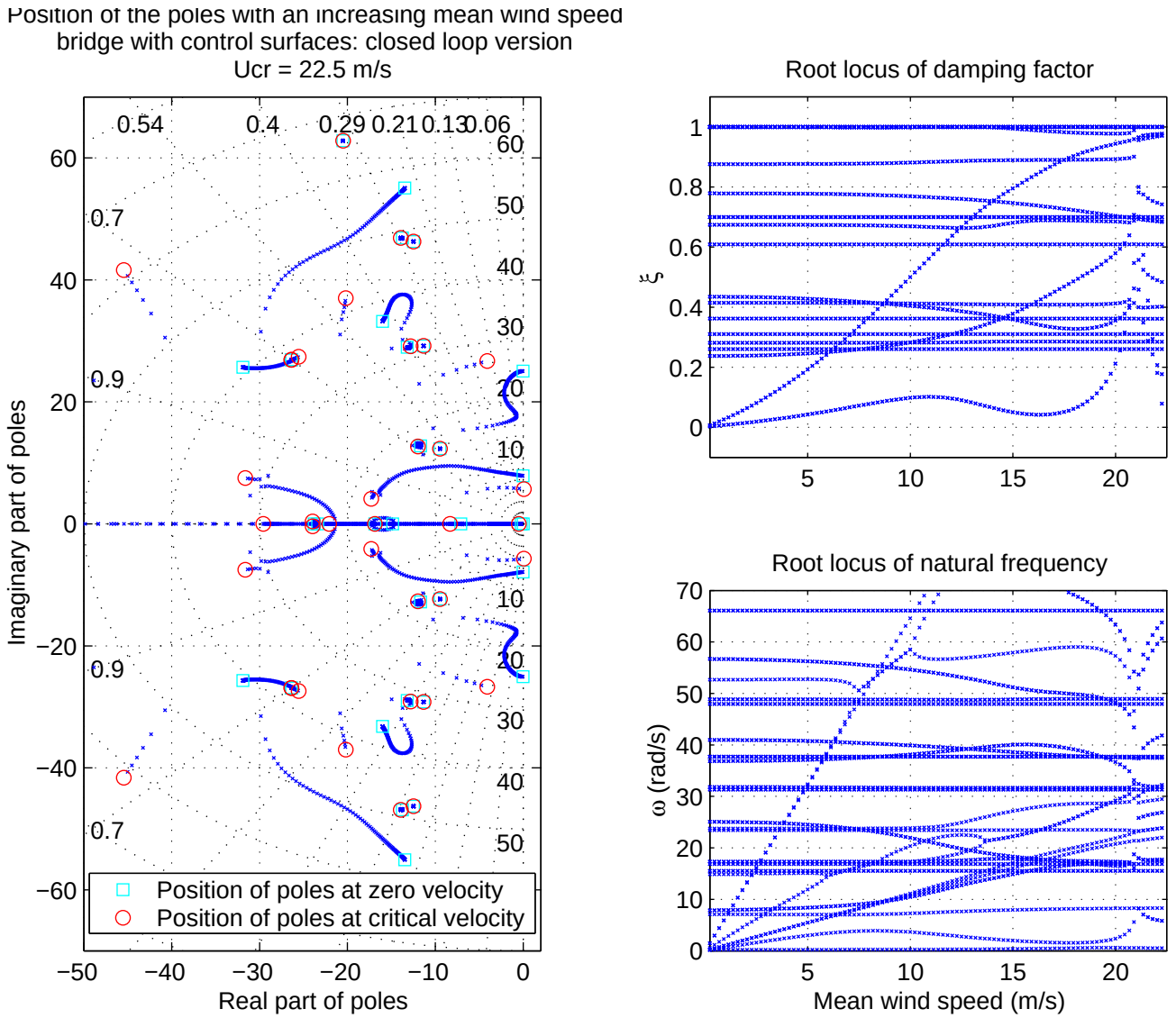

Figure A.6: Pole map for the BWCS in a closed loop configuration controlled by a stochastic regulator designed for $\bar{U} = 21$ m/s

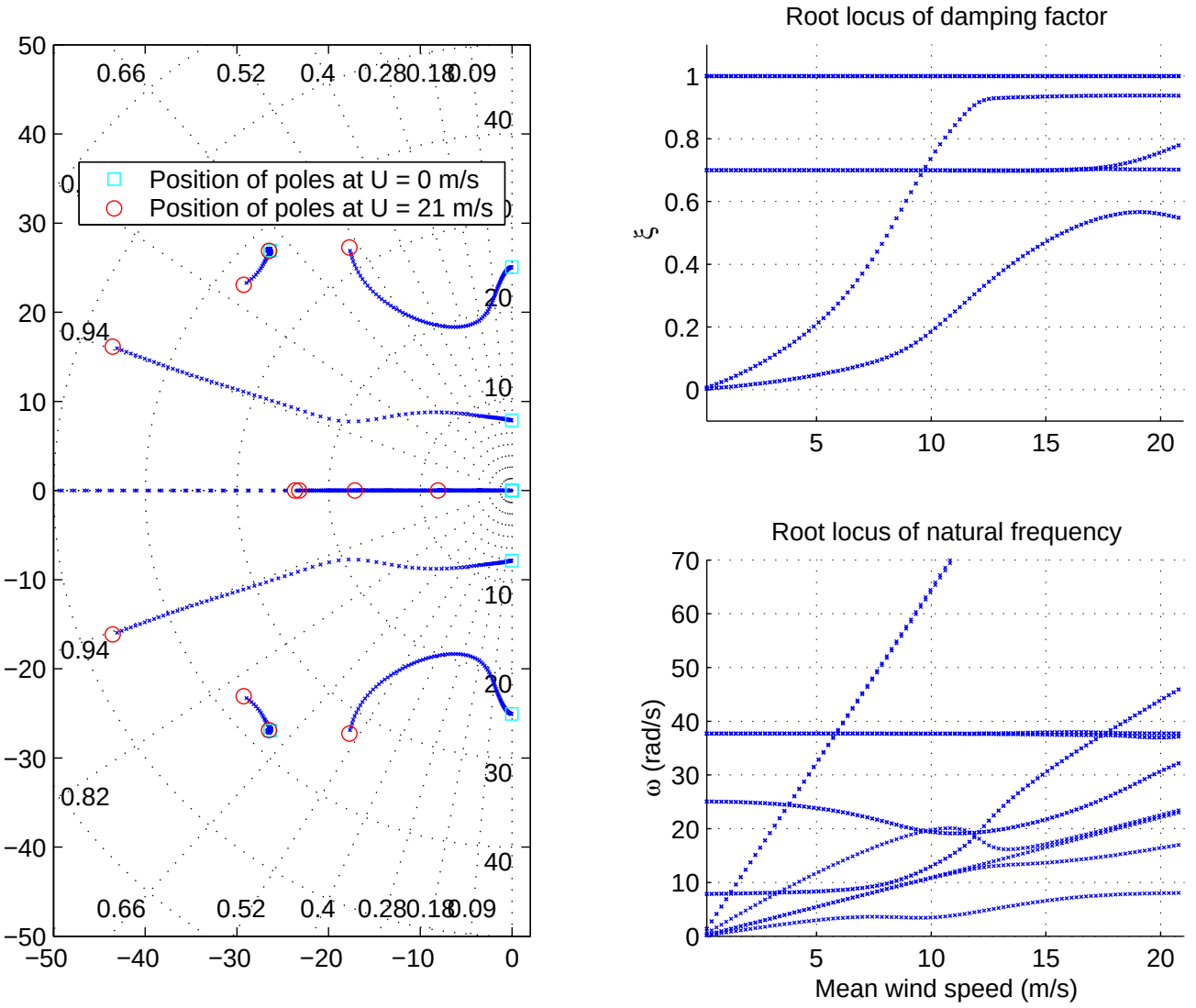

Figure A.7: Pole map for the BWCS in a closed loop configuration controlled by a variable gain LQR $\bar{U} = 0, \ldots, 21\mathrm{m/s}$

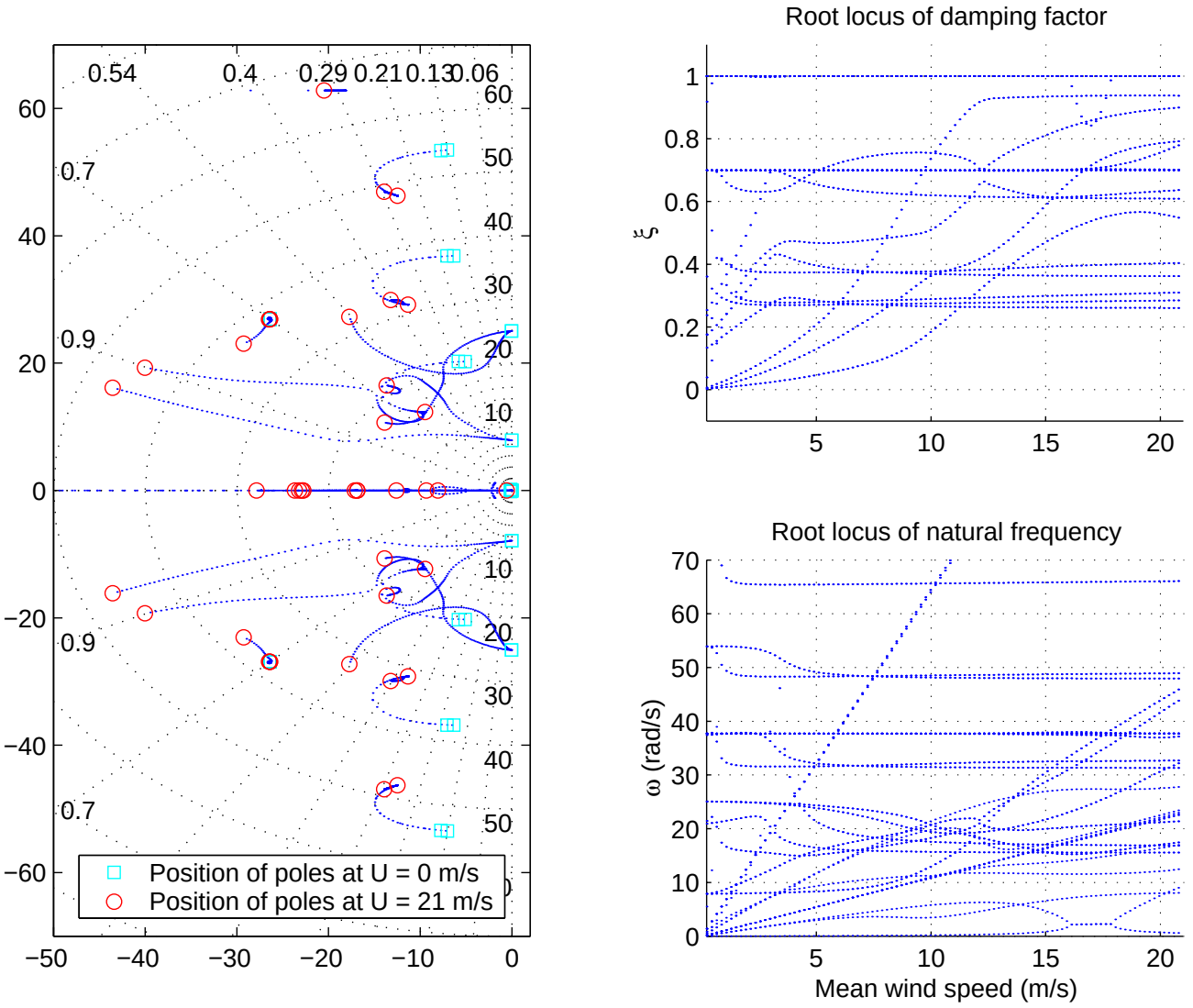

Figure A.8: Pole map for the BWCS in a closed loop configuration controlled by a variable gain stochastic regulator $\bar{U} = 0, \ldots, 21\mathrm{m/s}$

Bibliography

Ackkire, Y. and Preumont, A. (1996). Active tendon control of cable-stayed bridges. *Earthquake Engineering and Structural Dynamics*, 25:585–597.

Astiz, M. A. (1998). Flutter stability of very long suspension bridges. *ASCE, Journal of Bridge Engineering*, 3(3):132–139.

Billah, K. Y. and Scanlan, R. H. (1991). Resonance, Tacoma Narrows bridge failure, and undergraduate physics textbooks. *American Journal of Physics*, 59(2):118–124.

Boonyapinyo, V., Miyata, T., and Yamada, H. (1999). Advanced aerodynamic analysis of suspension bridges by state-space approach. *ASCE, Journal of Structural Engineering*, 125(12):1357–1366.

Bossens, F. and Preumont, A. (2001). Active tendon control of cable-stayed bridges: a large scale demonstration. *Earthquake Engineering and Structural Dynamics*, 30(961-979).

Branceleoni, F. (1992). The construction phase ans its aerodynamic issues. In Larsen, A., editor, *Aerodynamics of large bridges*, pages 147–158. A. A. Balkema, Rotterdam, The Netherlands.

Bucher, C. G. and Lin, Y. K. (1988). Stochastic stability of bridges considering coupled modes. *ASCE, Journal of Engineering Mechanics*, 114:2055–2071.

Bucher, C. G. and Lin, Y. K. (1989). Stochastic stability of bridges considering coupled modes: II. *ASCE, Journal of Engineering Mechanics*, 115:384–400.

Cai, C. S., Albrecht, P., and Bosch, H. R. (1999). Flutter and buffeting analysis. I: Finite-element and RPE solution. *ASCE, Journal of Bridge Engineering*, 4(3):174–180.

Cao, Y., Xiang, H., and Zhou, Y. (2000). Simulation of stochastic wind velocity field on long-span bridges. *ASCE, Journal of Engineering Mechanics*, 126(1):1–6.

Chen, C.-T. (1999). *Linear system theory and design*. Oxford series in electrical and computer engineering. Oxford University Press, New York, 3 edition.

Chen, X. and Kareem, A. (2001). Aeroelastic analysis of bridges under multicorrelated winds: integrated state-space approach. *ASCE, Journal of Engineering Mechanics*, 127(11):1124–1134.

Chen, X., Matsumoto, M., and Kareem, A. (2000). Aerodynamic coupling effects of flutter and buffeting of bridges. *ASCE, Journal of Engineering Mechanics*, 126(1):17–26.

Cobo del Arco, D. and Aparicio, A. C. (1998). Improving suspension bridge wind stability with aerodynamic appendages. *ASCE, Journal of Structural Engineering*, 125(12):1367–1375.

Davenport, A. G. (1968). The dependence of wind load upon meteorological parameters. In *Proc. of the Int. Res. Seminar of Wind Effects on Build. and Struct.*, pages 19–82, Toronto, Canada. University of Toronto Press.

Deodatis, G. (1996). Simulation of ergodic multivariate stochastic processes. *ASCE, Journal of Engineering Mechanics*, 122(8):778–787.

Deodatis, G. and Shinozuka, M. (1989). Simulation of seismic ground motion using stochastic waves. *ASCE, Journal of Engineering Mechanics*, 115(12):2723–2737.

Dyke, S., Caicedo, J. M., Turan, G., Bergman, L., and Hague, S. (2003). Phase I: Benchmark control problem for seismic response of cable-stayed bridges. *ASCE, Journal of Structural Engineering*, 129(7):857–872.

Dyke, S. J., Turan, G., Caicedo, J. M., Bergman, L. A., and Hague, S. (2000). Benchmark control problem for seismic response of cable-stayed bridges. In *Proceedings of the Second European Conference on Structural Control*, Paris, France. Available in `http://wusceel.cive.wustl.edu/quake/bridgebenchmark/index.htm`.

Field, R. V., Voulgaris, P. G., and Bergman, L. A. (1996). Probabilistic stability robustness of structural systems. *ASCE, Journal of Engineering Mechanics*, 122(10):1012–1021.

Frandsen, J. (2002). Computational bridge aerodynamics. `http://www.eng.ox.ac.uk/~oedjbf/index.html`.

Fujino, Y., Iwamoto, M., Ito, M., and Hikami, Y. (1992). Wind tunnel experiments using 3d models and response prediction for a long-span suspension bridge. *Journal of Wind Engineering and Industrial Aerodynamics*, 41–44:1333–1344.

Hansen, H. I. and Thoft-Christensen, P. (1998). Active vibration control of long bridges using flaps. Proceedings of the Second World Conference on Structural Control.

Housner, G. W., Bergman, L. A., Caughey, T. K., Chassiakos, A. G., Claus, R. O., Masri, S. F., Skelton, R. E., Soong, T. T., Spencer, B. F., and Yao, J. T. P. (1997). Structural control: past, present and future. *ASCE, Journal of Engineering Mechanics*, 123(9). Special Issue.

Hurtado, J. E. and Alvarez, D. A. (2001). Neural network-based reliability analysis: A comparative study. *Computer Methods in Applied Mechanics and Engineering*, 191:113–132.

Hurtado, J. E. and Alvarez, D. A. (2003). A classification approach for reliability analysis with stochastic finite element modelling. *ASCE, Journal of Structural Engineering*, 129(8):1141–1149.

Huston, D. R. (1986). *The effect of upstream gusting on the aeroelastic behaviour of lon suspended-span bridges*. Ph. D. dissertation, Princeton University.

Huynh, T. and Thoft-Christensen, P. (2001). Suspension bridge flutter for girders with separate control flaps. *ASCE, Journal of Bridge Engineering*, 6(3):168–175.

Ibrahim, R. A. (1985). *Parametric random vibration*. Research Studies Press Ltd., Taunton.

Jain, A., Jones, N. P., and Scanlan, R. H. (1996). Coupled flutter and buffeting analysis of long-span bridges. *ASCE, Journal of Structural Engineering*, 122(7):716–725.

Jurado, J. A. and Hernández, S. (2000). Theories of aerodynamic forces on decks of long span bridges. *ASCE, Journal of Bridge Engineering*, 5(1):8–13.

Kaimal, J. C. and et. al. (1972). Spectral characteristics of surface-layer turbulence. *J. Royal Meteorological Soc.*, 98:563–589. London, England.

Kalman, R. E. (1960). A new approach to linear filtering and prediction theory. *Journal of Basic Engineering*, 82:34–35.

Kalman, R. E. and Bucy, R. (1961). New results in linear filtering and prediction theory. *Journal of Basic Engineering*, 83:83–95.

Karpel, M. (1981). Design for active and passive flutter suppression and gust alleviation. CR 3482, NASA, Washington D.C.

Katsuchi, H., Jones, N. P., and Scanlan, R. H. (1999). Multimode coupled flutter and buffeting analysis of the Akashi-Kaikyo Bridge. *ASCE, Journal of Structural Engineering*, 125(1):60–70.

Kobayashi, H. and Nagaoka, H. (1992). Active control of flutter of a suspension bridge. *Journal of Wind Engineering and Industrial Aerodynamics*, 41–44:143–151.

Lin, Y. K. (1979). Motion of suspension bridges in turbulent winds. *ASCE, Journal of Engineering Mechanics*, 105(6):921–932.

Lin, Y. K. (1996). Stochastic stability of wind-excited long-span bridges. *Probabilistic Engineering Mechanics*, 11:257–261.

Lin, Y. K. and Ariaratnam, S. T. (1980). Stability of bridge motion in turbulen winds. *ASCE. Journal of Structural Mechanics*, 8(1):1–15.

Mitra, S. K. (1998). *Digital signal processing: a computer-based approach.* Series in electrical and computer engineering. McGraw Hill, Singapore.

Morguental, G. (2000). Fluid-structure interaction and bluff-body aerodynamics and long-span bridge design: phenomena and methods. Technical Report CUED/D-Struct/TR. 187, Magdalena College.

Nobuto, J., Fujino, Y., and Ito, M. (1988). A study on the effectiveness of tuned mass dampers to supress a coupled flutter of bridge deck. *Journal of Structural Mechanics and Earthquake Engineering*, Tokyo, Japan No. 398(I-10):413–416. (in Japanese).

Ogata, K. (1997). *Modern Control Engineering.* Prentice Hall Inc., Mexico, 3 edition.

Ostenfeld, K. H. and Larsen, A. (1992). Bridge engineering and aerodynamics. In Larsen, A., editor, *Aerodynamics of large bridges*, pages 3–22. Balkema, Rotterdam, The Netherlands.

Ostenfeld, K. H. and Larsen, A. (1997). *New Technologies in structural engineering*, chapter Elements of active flutter control of bridges, pages 683–694. Laboratorio Nacional de Engenharia Civil, Lisbon, Portugal.

Papoulis, A. (1991). *Probability, random variables and stochastic processes*. Series in Electrical Engineering. McGraw Hill, Singapore, 3 edition.

Pollock, D. (1999). *A handbook of time-series analysis, signal processing and dynamics*. Academic Press, London.

Raggett, J. D. (1987). Stabilizing pair of winglets for slender bridge decks. In *Bridges and transmission line structures*, New York. American Society of Civil Engineers.

Rice, S. O. (1954). Mathematical analysis of random noise. In Wax, N., editor, *Selected papers on noise and stochastic processes*, pages 133–294. Dover Publications Inc., New York.

Richardson, J. R. (1981). The development of the concept of the twin deck suspension bridge. *NMI R 125 National Maritime Institute*. Feltham , Middlesex, U.K.

Roger, K. (1977). Airplane math modeling for active control design: structural aspects of active control. Technical Report AGARD-CP-228, Advisory Group for Aerospace Research and Development, Neuilly-sur-Seine, France.

Scanlan, R. H. and Tomko, J. J. (1971). Airfoil and bridge deck flutter derivatives. *ASCE, Journal of Engineering Mechanics*, 97:1717–1737.

Shinozuka, M. (1972). Monte Carlo solution of structural dynamics. *Computers and Structures*, 2(5+6):855–874.

Shinozuka, M. (1974). Digital simulation of random processes in engineering mechanics with the aid of the FFT technique. In Ariaratnam, S. T. and Leipholz, H. H. E., editors, *Stochastic problems in mechanics*, pages 277–286. University of Waterloo Press, Waterloo, Canada.

Shinozuka, M. and Jan, C.-M. (1972). Digital simulation of random processes and its applications. *Journal of Sound and Vibration*, 25(1):111–128.

Shinozuka, M., Kamata, M., and Yun, C.-B. (1989). Simulation of earthquake ground motion as multi-variate stochastic process. Technical Report 1989.5, Princeton-Kajima Joint Res.,

Department of Civil Engineering and Operations Research, Princeton University, Princeton, N. J.

Simiu, E. and Scanlan, R. H. (1996). *Wind effects on structures: fundamentals and applications to design*. Wiley, New York, 3 edition.

Soong, T. T. (1990). *Active structural control: theory and practice*. Longman Scientific and Technical, Great Britain.

Soong, T. T. and Grigoriu, M. (1993). *Random Vibration of Structural and Mechanical Systems*. Prentice Hall, Englewood Cliffs.

Stengel, R. F. (1986). *Stochastic optimal control: theory and application*. John Wiley and Sons, United States of America.

Szidarovszky, F. and Bahill, A. T. (1998). *Linear systems theory*. CRC Press, Boca Raton, 2 edition.

Theodorsen, T. (1935). General theory of aerodynamic instability and the mechanism of flutter. Technical Report NACA496, U.S. Naval Advisory Committee for Aeronautics, Langley, Virginia.

Tiffany, S. H. and Adams, W. M. J. (1988). Nonlinear programming extensions to rational function approximation methods for unsteady aerodynamic forces. CR 2776, NASA, Washington D.C.

Walther, R., Houriet, B., Isler, W., and Moïa, P. (1988). *Cable stayed bridges*. Thomas Telford.

Wilde, K. (2003). Personal communication.

Wilde, K. and Fujino, Y. (1998). Aerodynamic control of bridge deck flutter by active surfaces. *ASCE, Journal of Engineering Mechanics*, 124(7):718–727.

Wilde, K., Omenzetter, P., and Fujino, Y. (2001). Supression of bridge flutter by active-deck-flaps control system. *ASCE, Journal of Engineering Mechanics*, 127(1):80–89.

Wong, E. and Zakai, M. (1965). On the relation between ordinary and stochastic equations. *Int. J. Engrg. Sci.*, 3(2):213–229.

Yamazaki, F. and Shinozuka, M. (1988). Digital generation of non-gaussian stochastic fields. *ASCE, Journal of Engineering Mechanics*, 114(7):1183–1197.

Yang, J.-N. (1972). Simulation of random envelope processes. *Journal of Sound and Vibration*, 25(1):73–85.

Yang, J.-N. (1973). On the normality and accuracy of simulated random processes. *Journal of Sound and Vibration*, 26(3):417–428.

Yao, J. T. P. (1972). Concept of structural control. *J. Struct. Div. ASCE*, 98:1567–1574.